KTH ROYAL INSTITUTE
OF TECHNOLOGY

Doctoral Thesis in Energy Technology

Waste Heat Driven Membrane Distillation for Industrial Wastewater Treatment

IMTISAL-E-NOOR

Stockholm, Sweden 2021

Waste Heat Driven Membrane Distillation for Industrial Wastewater Treatment

IMTISAL-E-NOOR

Doctoral Thesis 2021

Academic Dissertation which, with due permission of the KTH Royal Institute of Technology and Aalto University, is submitted for public defense on Monday the 1st March 2021, at 8:00 a.m. via Zoom in KTH Royal Institute of Technology, Sweden.

Department of Energy Technology
School of Industrial Engineering and Management
KTH Royal Institute of Technology
Stockholm, Sweden

Department of Bioproducts and Biosystems
School of Chemical Engineering
Aalto University
Espoo, Finland

This doctoral dissertation is completed under Erasmus Mundus Joint Doctoral Programme, Environomical Pathways for Sustainable Energy Services (SELECT+) for the degree of Doctor of Philosophy from KTH Royal Institute of Technology, Sweden and degree of Doctor of Science (Technology) from Aalto University, Finland.

Aalto University publication series
DOCTORAL DISSERTATIONS 184/2020
ISBN (printed): 978-952-64-0131-7
ISBN (pdf): 978-952-64-0132-4
ISSN 1799-4934
ISSN 1799-4942 (electronic)

TRITA-ITM-AVL 2021:2
ISBN: 978-91-7873-774-1

Printed by: Universitetsservice US-AB, Sweden, 2021

Supervising Professors and Thesis Advisers
Prof. Andrew Martin, KTH Royal Institute of Technology, Sweden
Prof. Olli Dahl, Aalto University, Finland

Preliminary Examiners
Prof. Wojciech Kujawski, Nicolaus Copernicus University, Poland
Dr. Alessandra Criscuoli, Institute on Membrane Technology (CNR-ITM), Italy

Opponent
Prof. Mikel Duke, Victoria University, Melbourne Australia

Examination Committee Members
Prof. Corinne Cabassud, INSA Toulouse, France
Prof. Erik Dahlquist, Mälardalen University, Sweden
Prof. Riitta Keiski, University of Oulu, Finland

To my beloved parents Azhar Iqbal Sheikh and Zahida Jabeen

Abstract

The European Union has placed a high priority on reaching the goals described in the 2030 Agenda for Sustainable Development. This aim has provided added momentum to member-state environmental regulatory authorities to further tighten the discharge limits of industrial wastewater. These measures strongly influence existing industrial practices as many traditional wastewater treatment methods cannot achieve these strict release limits. Moreover, industrial sectors are encouraged to employ a zero liquid discharge strategy for advanced wastewater management, particularly for process water reuse. Emphasis is thus now placed on improved water treatment systems to recover, reuse and release water in a manner that protects natural resources, guarantees stringent regulatory constraints and ensures financial viability. In this context membrane distillation (MD) is a promising industrial wastewater treatment technology capable of meeting these requirements while utilizing low-grade heat sources.

This thesis focuses on experimental investigations and techno-economic analysis of waste heat driven MD systems for water purification in two water-intensive industries: nano-electronics facilities and cogeneration plants. Samples collected at relevant facilities were tested in an air gap MD bench unit and a semi-commercial pilot plant, with a focus on separation efficiency and potential for achieving high recovery ratios. For the techno-economic analysis of the industrial scale system, the performance of the chosen semi-commercial unit was considered to evaluate the full-scale system operation in terms of thermal energy demand and expected water purification cost. Various thermal integration approaches were investigated while considering locally available heat sources to realize the energy requirements of the specific MD system. The selected case studies include: removal of tetramethylammonium hydroxide (TMAH) from photolithography process wastewater in nano-electronics industries; treatment of chemical mechanical planarization (CMP) process wastewater in nano-electronics industries; and water recovery through advanced flue gas condensate treatment from municipal solid waste incineration and biofuel fired cogeneration plants.

The results from nano-electronics wastewater treatment tests showed that high-quality permeate could be recovered while observing good to excellent separation efficiencies of analyzed contaminants. Moreover, the proposed advanced flue gas condensate treatment is also proved successful while removing the pollutants up to the concentration levels of parts per billion. The proposed pretreatment step, pH adjustment of MD feeds, enhanced ammonia removal efficiency in all cases. Compared to current practices, the separation efficiencies of the considered MD based processes are improved. The simulation results indicate that the required thermal energy for operating large scale MD systems is readily available via internal waste heat sources of nano-electronics facilities for handling typical volumes of the mentioned wastewaters. In cogeneration plants, district heating supply and return lines are well suited as the heat source and heat sink to manage industrial-scale MD systems effectively. The process economy shows that the unit water treatment cost is mainly constrained by thermal energy cost. In case when the price of heat is considered negligible, the unit water treatment cost is significantly lower than the competing technologies.

Keywords: Membrane Distillation, Experimental investigations, Techno-economic, Wastewater, Flue gas condensate, Waste heat, District heating, Nano-electronics, Cogeneration, Sustainable development

Sammanfattning

Den Europeiska Unionen har lagt högt prioritet på uppfyllelsen av de målen som finns i 2030 Agenda för Hållbar Utveckling. Denna ambition har gett ytterligare fart till medlemsländernas miljöförvaltningar för att strama åt utsläppsnivåer av industriella avloppsvatten. Dessa åtgärder har stor betydelse för existerande förhållningssätt i industrin eftersom många traditionella metoder för rening av avloppsvatten når inte de åtstramade utsläppsnivåerna. Dessutom finns det en uppmaning hos industrin att implementera strategier för noll utsläpp, framför allt för återanvändning av processvatten. Betoningen ligger på förbättrad vattenreningsteknik för återhämtning, återanvändning och utsläpp av vatten på det sättet som skyddar naturresurser, garanterar tuffa miljölagstiftningar och säkerställer ekonomin. I detta sammanhang är membrandestillering (MD) en lovande teknik för rening av avloppsvatten och är kapabel att bemöta dessa krav genom utnyttjandet av låg-temperatur värmekällor.

Denna avhandling fokuserar på experimentella undersökningar och tekno-ekonomiska utvärderingar av spillvärmedrivna MD-system för vattenrening i två vattenintensiva industrier: nano-elektronisk tillverkning och kraftvärmeverk. Vattenprover hämtade från relevanta anläggningar testades i en luftspalt MD rigg i bänkskala och hos en halv-kommersiell pilotanläggning, med fokus på separationsverkningsgrad och möjligheten att nå en hög grad av uppkoncentrering. För den tekno-ekonomiska analysen av ett system i industriellt skal undersöktes prestandan hos den valda halv-kommersiell enhet för att utvärdera drift i fullt skal gällande termiskt energibehov och förväntad kostnad för renat vatten. Olika termiska integreringssätt utvärderades med hänsyn till lokala värmekällor för att tillgodose energibehoven hos det specifika MD-systemet. De valda fallstudierna omfattar: avskiljning av tetrametylammonium hydroxid (TMAH) från fotolitografiska avloppsvatten i nano-elektronisk tillverkning; behandling av kemisk-mekanisk utjämning (CMP) avloppsvatten i nano-elektronisk tillverkning; och uppkoncentrering genom avancerad rening av rökgaskondensat från kraftvärmeverk med hushållsavfall och biobränsle som energikällor.

Resultat från rening av avloppsvatten hos nano-elektronisk tillverkning visade att permeat med hög kvalité kunde åstadkommits med hög separationsverkningsgrad hos de analyserade föroreningarna. Det föreslagna systemet för rening av rökgaskondensat var också framgångsrikt med avskiljning av föroreningar upp till miljarddelar. Förbehandlingen genom pH-justering av råvattnet ledde till förbättrad ammoniak-avskiljning i alla fallstudier. I jämförelse med dagens tekniker fanns det en förbättring med MD-teknik gällande separationsverkningsgrad. Resultaten från simuleringar för nano-elektronisk tillverkning visade att den nödvändiga termiskenergin finns tillgänglig för MD-system i stort skal genom utnyttjandet av intern spillvärme. Hos kraftvärmeverk passar fjärrvärmeledning och –returlinjor bra som värmekällor respektive värmesänka. Processekonomin visar att kostnaden för renat vatten är mest beroende av kostnaden för värmen. I de fall där värmekostnaden är noll ligger reningskostnaden mycket lägre än konkurrerande teknik.

Nyckelord: membrandestillering, experimentella undersökningar, tekno-ekonomin, avloppsvatten, rökgaskondensat, spillvärme, fjärrvärme, nano-elektronik, kraftvärme, hållbar utveckling

Acknowledgements

All the praise be to Allah, the Almighty. Here, first, I would like to thank Him for His continued kindness, favor and blessings which enabled me to reach this level of my education. Though being far from home and living alone for years was a bit hard for me yet the outcome of the endeavor proved more rewarding. Therefore, I collectively count this period of my life as one of the best times, and it was wonderful. Obviously, this became possible with the help, support, guidance, timesharing, and the more, generous cooperation extended by the ones connected to me. I, therefore, want to thank every one of them individually.

I would like to express my sincere gratitude to my principal advisors, Prof. Andrew Martin at KTH Royal Institute of Technology, Sweden and Prof. Olli Dahl at Aalto University, Finland for their continued guidance, support and encouragement throughout the course of my Ph.D. Special thanks to my industrial mentor, Aapo Sääsk (Scarab Development AB) for the enlightening discussions with him throughout my Ph.D. study.

I appreciate the valuable feedback and constructive comments offered by Dr. Daniel M. Woldemariam (Waterapp), Dr. Alaa Kullab (Scarab Development AB) and Dr. Ershad Khan (Xzero AB). I am grateful for the technical support and suggestions from Henrik Dolfe (Scarab Development AB), Jaime Camalich (HVR Water Purification), Miriam Åslin (Xzero AB), Alexander Fornsäter (Xzero AB), Leif Pettersson (KTH) and Göran Arntyr (KTH). Advices and comments given by Jan Coenen (imec), Bo Bängtsson (Bäcken Industrifysik), Andreas Neuber (Applied Materials), Rushikesh Matkar (Intel Corporation), Jan Lundgren (Stockholm Exergi), Mohammad Bisher Kazkaz (Stockholm Exergi) and Sara Sjögren (Stockholm Exergi) have been a great help for the industrial case studies. I take this chance to thank Prof. Massimo Santarelli (Politecnico di Torino) for his feedback and contribution as a co-author in one of the publications.

I want to express my greatest appreciation to Assoc. Prof. Kerstin Forsberg from the Department of Chemical Engineering (KTH) for evaluating the midterm and final seminars and giving valuable feedback on the draft thesis that helped me improve its quality. I am also thankful to Dr. Maryna Henrysson, Dr. Francesco Gardumi and Dr. Jens Fridh from the Department of Energy Technology (KTH) for their constructive feedback on the progress of this research.

I am grateful to the pre-examiners Prof. Wojciech Kujawski (Nicolaus Copernicus University) and Dr. Alessandra Criscuoli (Institute on Membrane Technology, ITM-CNR) for their time in reviewing and evaluating this Ph.D. thesis. Many thanks to my Ph.D. thesis opponent Prof. Mikel Duke (Victoria University) and all the jury members Prof. Corinne Cabassud (INSA Toulouse), Prof. Erik Dahlquist (Mälardalens University) and Prof. Riitta Keiski (University of Oulu) for their participation in the Ph.D. defense.

I would like to acknowledge the Erasmus Mundus Joint Doctoral Programme SELECT+, Swedish Energy Agency, Xzero AB and KTH Royal Institute of Technology for their financial support for the research I conducted. I also would like to express my gratitude to the InnoEnergy organization for providing me a great platform to foster innovation and entrepreneurship skills through the Ph.D. school program. I would like to offer my special thanks to Chamindie Senaratne for facilitating all activities involving SELECT+ mobility and the joint doctoral program issues. I want to express my gratitude to Sirje Liukko for her support in practical and administrative issues related to Ph.D. thesis pre-examination to graduation. I truly appreciate all the staffs in the Department of Energy Technology at KTH and in the Department of Bioproducts and Biosystems at Aalto University who made my stay at the two institutes comfortable and fruitful.

I want to show my appreciation to my colleagues and friends who contributed to my study and personal life in one way or the other. Special thanks to Getnet Tadesse Ayele, Moritz Wegener, Mahrokh Samavati, Manuel Betancourt, Mexitli Eva, Azhar Uddin and all of those who are affiliated with the SELECT+ Ph.D. programme who shared with me their experiences. I deeply thank all my other colleagues and friends at KTH and Aalto University. I owe my deepest gratitude to Komal Khan who has been always there for me with great compassion and support.

My heartfelt appreciation goes to my parents Azhar Iqbal Sheikh and Zahida Jabeen for making me what I am today. Their selfless fatherly and motherly support and encouragement made me explore new avenues and directions in life for seeking my own destiny at its best possible. As a result, it paved the way for me to reach up to here. Without their continuous and unparalleled love, help and support, I could never experience the joy of life. This journey would not have been possible without them, and I dedicate this milestone to them. I am grateful to my lovely siblings, Taal Azhar, Arsalan Azhar Sheikh and Gul Jabeen for being part of my life. I feel extremely lucky to have them in my life. Finally, to my caring husband M. Hussam Khaliq, you are my encouragement and hope.

Imtisal-E-Noor
March 2021, Stockholm

Publications appended to thesis

Journal Articles

I. **Imtisal-e- Noor**, Jan Coenen, Andrew Martin, Olli Dahl and Miriam Åslin, "Experimental investigation and techno-economic analysis of tetramethylammonium hydroxide removal from wastewater in nano-electronics manufacturing via membrane distillation," Journal of Membrane Science, 2019, Volume 579, p. 283-293. https://doi.org/10.1016/j.memsci.2019.02.067.

II. **Imtisal-e- Noor**, Jan Coenen, Andrew Martin and Olli Dahl, "Performance assessment of chemical mechanical planarization wastewater treatment in nano-electronics industries using membrane distillation," Separation and Purification Technology, 2020, Volume 235, 116201. https://doi.org/10.1016/j.seppur.2019.116201.

III. **Imtisal-e- Noor**, Andrew Martin and Olli Dahl, "Techno-economic system analysis of membrane distillation process for treatment of chemical mechanical planarization wastewater in nano-electronics industries," Separation and Purification Technology, 2020, Volume 248, 117013. https://doi.org/10.1016/j.seppur.2020.117013.

IV. **Imtisal-e- Noor**, Andrew Martin and Olli Dahl, "Water recovery from flue gas condensate in municipal solid waste fired cogeneration plants using membrane distillation," Chemical Engineering Journal, 2020, Volume 399, 125707. https://doi.org/10.1016/j.cej.2020.125707.

V. **Imtisal-e- Noor**, Andrew Martin and Olli Dahl, "District heating driven membrane distillation for advanced flue gas condensate treatment in combined heat and power plants," Journal of Cleaner Production, 2021, In press, 125979. https://doi.org/10.1016/j.jclepro.2021.125979.

Author’s Contributions

Paper I: Lead author **IN** performed the literature review, curated and analyzed industrial data, developed the methodology, executed experiments and done techno-economic studies, performed analysis and interpretation of the results, and was the main responsible person for writing the original manuscript. **JC** and **MÅ** were also involved in performing experiments and sample analysis. The roles of **AM** and **OD** included mentoring and reviewing the article.

Paper II: Lead author **IN** performed the literature review, developed the methodology, executed experiments, performed analysis and interpretation of the results, and was the main responsible person for writing the original manuscript. **JC** participated in sample analysis. The roles of **AM** and **OD** included mentoring and reviewing the article.

Paper III: Lead author **IN** performed the literature review, curated and analyzed industrial data, developed the methodology, done techno-economic studies, performed analysis and interpretation of the results, and was the main responsible person for writing the original manuscript. The roles of **AM** and **OD** included mentoring and reviewing the article.

Paper IV: Lead author **IN** performed the literature review, curated and analyzed industrial data, developed the methodology, executed experiments and done techno-economic studies, performed analysis and interpretation of the results, and was the main responsible person for writing the original manuscript. The roles of **AM** and **OD** included mentoring and reviewing the article.

Paper V: Lead author **IN** performed the literature review, curated and analyzed industrial data, developed the methodology, executed experiments and done techno-economic studies, performed analysis and interpretation of the results, and was the main responsible person for writing the original manuscript. The roles of **AM** and **OD** included mentoring and reviewing the article.

Publications not appended to thesis

Peer-reviewed Conference Articles

1. **Imtisal-e- Noor**, Andrew Martin and Olli Dahl, "Membrane distillation - A new approach for treating wastewater in nano-electronics industries," Proceedings of the 31st International Conference on Efficiency, Cost, Optimization, Simulation and Environmental Impact of Energy Systems, June 17-22, 2018, Guimarães, Portugal, Article ID: 462.

2. **Imtisal-e- Noor**, Andrew Martin and Massimo Santarelli, "Exergy analysis of air gap membrane distillation unit for chemical mechanical polishing wastewater treatment," Proceedings of the International Conference on Innovative Applied Energy, March 14-15, 2019, Oxford, UK, ISBN: 978-1-912532-05-6, Article ID: 159.

3. **Imtisal-e- Noor**, Mahrokh Samavati and Andrew Martin, "Modelling and techno-economic analysis of membrane distillation system for flue gas condensate cleaning," Proceedings of the 33rd International Conference on Efficiency, Cost, Optimization, Simulation and Environmental Impact of Energy Systems, June 29-July 3, 2020, Osaka, Japan, ISBN: 978-1-713814-06-1, p. 2132-2140, Article ID: 354.

Peer-reviewed Conference Abstracts

4. **Imtisal-e- Noor**, Andrew Martin and Olli Dahl, "Waste water treatment in semiconductor industry through membrane distillation," 5th International Scientific Conference on Pervaporation, Vapor Permeation and Membrane Distillation, June 20-23, 2017, Torun, Poland.

5. **Imtisal-e- Noor**, Andrew Martin, Miriam Åslin, Jan Coenen and Henrik Dolfe, "Performance of membrane distillation for TMAH wastewater treatment in nano-electronics industries - Case study: imec, Belgium," Ultrapure Micro 2018, May 30-June 1, 2018, Austin, Texas, USA.

6. **Imtisal-e- Noor**, Andrew Martin and Olli Dahl, "PureBlue–Water purification solutions," InnoEnergy PhD School Annual Conference 2018, October 3-5, 2018, Budapest, Hungary.

7. **Imtisal-e- Noor**, Andrew Martin, Miriam Åslin, Jan Coenen and Olli Dahl, "Chemical mechanical planarization wastewater treatment using membrane distillation," Ultrapure Micro 2019, June 5-7, 2019, Phoenix, Arizona, USA.

8. **Imtisal-e- Noor**, Andrew Martin and Henrik Dolfe, "Flue gas condensate cleaning via air gap membrane distillation," International Membrane Science & Technology Conference, February 2-6, 2020, Sydney, Australia.

Method Articles

9. **Imtisal-e- Noor**, Andrew Martin and Olli Dahl, "Process design of industrial-scale membrane distillation system for wastewater treatment in nano-electronics fabrication facilities," MethodsX, 2020, Volume 7, 101066. https://doi.org/10.1016/j.mex.2020.101066.

10. **Imtisal-e- Noor**, Andrew Martin and Olli Dahl, "Evaluation of membrane distillation technology for condensate cleaning in MSW-fired cogeneration plants," MethodsX, submitted.

Nomenclature and Abbreviations

Symbols

A	area, m^2
C	cost, USD
c_p	specific heat, J/kgK
c'	concentration, ppm
$c'F$	concentration factor
d	degression constant
E	electrical power, kW
Ex	exergy flow rate, kW
h	heat transfer coefficient, W/m^{2}K
i	index
J	transmembrane flux, L/m^{2}h
L	lang factor
mw	molecular weight, g/mol
$\dot{m}$	mass flow rate, kg/s
n	lifetime, years
N	number
P	pressure, bar
Q	heat transfer rate, kW
$\dot{Q}$	specific energy, kWh/m^3
r	recovery ratio
R	gas constant, J/molK
T	temperature, °C
U	overall heat transfer coefficient, W/m^{2}K
V	volume, m^3
$\dot{V}$	volumetric flow rate, m^3/h
X	capacity of equipment
z	interest rate, %
ß	number of dissociation species in contaminant
ρ	density, kg/m^3
η	exergy efficiency, %
φ	heat recovery factor
μ	pump efficiency, %
Δ	difference

Subscripts

a	annual
A	atmospheric
c	coolant
cap	capital
CEPCI	chemical engineering plant cost index
CF	contingencies fees
ch	chemical
CO	contractor fees

comp	component of the system
cv	convective heat transfer
DPC	direct permanent capital
des	destruction
el	electrical
eq	equipment
f	feed
HX	heat exchanger
i	inlet
I	insurance
ISBL	inside battery limits
ir	irreversibility
j	contaminant in stream
k	stream in process
L	location
LS	land and site development
m	membrane
mech	mechanical
n	net
o	outlet
om	operating and maintenance
OSBL	outside battery limits
p	permeate
PS	plant startup
r	retentate
rf	retrofitting
R	reference
s	surface
solv	solvent
sys	system
T	total
TCI	total capital investment
TDC	total depreciable capital
TPC	total permanent capital
th	thermal
w	water
WC	working capital
v	vapor

Abbreviations

AGMD	Air Gap Membrane Distillation
CAPEX	Capital Expenditure
CHP	Combined Heat and Power
CMP	Chemical Mechanical Planarization
COD	Chemical Oxygen Demand
CV-AFS	Cold Vapor-Atomic Fluorescence Spectrometry

DCMD	Direct Contact Membrane Distillation
DH	District Heating
ED	Electrodialysis
EDI	Electrodeionization
EPA	Environmental Protection Agency
ICs	Integrated Circuits
IC	Ion Chromatography
ICP-MS	Inductively Coupled Plasma-Mass Spectrometry
ICP-OES	Inductively Coupled Plasma-Optical Emission Spectrometry
imec	Interuniversity Microelectronics Centre
IVL	Svenska Miljöinstitutet (Swedish Environmental Research Institute)
KTH	Kungliga Tekniska Högskolan (Royal Institute of Technology)
LCOW	Levelized Cost Of Water
LEP	Liquid Entry Pressure
MGMD	Material Gap Membrane Distillation
MD	Membrane Distillation
MF	Microfiltration
MEMD	Multi-Effect Membrane Distillation
NF	Nanofiltration
MSW	Municipal Solid Waste
OPMEX	Operational and Maintenance Expenditure
OMD	Osmotic Membrane Distillation
PV	Photovoltaic
PE	Polyethylene
PP	Polypropylene
PTFE	Polytetrafluoroethylene
PVDF	Polyvinylidene fluoride
PFA	Perfluoroalkoxy alkanes
RO	Reverse Osmosis
SDGs	Sustainable Development Goals
SGMD	Sweeping Gas Membrane Distillation
TDS	Total Dissolved Solids
TMAH	Tetramethyl Ammonium Hydroxide
TOC	Total Organic Carbon
TSGMD	Thermostatic Sweeping Gas Membrane Distillation
UF	Ultrafiltration
UNEP	United Nations Environment Programme
UV	Ultraviolet
VMD	Vacuum Membrane Distillation
VMEMD	Vacuum Multi-Effect Membrane Distillation
VOCs	Volatile Organic Compounds
VRF	Volume Reduction Factor
ZLD	Zero Liquid Discharge

Table of Contents

List of Figures

List of Tables

Chapter 1 Introduction

Water is one of the key pillars of sustainable development. However, the continuously increasing world population and changing consumption patterns place extreme pressure on finite, vulnerable water resources. Additionally, the water footprint of the industrial sector continues to grow exponentially in concert with rapid economic development, which puts substantial demand for fresh water supplies. Figure 1.1 shows the projected water scarcity in 2040. According to one estimate, industries account for about 19% of total water extractions [1]. Industries use freshwater in several steps of the particular operations, including fabrication, processing, washing, diluting, cooling, or transporting a product. Moreover, water is also needed in energy utilities, for cooling and space heating. Along with consuming enormous volumes of freshwater, industries also generate wastewater containing contaminants from chemicals used during the production process. As stated in the United Nations Environment Programme (UNEP) Report, 300-400 million tons of heavy metals, toxic sludge, solvents, and other pollutants are released each year from industries, many of which are later discharged to freshwater bodies [2]. This ultimately raises concerns about sustainable development.

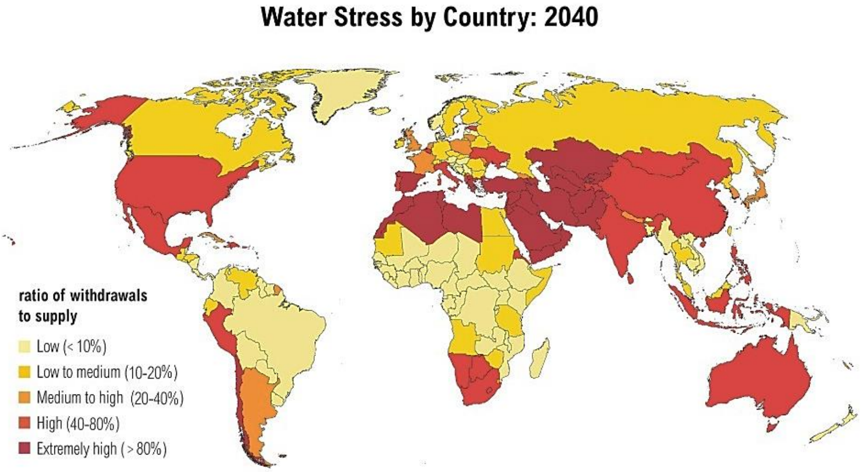

Figure 1.1 Projected water stress in 2040 [3]

According to the United States Environmental Protection Agency (EPA), two of the leading industrial sectors in terms of high water demand are electronics manufacturing and heat and power generation [4]. To put this into perspective: a typical nano-electronics fabrication facility (fab) consumes up to 40 kg of fresh water per cm^2 of silicon processed [5] and solid-fueled power plants (steam-Rankine cycle) require 100 kg of freshwater per kWh electricity [6]. Subsequently, these industries generate a corresponding amount of wastewater, which mainly include metallic, acidic and alcoholic compounds and nano-particles. Strict environmental regulations embodied in UN sustainable development goals (SDGs) 6 (Clean Water and Sanitation), 9 (Industry, Innovation, and Infrastructure) and 12 (Responsible Consumption & Production) mandate the use of advanced pollution controls to realize tightened discharge limits of industrial effluent. Moreover, industries are recommended to adopt a zero liquid discharge (ZLD) approach for advanced water management. In the nano-electronics sector, the focus is to improve wastewater treatment systems for ensuring high environmental performance, along with the reduction of wastewater volumes. In combined heat and power (CHP) plants, the emphasis is placed on advanced methods for flue gas condensate cleaning for the elimination of toxic compounds in effluents, including recovery for boiler make-up water.

Industries have considered various technologies for treating industrial effluents involving either mechanical, electrical or thermal separation. Membrane separation methods are widespread due to their outstanding performance and other favorable traits. The conventional membrane technologies include reverse osmosis (RO), micro-filtration (MF), ultra-filtration (UF), nano-filtration (NF) and pervaporation [7]–[9]. Among them, RO is a proven and well-established technology and is typically considered the core of a water treatment system. However, many fundamental shortcomings are associated with RO based systems which are yet to be overcome [10]. For instance, RO has comparatively higher electrical energy demand to manage high operating pressures. The necessarily-high mechanical load subsequently reduces membrane performance efficiency. Moreover, RO requires harsh pretreatment chemicals for countering bio-fouling on membrane surfaces. Furthermore, RO cannot efficiently handle certain high-concentration feedstocks due to some practical constraints, mainly, limitations associated with higher pressure levels. Additionally, many RO applications struggle with sludge disposal problems, which are required to be resolved by improving the water recovery ratio in order to minimize sludge volumes. Hence alternative membrane techniques are of high interest, which may retain the advantages of the established methods while enhancing robustness, achieving high recovery ratios, reducing electrical energy demand, minimizing chemical requirements, decreasing sludge volumes, diminishing bio-fouling issues, and simplifying process integration.

In this context, membrane distillation (MD) is a promising technology with highly favorable water purification characteristics. MD employs a hydrophobic membrane to allow only water vapor and volatiles (if present) to pass through the membrane pores while leaving behind the dissolved contaminants in the feed solution [11]. The vapor transport is primarily driven by the temperature difference between the feed and permeate sides. The process theoretically provides complete removal of non-volatiles, including cells, metals, ions, macromolecules and colloids. It typically operates at lower temperatures than the conventional distillation and much lower pressure than the RO process [12]. Additionally, MD has other potential advantages compared to RO as follows: (1) improved separation efficiency; (2) higher recovery ratios; (3) reduced fouling issues; (4) lower mechanical stress; (5) less-sensitivity to fluctuating concentration levels; (6) lower electricity demand; (7)

highly concentrated retentate; and (8) reduced capital expenditures. These attributes ensure enhanced performance of MD technology as compared to RO-based alternatives.

Since MD is a thermally driven process, the principal challenge for realizing its industrial applications is linked with high thermal power demand and concurrent operational expenses that limit the technology's commercialization. Nonetheless, a considerable amount of sustainable, affordable and locally derived waste heat is available in numerous industries and can offer MD scope to showcase its potential. To this end, it is also necessary to draw attention to thermal integration with due consideration of thermal energy supply from heat sources along with dissipation to heat sinks for the specific application. Utilization of locally available energy (waste heat) sources for driving an MD system can not only treat wastewater within or beyond the governing environmental regulations but can also enhance sustainability and potentially reduce carbon dioxide emissions for a particular process. This situation results in a dual benefit in terms of ecological aspects.

1.1 Research objectives and questions

The main aim of this research is to introduce and evaluate waste heat driven membrane distillation for industrial wastewater treatment in nano-electronics manufacturing facilities and cogeneration plants. In alignment with the primary aim, the sub-objectives are defined including:

1) Identification of potential wastewater treatment applications of MD technology in nano-electronics industries and cogeneration plants, and thorough understanding of the types of locally available waste heat sources applicable to industrial-scale MD based processes;

2) Characterization of single-cassette laboratory-scale and multi-cassette pilot-scale air gap MD facilities in terms of their technical performance for different feedstocks obtained from nano-electronics and cogeneration facilities while varying operating conditions;

3) Techno-economic assessment of thermal integration options for industrial-scale MD systems for effluent treatment in selected industries.

Within the defined scope of the aforementioned aim and sub-objectives, three research questions were posed as follows:

1) What are the separation efficiencies of the MD systems for various contaminants considering the selected wastewaters as feedstocks? Is there a need for any other complementary pretreatment or post-treatment processes for complete separation?

2) What are product yield, specific thermal and electrical energy demand and exergy efficiency, and how is the energy distributed and exergy destroyed by different components of the system?

3) Are the proposed waste heat driven MD systems technically viable and have economic superiority for the industrial effluent treatment compared with existing systems? How do different techno-economic parameters affect the process economy?

1.2 Contributions to state of the art

Taking the above-mentioned research objectives and questions into consideration, contributions of this thesis linked to the appended papers are summarized in Table 1.1.

Table 1.1 Summary of the main contributions of the papers appended in this thesis

	Papers I, II, IV and V
Research topic	Introduction of MD systems in water-intensive industries
Contributions to state of the art	• Exploration of photolithography and chemical mechanical planarization wastewaters treatment as the potential applications for MD technology in nano-electronics facilities • Comparison of flue gas condensate treatment in municipal solid waste incineration and biofuel-fired cogeneration facilities using MD systems • Inspection for required pre/post-treatment steps and determination of potential mechanisms attributed to the separation of contaminants • Yield, energy and exergy analyses of the MD systems for different conditions
	Papers I, III, IV and V
Research topic	Techno-economic system analysis of thermally integrated industrial-scale MD for wastewater treatment in nano-electronics and cogeneration facilities
Contributions to state of the art	• Identification and comparison of locally available waste heat sources applicable for thermal integration with MD in nano-electronics and cogeneration facilities • Process design of thermally integrated industrial-scale MD based systems for particular applications according to the requirements of generic nano-electronics and cogeneration facilities • Economic assessment of thermally integrated MD systems at different scales for retrofitted and new wastewater treatment facilities

1.3 Outline of the thesis

The thesis is divided into six chapters, as follows:

Chapter 1 states the context and motivation for this research work and includes objectives, research questions, a summary of the main contributions to state of the art and an outline of the thesis report.

Chapter 2 provides a review of membrane distillation technology, along with specific industrial applications under consideration.

Chapter 3 presents the methodology of the thesis for performed experimental and techno-economic studies.

Chapter 4 includes the experimental investigation of membrane distillation for the treatment of different wastewaters released from the nano-electronics manufacturing facilities. This chapter also consists of the techno-economic feasibility of locally available waste heat driven membrane distillation for wastewater treatment in nano-electronics industries.

Chapter 5 explores the competitiveness of membrane distillation versus conventional approaches for water recovery from flue gas condensate in municipal solid waste and biofuel-fired cogeneration plants. This chapter also covers the techno-economic system analysis of district heating driven MD for advanced flue gas condensate treatment in cogeneration plants.

Chapter 6 provides a conclusion and future outlook.

Chapter 2 Context and literature review

This chapter provides an overview of the membrane distillation technology, including its industrial applications. Background of the industries under consideration, their wastewater streams and locally available waste heat sources are also presented.

2.1 Membrane distillation

In 1963, Bruce R. Bodell [13] introduced a system based on the air-filled porous hydrophobic membrane for converting the non-portable liquids to drinkable water. However, the research did not publish the membrane geometry and structure and did not quantify the results. Later, in 1967, Peter K Weyl [14] investigated the polytetrafluoroethylene (PTFE) hydrophobic membrane (thickness: 3.2 mm, pore size: 9 mm and porosity: ~ 42 %) to improve the efficiency of water desalination. In the same year, Findley [15] was the first to publish the fundamental principles and outcomes of direct contact membrane distillation. However, in the mid-1980s, with the introduction of highly porous hydrophobic materials, the interest in membrane distillation technology was boosted substantially [16]. Lawson et al. [17], Alklaibi et al. [18], Tomaszewska et al. [16], Drioli et al. [19]–[21], El-Bourawi et al. [22], Alkhudhiri et al. [23], Khayet et al. [24], [25], Wang et al. [26], Thomas et al. [27] and Tibi et al. [28] have presented detailed reviews on membrane distillation (MD), including its development, membrane properties and potential applications. These studies show that MD technology has been investigated at the academic level quite extensively, where publications regarding experimental studies are mostly focused on the development of membrane materials and parametric investigations. However, very few are related to industrial applications of MD technology, although the process has been known for more than forty years.

2.1.1 Working principles

Membrane distillation, a non-isothermal membrane separation process, presents a two-fold barrier during purification: membrane hydrophobicity that provides high recovery ratios with high-quality permeate production; and separation owing to differentiation in the volatility of various contaminants. The term ‘membrane distillation’ is originated from a conventional distillation process modified with membrane separation. The main driving force is the temperature difference across the membrane, which ultimately creates a vapor pressure difference between the feed and the permeate sides of the membrane [23]. The MD feed operating conditions are usually temperature in the range of 50-90°C and ambient pressure [18], [21], [23]. The water transport in the MD system can be summarized in three stages: (1) vapor gap is formed at the interface of hot feed solution and membrane surface; (2) water vapor is transported through the hydrophobic membrane; (3) water vapor is condensed at the interface of cold side membrane and permeate solution [29]. The involved phase separation in the MD process is attributed to the vapor-liquid equilibrium, where the latent heat of evaporation/condensation induces the phase change process [30]. During the process, the latent heat associated with permeate vapor dissipated on the other side of the membrane to the cold stream.

The mass transfer phenomenon in the MD process is governed by three principal mechanisms: Poiseuille flow (viscous flow), Knudsen diffusion and molecular diffusion. Consequently, specific resistances are associated with the momentum transfer to the membrane (viscous resistance), with the membrane itself (Knudsen resistance) and with the collision of molecules (molecular resistance). The concentration boundary layer and surface resistances are usually negligible during the mass transfer phenomenon. In contrast, the thermal boundary layer significantly affects mass transfer in the MD process [20], [23]. Figure 2.1 presents mass transfer resistances in the MD process.

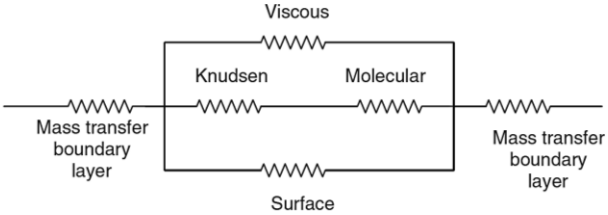

Figure 2.1 Mass transfer resistances in MD [23]

In the MD separation process, heat transfer through the membrane occurs through two parallel mechanisms: latent heat and conduction heat transfer [23], [31]. As a result, different heat transfer resistances are experienced during the heat flow, as demonstrated in Figure 2.2.

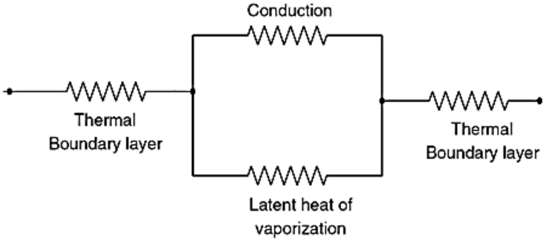

Figure 2.2 Heat transfer resistances in MD [23]

2.1.2 Membrane materials and properties

The primary purpose of the MD membrane is to transport vapor with no wetting and minimal resistance [32]. In this regard, it was found that macro-porous materials with high porosity and open-cell pore structures with low tortuosity help to mitigate vapor transfer resistance [33]. Thus, the product flux is directly proportional to the porosity and pore size; however, it is inversely proportional to the tortuosity and membrane thickness. Moreover, the temperature polarization effect is linked to the thermal conductivity of the membrane material. By increasing the porosity and pore-size, the thermal conductivity of the membrane is reduced due to the air captured inside the polymer matrix. This leads to a reduction in conductive heat transfer through the membrane. On the contrary, the convective heat transfer associated with the transmembrane flux increases across the membrane**.** Furthermore, high hydrophobicity, small pores and high tortuosity contribute to the anti-wetting properties [32], [34]. Therefore, for an effective MD application following properties of the membrane material are suggested [33], [34]:

1. Moderately small pore size (0.1-1µm)
2. High porosity (80-90%)
3. Low tortuosity factor (1-3)
4. Adequate chemical, thermal and physical resistance
5. Reasonable liquid entry pressure (LEP, 2.5 bar) and contact angle (>105°)
6. Long term stability
7. High heat transfer and low mass transfer resistances
8. Reduced thickness (10-200 µm)

Considering these properties, polymeric materials are generally used owing to their low cost and ease in manufacturing [28]. (Presently, membranes composed of ceramics, metals and carbon nanotubes are also under consideration for this purpose [35]–[38].) Commonly applied membrane materials are polytetrafluoroethylene (PTFE), polyethylene (PE), polypropylene (PP), polyvinylidene fluoride (PVDF), and perfluoroalkoxy alkanes (PFA) [39]–[44].

Hollow fiber and flat-sheet membrane geometries are traditionally used in MD modules [26], [42], [45]. The hollow fiber module has a very high packing density. It has a large membrane active area with a compact structure that makes it favorable for commercial usage. On the other hand, plate and frame modules can easily be constructed and cleaned, but they have lower packing density than the hollow fiber modules [46]. However, the active membrane area can be increased while introducing layers of flat-sheet MD membranes. The damaged membranes are readily detachable in the flat-sheet modules; therefore, it is widely employed for both laboratory and industrial-scales applications [42].

2.1.3 MD module configurations

Apart from different membrane geometries, there are also various primary module configurations that can be categorized based on the way of vapor condensation in the permeate side. Figure 2.3 and Figure 2.4 present different primary and modified types of MD module configurations.

- In direct contact membrane distillation (DCMD), the hot feed is in direct contact with the feed side of the membrane, and vapor passing through the membrane condenses on the cold permeate side inside the module. DCMD gives a considerably high permeation flux with low energy efficiency, a drawback linked to heat losses due to conduction. [21], [41], [47].

- In air gap membrane distillation (AGMD), the hot feed is in direct contact with the membrane, but stagnant air is introduced between the membrane and condensation surface to reduce the heat loss. The vapor condenses on the cold condensation surface. Due to the air gap, additional mass transfer resistance is experienced in this structure. [23], [34], [48].

- In sweeping gas membrane distillation (SGMD), the cold, inert sweeping gas is introduced at the permeate side, which reduces the heat loss and enhances the mass transfer coefficient. Condensation of water vapors takes place outside the membrane module. The drawback involves in this configuration is the diffusion of a small volume of permeate in a high volume of sweep gas. [34], [49].

- In vacuum membrane distillation (VMD), a pump is used to form a vacuum at the permeate side, whereas the condensation happens outside the module, and heat loss is insignificant due to conduction. However, a high risk of pore wetting is associated with VMD configuration [32], [34], [48].

- In thermostatic sweeping gas membrane distillation (TSGMD), a combination of AGMD and SGMD is considered. Here, sweep gas is introduced in the air gap between the membrane and condensation surface. Vapors are partially condensed on the condensation surface inside the membrane module as in AGMD and partially on the external condenser as in SGMD [25], [50].

- In material gap membrane distillation (MGMD), different materials, e.g., polyurethane or polypropylene, can be introduced in the air gap to overcome the inherent disadvantage of AGMD (lower permeation flux due to stagnant air). It can be observed from the literature that the permeation flux rate is increased by 200-800 % [51].

- In osmotic membrane distillation (OMD), the concentration gradient across the membrane is owing to the stripping solution at the permeate side. The permeate is continuously drawn by the stripping solution. The OMD process is isothermal and operates at a much lower temperature (nearly ambient temperature) than conventional MD configurations [11].

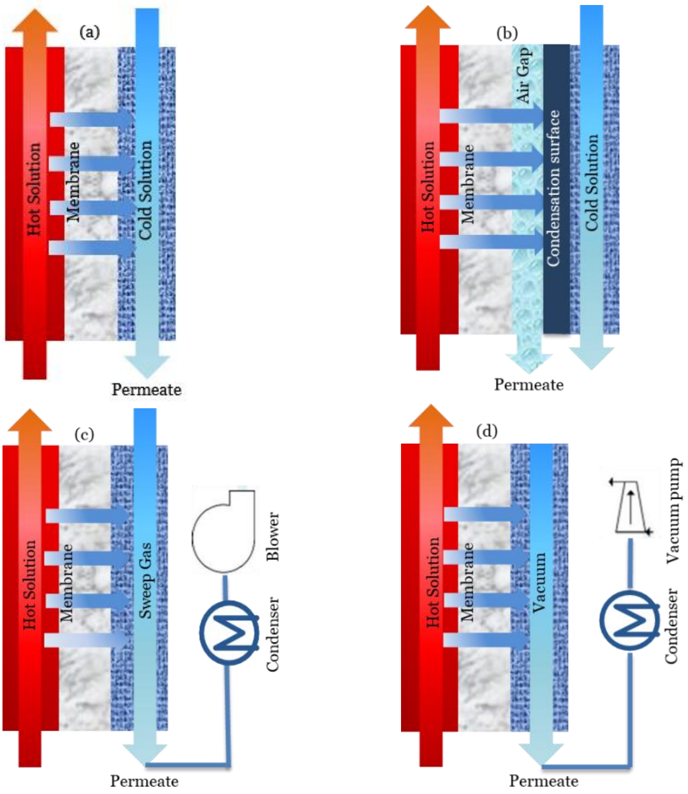

Figure 2.3 Four primary MD configurations a) DCMD, b) AGMD, c) SGMD, d)VMD

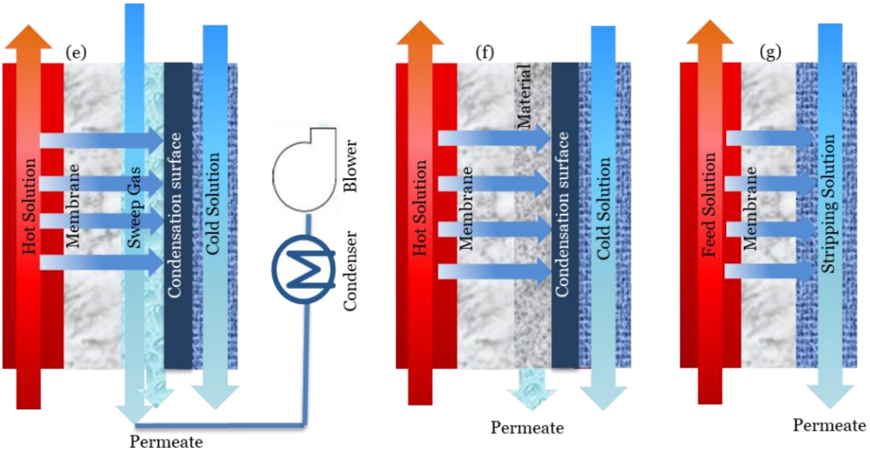

Figure 2.4 Modified MD configurations e) TSGMD, f) MGMD, g) OMD

2.1.4 Integrated MD module configurations

For providing the required driving force to produce and transport permeate vapors, most single-stage MD modules have a thermal energy demand of around 1200 kWh/m^3 with associated gained output ratios of less than unity [24]. (Gained output ratio can be defined as a ratio of latent heat of evaporation associated with transmembrane flux to the input thermal energy of the MD system.) The thermal performance of the MD system can be improved when the concept of internal heat recovery is adopted while adding stages in series (cascading), employing thermal storage to recover surplus energy, using concentrate recycle loops, or recovering dissipated heat. Therefore, extensive work has been done to introduce multi-effect membrane distillation (MEMD) configuration, which involves the heat recovery system that gives better thermal efficiencies. MEMD usually considers primary MD configurations (DCMD and AGMD) combined with an internal heat recovery system. In these configurations, the GOR values can be increased up to 20 [52]. It is claimed by Memstill® after pilot trails that only 56-100 kWh/m^3 has been consumed while using spiral-wound design [53]. The concept of Scarab Development AB (Sweden) includes the plate and frame design, and with a single-module thermal energy demand was 600-1000 kWh/m^3 [47], [54]. Memsys designed a vacuum multi-effect membrane distillation (VMEMD) configuration that follows the comparable model as MEMD except for high vacuum utilization. This VMEMD uses a plate and frame module and involves multiple evaporator-condensation stages with an external heater and condenser. Memsys claimed it to consume specific thermal energy of 175-350 kWh/m^3 with GOR of up to 3.6 [42], [55], [56]. The reported specific electrical energy demand of MD systems typically varies from 0.3-3 kWh/m^3 depending upon MD feed flow rates and different system configurations [54], [57]. Figure 2.5 shows an example of a vacuum multi-effect membrane distillation configuration, and Table 2.1 presents commercial MD modules.

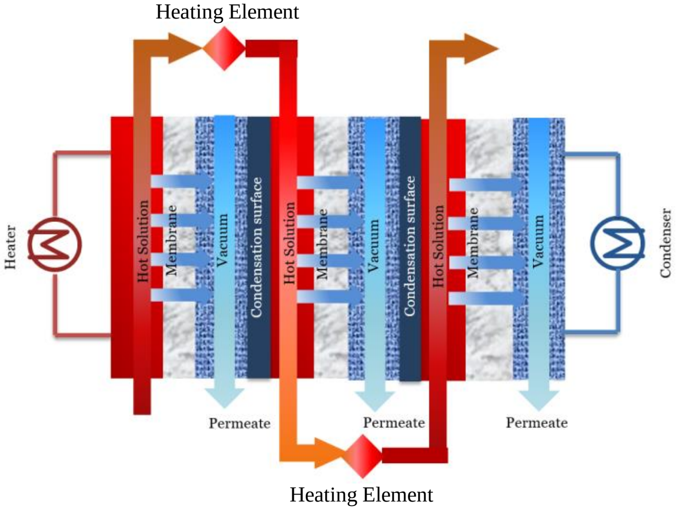

Figure 2.5 VMEMD configuration (adapteded from [29])

Table 2.1 Commercial MD systems [27]

Technology developer	Technology/system	MD configuration and membrane geometry
Scarab Development AB, Sweden	Xzero system	AGMD (flat-sheet)
Solar Springs GmbH, Germany	A spin-off from Fraunhofer Institute for solar energy systems	AGMD (spiral-wound)
TNO, Netherlands	Memstill promoted by Aquastill, Keppel Seghers and Bule Gold technologies	DCMD and AGMD (spiral-wound and flat-sheet)
Memsys GmbH, Germany	Licensed to Aquaver. New Concept Holdings Limited acquired assets of Memsys in 2016	VMEMD (flat-sheet)
KmX Corporation, Canada	Aqua-sep^{TM} technology	VMD (hollow-fiber)

2.2 Potential low-grade heat sources

MD operates at lower temperatures, yet it has comparatively higher thermal energy demand than other membrane techniques. Therefore, it is instructive to couple MD with the inexpensive low-grade heat sources for fulfilling the thermal energy requirement of the operation while making the technology sustainable, environmentally friendly and profitable [12], [58]. Potential low-grade heat sources for thermally integrated MD systems include solar energy, geothermal energy and waste heat.

2.2.1 Solar energy

For the last few decades, solar-powered MD systems are the most investigated integrations for desalination purposes where different MD module configurations were considered, including DCMD, AGMD and VMEMD [59], [60]. Different geometries of solar collectors have been employed for this purpose: flat plate [60]–[63]; evacuated tube [59], [64], [65]; compound parabolic [60], [65]; solar still and solar pond [66]–[68]. These solar collectors can either be connected with MD via a single loop or two loops [61], [69]. In some studies, along with solar thermal collectors, photovoltaic (PV) panels are also integrated with the MD systems to provide electrical energy for the pumps and other usages [61], [69], [70]. The examined solar-powered MD plants have a capacity of few liters per day to 10 m^3/day where the heat is supplied at low temperature (50-85°C) [59], [62], [69]. The reported levelized cost of water (LCOW) ranged from 5-85 \$/m^3 when solar-powered MD systems were used [27], [71]. For small-scale application and remote areas, solar-powered MD systems are quite competitive to comparative technologies; however, its commercialization for industrial applications is very limited due to low flux, large collector area requirement and the intermittent nature of solar radiation.

2.2.2 Geothermal energy

In contrast to solar energy, there is a negligible daily or seasonal shift associated with a geothermal energy source; however, it is quite variable depending upon the geographical location. There are very few studies that presented the concept of either geothermal energy driven MD system or MD for geothermal water purification using DCMD, AGMD and VMD [72]–[75]. Geothermal energy driven MD systems are specified for the locations where geothermal fields are present, and there is a need to obtain potable water and/or water for crop irrigation (due to critical water shortage and contaminated available water). The temperature range for geothermal energy can be between 40-95°C. The considered locations include Cerro Prieto in Mexico, Momotombo in Nicaragua and Lake Poopó in Bolivia [72]; Ranau, Sabah in Malaysia [73]; Masson Greenhouse in New Mexico [74] and Tunisian geothermal springs [75], [76]. Considering warm geothermal water can save up to 95% of the total energy consumption of the MD system [73]. The LCOW can be between 0.50-130 $\$/m^3$ when the plant is operated with geothermal energy [24], [27].

2.2.3 Waste heat

Waste heat may be present in different forms, but the key source of waste heat is hot streams from power generation and industrial processes. Waste heat is broadly defined as a form of sustainable energy, and its temperature ranges between 50–800°C [77]. Various waste heat sources are identified in the literature to fulfill the thermal energy requirement of the MD system. These waste heat sources include heat recovery chiller water [78], boiler blowdown, steam diverted from bleed streams and cooling water system stream [79], diesel engine exhaust [80], cooling tower blowdown [81], district heating [54], [82] and exhaust flue gas/sanitized sludge in biogas plant/anaerobic membrane bioreactor [83]–[86]. Moreover, hybrid sources, i.e., combined solar energy and waste heat sources, are also investigated to operate MD systems [87].

The concept of waste heat driven MD systems has been used by most of the main companies in the market. Pilot and commercial MD projects have considered AGMD and VMEMD modules with the flat sheet, hollow fiber and spiral wound membrane geometries. The reported LCOW is 0.26-5.5 $\$/m^3$ [24], [27]. The comparison among different low-grade heat sources depicts that waste heat sources can be more reliable, environmentally friendly and inexpensive. Table 2.2 summarizes waste heat sources driven pilot and commercial MD projects.

Table 2.2 Waste heat driven pilot and commercial MD projects [27], [42].

Executing company	Location	Capacity (m^3/day)	Waste heat sources
Keppel Seghers (2006)	Rotterdam, Netherlands	0.5–1	2 bar steam from the coal-fired power plant
Keppel Seghers (2008)	Rotterdam, Netherlands	0.5–1	Incineration plant
Keppel Seghers (2011)	Jurong Island, Singapore	100	Tempered water
XZero (2011)	Hammarby Sjöstadsverk, Sweden	1-2	District heating network
Scarab Development (2011)	Nyköping, Sweden	1–2	District heating network
Aquaver, Memsys Clearwater (2012)	Senoko Power Plant, Singapore	50	Boiler blowdown from the refinery
Aquaver (2013)	Kamperland, Zeeland, Netherlands	1.5	Diesel generator
Aquaver, Memsys Clearwater (2014)	Kunfunadhoo Island, Maldives	100	Diesel generator
Aquaver, Memsys Clearwater (2014)	Gulhi Island, Maldives	10	Diesel generator
Abengoa Water (2016)	Ghantoot, United Arab Emirates	60	Diesel generator
Global MVP/Econity (2013-2018)	South Korea	400	Partial energy requirement met by using MD brine as a draw solution for pressure-retarded osmosis energy generation

2.3 MD applications

Membrane distillation can be employed in a variety of applications such as seawater desalination, wastewater treatment from chemical industries and concentration of non-volatile compounds. Different MD configurations were used commercially for water purification purpose which includes DCMD, AGMD and VMEMD [42], [47], [54], [55], [88].

MD is considered as a competitive technology for desalination of seawater and brackish water [23], [42], [69]. For the removal of small molecules and heavy metal ions, MD gives a higher water recovery ratio compared to RO, NF and electrodialysis (ED) [89]. It has been reported that boron contaminated water can be purified with rejection efficiency greater than 99.5% [90]. Nickel can be recovered from electroplating wastewater by increasing concentration more than 100-fold using MD [91]. Other heavy metals, for example, arsenic [72], [92], zinc [93], chromium [93] and gold [94], can also be removed entirely from the contaminated water.

It is also found that MD is favorable for the treatment of polluted water with radioactive substances [95], [96]. Moreover, MD has the potential to treat the oily water/produced water from the industries [97]–[99]. MD process can also be considered for the removal of inorganic matters like ammonia [100]–[102] and halogenated volatile organic compounds (VOCs) [103]–[105].

Mineral acids (hydrochloric acid [106], [107], sulfuric acid [108], [109]), fruit juices [110]–[112], sugar [113] and alcohol [114]–[116] can be concentrated either in the permeate stream or in feed stream depending upon the volatility and vapor pressure of the components. MD can also be used for the concentration of natural food colorants [117] and de-alcoholization of wine [118]. MD showed a high rejection percentage (>99%) for all dairy components while concentrating skimmed milk and whey processing [119].

Furthermore, MD is a promising technique in the field of pharmaceuticals, where it can be used as a waste concentration method. Low-level pharmaceutical contamination in wastewater can be removed with the help of this separation technique [54], [120]. Anti-inflammatory, topical anesthetic, analgesic, and antihistamine medicines such as ibuprofen, dibucaine, acetaminophen, and diphenhydramine, respectively, were reported to be concentrated through MD with carbon nanotube immobilized membranes [120]. The textile industry is another sector where the MD separation technique could treat wastewater with a high recovery rate. The successful treatment of synthetic feed solutions containing dyes and salts was shown in previous works where chemical oxygen demand (COD) removal was better through MD than RO and NF [121], [122].

In the nano-electronics industries, MD was considered for supplying ultrapure water from freshwater [78]. However, more complex wastewater streams were not investigated using the MD process. There are also some preliminary experimental studies where MD was employed in the power industry for flue gas desulfurization wastewater treatment [123], concentrating cooling tower blowdown [124], [125] and for flue gas condensate cleaning [126]–[128]. It was observed that particles and heavy metals could be separated successfully; however, ammonium could not be readily managed, which needs to address further.

Based on the previous record of MD applications and current requirement of advanced wastewater management in water-intensive industries, the following industrial case studies are selected and included in this work as potential MD applications:

- Treatment of wastewater released from Interuniversity Microelectronics Centre (imec), Belgium: Nano-electronics manufacturing employs various specialty chemicals, thus necessitating wastewater treatment. This case study determines the feasibility of MD separation technology for the treatment of challenging wastewaters released from nano-electronics fab and identifies locally available waste heat sources required for MD operation. Research campaigns include experiments and techno-economic system analysis. The findings are presented in Chapter 4.

- Water recovery from flue gas condensate released from Stockholm Exergi cogeneration facilities, Sweden: The concept involves replacing multistep RO based flue gas condensate treatment with MD based technology. Högdalen and Brista CHP facilities are considered as examples for municipal solid waste incineration and biofuel-fired cogeneration plants, where along with the removal of non-volatile contaminants, ammonium separation was also studied. The detailed experimental investigation and district heating driven MD system analysis for this case study are discussed in Chapter 5.

The additional background information about selected industries, their wastewaters and locally available thermal energy sources has been described in sections 2.4 and 2.5.

2.4 Nano-electronics industries: wastewater and waste heat

In 1958 Jack Kilby, from Texas Instruments labs, was the first person to publish a patent on the fundamental principles of integrated circuits (ICs) manufacturing. Following then, fabricating transistors on a silicon wafer became a practice to manufacture ICs [129]–[131]. The fabrication method of these ICs is quite complicated, as described in Figure 2.6.

1. In the first step, a high-purity silicon ingot is created, which is further divided into the silicon wafers of 200-300 mm diameter.
2. In the second step, these silicon wafers are coated with a silicon dioxide film, and then a dopant is diffused to modify its electrical features. Following that, layers of desired conducting/insulating materials are deposited on the top of the doped silicon substrate, depending upon the application.
3. In the next step, the wafer surface is coated with photoresist. Later on, the circuit pattern is printed on the device's specific zones using photolithography technology. In this method, a photomask is employed to project a particular ICs pattern on the wafer by exposing the photoresist to ultraviolet (UV) light. The weakened/soluble photoresist is then removed using a developer solution.
    - After that, a plasma stream is used for etching the pattern trace to eliminate materials and chemically reactive free radicals. The etching process typically helps produce vertical profiles necessary for the minuscule features in today's densely packed chip designs.
    - Following plasma etching, a photoresist stripper is employed to remove the residual photoresist. These steps are recurred 30-40

times to create several layers of circuits, with zonal connections via bonding pads during the metallization process.

4. Afterward, the entire wafer is covered with a finishing layer of the conductive material to protect the circuit from contamination and damage. Eventually, a combination of chemical etching and free abrasive polishing is used to smoothen the wafer surfaces. The fabricated chips are later diced and tested before packaging.

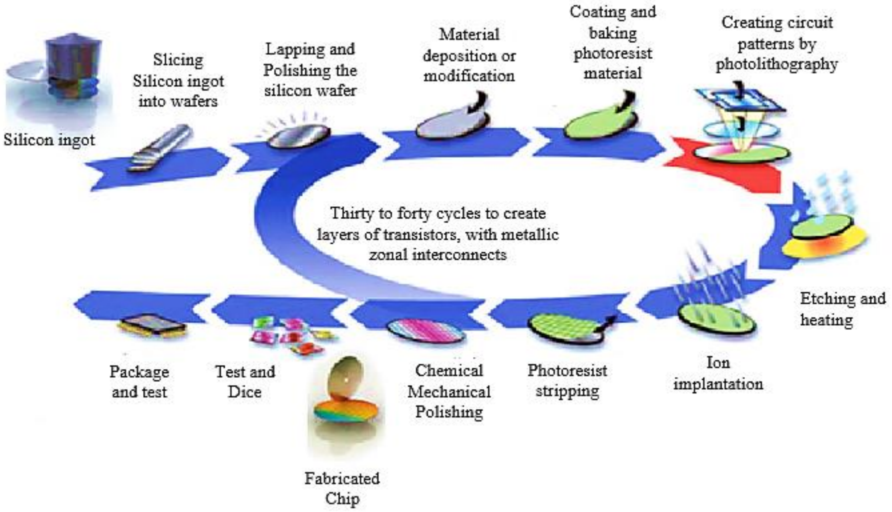

Figure 2.6 Semiconductor chips manufacturing process steps in nano-electronics industries (adapted from [132])

Such a complicated fabrication method includes numerous chemical inputs, resulting in the generation of several wastewater streams. In a typical nano-electronics fabrication facility (fab), approximately 0.4 Mm^3 of freshwater is required annually [133], [134]. Consequently, the nano-electronics manufacturing units generate an enormous volume of wastewater from many processes, including silicon growth, crystal production, oxidation, doping, dicing, ion implantation, photolithography (etching and stripping), metallization, chemical mechanical planarization (CMP), washing and cleaning [130], [135]–[137]. The mentioned processes need more than 200 types of various inorganic and organic compounds (proprietary and generic); thus, the wastewaters primarily comprise of metallic, acidic and alcoholic compounds and nano-particles [138]. According to the predefined standards set by local and international environmental regulatory authorities, these complex wastewater streams need to be treated before discharge to the recipient water bodies or reuse as process water. Table 2.3 presents the key wastewater generation processes in nano-electronics facilities.

Table 2.3 Key wastewater generation processes and the associated contaminants in nano-electronics facilities

Process	Contaminants	References
Metallization	Copper (Cu), chromium (Cr), lead (Pb), nickel (Ni), iron (Fe), magnesium (Mg), calcium (Ca), sodium (Na) and zinc (Zn)	[139]–[141]
Photolithography (Etching and Stripping)	Nitric acid (HNO_3), hydrofluoric acid (HF), tetramethylammonium hydroxide (TMAH) ($C_4H_{13}NO$), acetic acid (CH_3COOH), hydrogen peroxide (H_2O_2), ammonium hydroxide (NH_4OH), phosphoric acid (H_3PO_4) Isopropyl alcohol (C_3H_8O), dimethyl sulfoxide (C_2H_6OS), dimethyl disulfide ($C_2H_6S_2$), N-methyl-2-pyrrolidinone (C_5H_9NO), sulfuric acid (H_2SO_4), methyl diglycol ($C_5H_{12}O_3$) and trace amounts of toluene (C_7H_8) and acetone (C_3H_6O)	[142]–[149]
CMP	Silica (SiO_2), alumina (Al_2O_3), ceria (CeO_2), copper (Cu), ferric nitrate ($Fe(NO_3)_3$), potassium permanganate ($KMnO_4$), aminotriazole ($C_2H_4N_4$), hydrochloric acid (HCl), potassium hydroxide (KOH), nitric acid (HNO_3), oxalic acid ($C_2H_2O_4$), ammonium hydroxide (NH_4OH), polyethylene glycol ($C_{2n}H_{4n+2}O_{n+1}$) and biocides	[150]–[153]

The metallization process wastewater can be successfully treated by the traditional chemical separation process (ion-exchange), usually adopted to handle nano-electronics sewage. However, the photolithography and CMP wastewaters are only partially managed by conventional treatment methods. Researchers have investigated several techniques, including electrochemical and filtration methods, for the purpose (details are available in Chapter 4). These techniques have their merits, but they do not prove sufficient due to their fundamental issues. Therefore, many nano-electronics fabs simply accumulate their wastewaters for expensive off-site thermal destruction. Hence, there is a high interest in exploring novel approaches for the inexpensive and environmentally friendly handling of industrial effluent. MD can be a promising technology for the purpose.

Along with the wastewater treatment issue, there are also various waste heat sources available in nano-electronics industries that need to be taken care of to improve the resource efficiency of the nano-electronics fabs. These sources include [154]–[160]:

1. Condenser outlet water from chillers (temperature range: 35-90° C; thermal power: 3.5-12 MW)
2. Exhaust air from VOCs combustion abatement systems (temperature range: 350-400°C; thermal power: 0.25-0.5 MW)
3. Process cooling water from manufacturing tools (temperature range: 35-90° C; thermal power: 2.5-3.5 MW)
4. Spent stripper (sulfuric acid) from photoresist stripping and spent etchant (phosphoric acid) from nitride etching (temperature range: 90-200°C; thermal power: 0.5-1 MW)
5. Dissipated heat from steam generators, compressors and pumps (widely distributed temperature range)

Usually, the total amount of waste heat released from the typical nano-electronics facilities is about 35–40 MW [78]. Recovery of this waste heat can not only increase energy efficiency but also reduce CO_2 emissions.

2.5 Cogeneration plants: flue gas condensate and district heating

In 1882 Thomas Edison's Pearl Street Station in the United States was the first power plant to apply the concept of combined heat and power (CHP) generation [161]. Since then, CHP (also known as cogeneration) systems have been widely adopted to produce electricity and valuable thermal energy using an integrated approach. CHP facilities employ various fuels, including natural gas/oil, coal, biomass, or waste, to provide thermal energy to the system. There are principally three different thermodynamic cycles that are considered for CHP systems [162]:

1. Rankine or steam cycle where water is used as a working fluid that passes through four stages process including adiabatic/isentropic compression; isobaric heat addition (superheated steam formation); adiabatic/isentropic expansion (power generation); and isobaric heat rejection (heat recovered). The Rankine cycle is mostly considered for steam turbine-based CHP systems.
2. Brayton or Joule cycle where air/gas is considered as a working fluid. It mostly runs as an open cycle and generally follows the same stages as the Rankine cycle. Brayton cycle is typically opted for gas turbine-based CHP systems.
3. Otto cycle or Diesel cycle considers gas as a working fluid. In the Otto cycle, gas sequentially passes through adiabatic/isentropic compression, isochoric heat addition, adiabatic/isentropic expansion and isochoric heat release. For the Diesel cycle, the heat addition stage is isobaric instead of isochoric. These cycles are typical in the case of internal combustion engines.

For large-scale CHP plants, the steam turbine-based process is the most common one, whereas, for small-scale systems, gas turbines and engines are considered. Figure 2.7 shows the schematic of a typical steam turbine-based CHP facility where the process starts with the steam formation in a steam boiler. The steam passes through a turbine, which runs an electric generator. The exiting exhausted steam from the turbine is further sent to the condenser where the waste (useful) thermal energy is recovered (for district heating purpose). An economizer is typically installed to reduce energy consumption by preheating water prior to the steam boiler. To satisfy environmental regulations, ash is collected and disposed. In contrast, flue gas passes through the cleaning process to minimize airborne emissions of heavy metals, particulates, dioxins, nitrogen oxides and acid gases [163]. The clean flue gas is further directed to the stack.

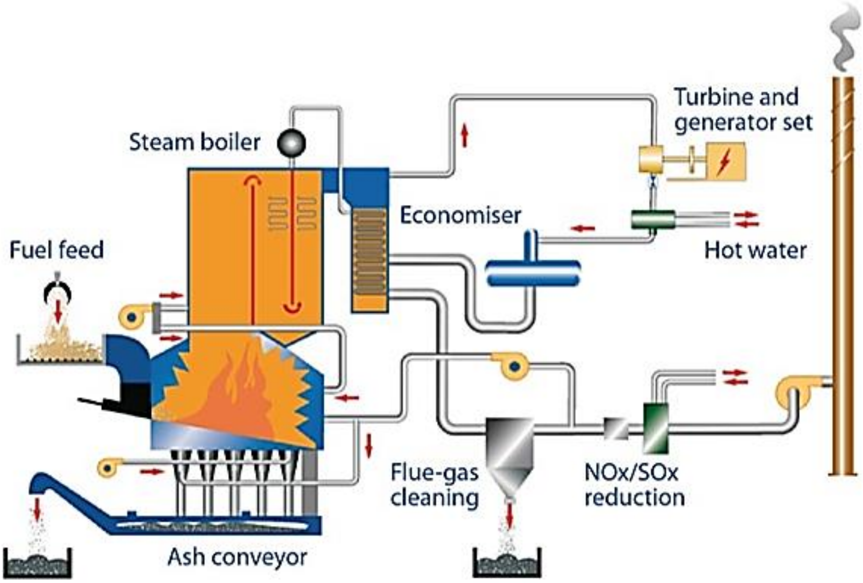

Figure 2.7 Cogeneration process steps in a steam turbine-based CHP facility [163]

Wet scrubbing is the most used flue gas cleaning process where high dew points encountered in the flue gas condensation system lead to thermal energy recovery for district heating (DH) or local heating along with water recovery [164]. The resulting flue gas condensate involves an aqueous mixture of salts, acids, heavy metals, and various particulate solids [165]. Series of membrane separation processes are typically considered for flue gas condensate treatment (details are available in Chapter 5) before its release into recipient water bodies; however, the existing techniques are insufficient to satisfy strict environmental regulations. Moreover, the concept of water reclamation as boiler feed water needs careful advancement in the water management system.

Electricity generated by CHP facilities is usually supplied to regional or national grids with immediate uptake. In contrast, the supply of thermal energy to DH systems is strongly dependent upon local customer demand, which is seasonal. Based on seasonal variance, DH temperature levels differ considerably; higher atmospheric temperature level demands lower DH temperature levels. Usually, the temperatures of DH supply lines differ from 70°C in the summer to 100°C in the winter, whereas the DH return lines temperatures range from 35 to 65°C correspondingly [166], [167]. In Sweden, more than half of the net heating demand of the residential sector was fulfilled by DH systems in 2017 [168]. Moreover, there are various industries where DH applications are commercial, such as food processing plants, electronics industries, forestry industries, steel and metal processing plants, vehicle manufacturing industries, beverage industries, pulp and paper industries, chemical industries, pharmaceuticals industries, and cogeneration facilities [169].

Chapter 3 Methodology

The present work includes feasibility studies of waste heat driven MD systems for wastewater treatment in different industries, namely nano-electronics fabs and cogeneration facilities. Extensive experimental investigations, large-scale system simulations and techno-economic analyses were performed for all the considered applications. A laboratory prototype and a semi-commercial MD system were employed to carry out experimental work. The separation efficiency of major contaminants was considered the critical performance factor, whereas other standard water quality parameters were also determined. Moreover, the effect of parametric variation on product yield, specific energy demand and exergy efficiency was examined in detail. Based on the findings of experimental work and input from considered industries, potential thermal integration strategies were identified, and large-scale integrated MD systems were simulated considering material and energy balances. Process economy analysis aims explicitly at finding out the optimal integration option in the view of unit water treatment cost, as an essential economic criterion.

For simplification, some particular aspects were not covered in the thesis: fouling/scaling problems of the membrane, methods for membrane regeneration, and concentrate disposal issues. Moreover, seasonal variations were neglected while considering district heating as a heat source/sink. Handling of continuous wastewater flow was not investigated experimentally, and long term studies were not considered due to limitation of equipment availability. Finally, suggested post-treatment options were not experimentally verified.

3.1 Experimental setups

Figure 3.1 a and b demonstrate the considered experimental facilities for this study: 1) Xzero laboratory prototype, and 2) Xzero pilot plant. (The Xzero pilot plant was built in a joint project between IVL Swedish Environmental Research Institute and KTH Royal Institute of Technology.) Both facilities consider air gap MD modules and employ PTFE membranes (with PP as back support material); however, their dimensions and other characteristics differ. Table 3.1 summarizes the features of them.

The design of the Xzero laboratory prototype is based on an earlier design [82] with some adjustments (imperative for MD application for ultra-high purity water production). The method for membrane attachment with the cassette is replaced to beam clamping and PTFE sealing to cope with higher pressures on the membrane and avoid leakages. Donaldson® membrane has been selected instead of Gore® admitting its attractive cost-performance comparison. Aluminum condensation plates are coated with the PVDF layer on the permeate side to provide improved permeate quality while resolving corrosion problems and providing an inert environment. The air gap is reduced, and flow spreaders are introduced to the cassette for improved mass transfer.

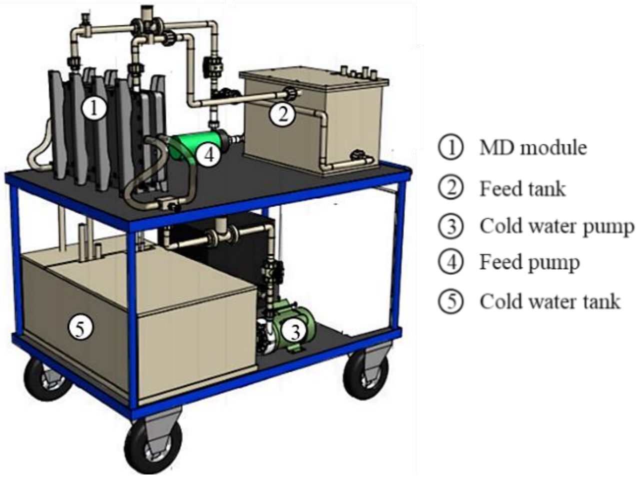

(a)

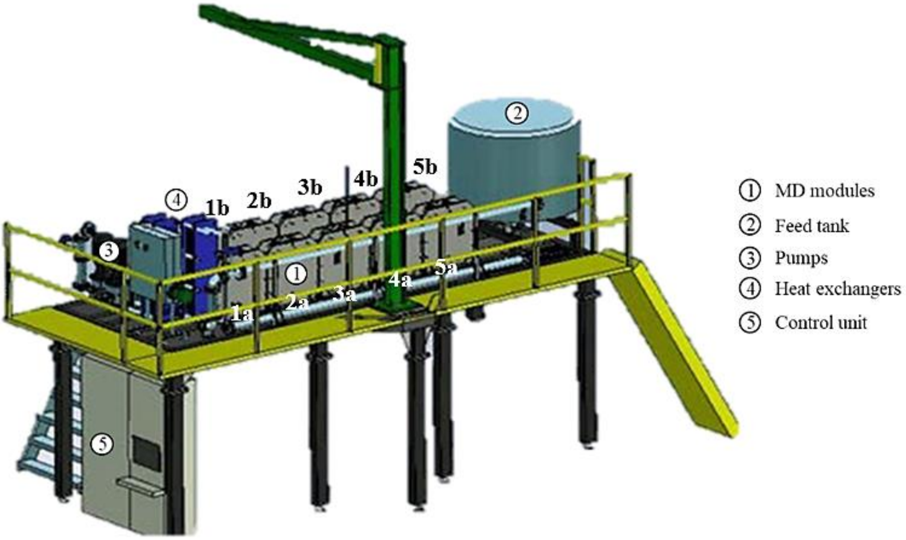

(b)

Figure 3.1 Membrane distillation experimental facilities a) Xzero laboratory prototype b) Xzero pilot-scale unit

Table 3.1 Features of considered AGMD units

Features	Xzero laboratory prototype	Xzero pilot plant
Number of cascades and configuration	1	5, in parallel
Number of modules each cascade	1	2, in series
Module width×height×thickness (cm^3)	55×40×16	63×73×17.5
Number of cassettes per module	1	10
Cassette material	PE	PP
Number of membranes each cassette	2	2
Membrane geometry	Flat-sheet	Flat-sheet
Membrane attachment method with cassette	Beam clamping and PTFE sealing	Thermal welding and O ring sealing
Membrane manufacturer	Donaldson®	Gore®
Membrane area per module (m^2)	0.194	2.3
Membrane thickness (mm)	0.254	0.2
Pore size of membrane (μm)	0.2	0.2
Porosity (%)	80	80
Liquid entry pressure (kPa)	345	368
Air gap (mm)	0.5-1	1
Condensation plate material	PVDF coated aluminum	PP
Feed water tank material	PVDF	Steel
Feed water tank volume (L)	30	900
Total capacity (L/hr permeate)	1-2	100-200
Immersion heaters capacity (kW)	2	24 (in addition DH)
Chiller capacity (kW)	1.8	-
Thermocouple type	PT-100	PT-100
Flowmeters	FIP flowX3 (paddlewheel)	Rotameters
Pumps supplier	Iwaki Sverige AB	Grundfos AB
Control system	Crouzet PLC	Citect Runtime SCADA and Melsoft
Modules supplier	Xzero AB	Xzero AB
Module installed	Xzero AB and imec	Hammarby Sjöstadsverk

Figure 3.2 displays the flow diagram of the AGMD process considered in the experimental facilities mentioned above. The system is separated into the feed side (hot side) and permeate side (cold side) through a hydrophobic membrane. The feed water is heated and recirculated in the feed channel of the module, with cold-water employed as a coolant in condensation plates. The higher temperature on the feed side is responsible for forming vapor in the main feed channel. The temperature difference across the membrane creates a vapor pressure gradient, which helps transport the vapor to the opposite side of the membrane. Following this, the vapor passes through a thin, stagnant air layer before condensing on a cold surface. The vapor condensation is primarily associated with heat dissipation to the coolant,

following the cold surface. The clean permeate is gravity fed to the bottom of the modules and collected into sample bottles. Various sensors and control systems are installed to regulate the process and ensure proper operation to meet safety standards. Figure 3.3 illustrates the exploded view of the AGMD cassette for a visual representation of the process.

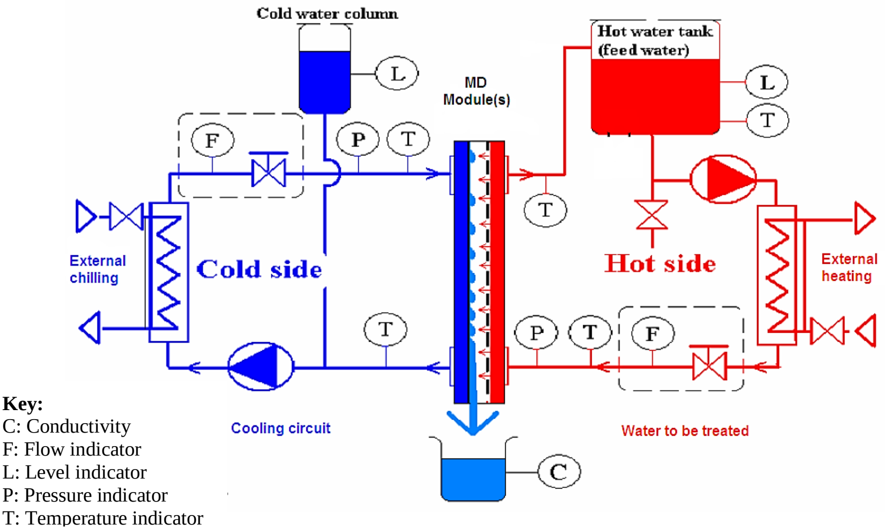

Figure 3.2 Schematic flow diagram of AGMD separation process

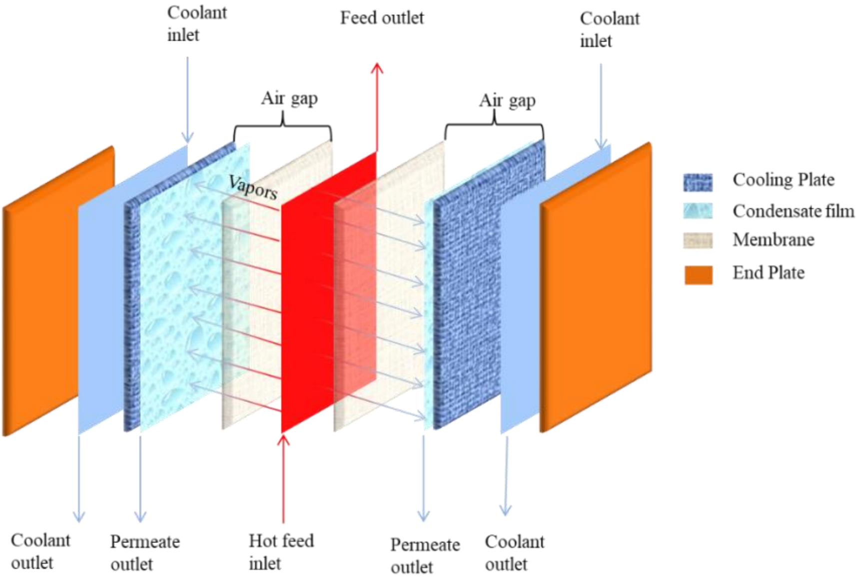

Figure 3.3 Exploded view of AGMD cassette

3.2 Experimental methods and system analyses

The experimental studies were carried out in two parts (I and II). In part I, wastewaters from nano-electronics facilities (imec, Belgium) were employed during tests. In contrast, in part II, experiments were executed using flue gas condensate samples from cogeneration facilities (Stockholm Exergi-Högdalenverket and Bristaverket, Sweden). During these experiments, temperatures and flow rates have been considered the main variables that affect the performance of MD systems. For a complete understanding of the impact of these parameters, ranges of feed and coolant inlet temperatures, and feed and coolant inlet flow rates were considered. The resultant permeate flow rate and temperature, feed and coolant outlet temperatures and module surface temperature were measured. Apart from experimental studies, complete technical and economic analyses were also conducted to examine the full potential and limitations of industrial-scale thermally integrated MD based processes for considered wastewaters treatment.

3.2.1 Separation efficiency

In both parts, the separation efficiencies of considered equipment at various operating conditions have been investigated for the major contaminants. For this purpose, the feed, retentate and permeate samples were collected in glass bottles (after realizing steady-state), and the following physicochemical analyses were performed: metallic and ionic concentration, conductivity, pH, total organic carbon (TOC), total dissolved solids (TDS), chemical oxygen demand (COD), turbidity, alkalinity and total hardness.

In part I, the analyses were performed in imec chemical laboratories, where several analytical methods have been considered to measure the mentioned water quality parameters. The concentration of metals was examined using inductively coupled plasma-optical emission spectrometry (ICP-OES) from PerkinElmer. The ionic concentration was analyzed with ion chromatography (IC). The conductivity was measured using a WTW LF3000 conductivity meter. The TOC was determined employing Sievers 900 TOC-analyzer, and COD was examined with Hach reagent LCI500. The pH was measured with a combined electrode (Yokogawa FU20) connected to a transmitter (Yokogawa EXA pH-402) with a display. The electrode was installed in the circulation route from the hot water tank before the modules and the pump. The pH was again verified for collected samples using an Orion Star Series meter with Orion Ross half-cell electrode and Ross reference electrode.

In part II, the collected samples were sent to independent laboratories for physicochemical analyses. The methods used for external analyses include inductively coupled plasma-mass spectrometry (ICP-MS) and cold vapor-atomic fluorescence spectrometry (CV-AFS) for determining metals concentrations; IC for measuring Cl^- concentration levels; spectrophotometry for estimating NH_4^+ and NH_3-N concentrations, TOC and COD; gravimetry for TDS; nephelometry for evaluating SO_4^{-2} level and turbidity; and potentiometry, conductometry and titration for measuring pH, conductivity and alkalinity, respectively. The total hardness was calculated by analysis of calcium (Ca) and magnesium (Mg). The accuracy of measurement for different analysis methods is presented in the appendix (Table A1).

It is important to mention that during lab and pilot-scale testing, the employed membranes were not replaced throughout the experimental investigations. However, the membrane distillation systems were washed with tap water to remove any impurities from the testing facilities, when required.

3.2.2 Transmembrane flux and reconcentration study

Along with determining the separation efficiency, transmembrane flux was also measured at different operating conditions. Transmembrane flux ($\mathrm{J_p}$) can be described as collected permeate volume over the elapsed experimentation time ($\dot{\mathrm{V}}_\mathrm{p}$) divided by active membrane area ($\mathrm{A_m}$) and can be determined with eq.1.

$$\mathrm{J_p} = \frac{\dot{\mathrm{V}}_\mathrm{p}}{\mathrm{A_m}} \tag{1}$$

Water recovery ratio ($\mathrm{r_w}$) can be described as a ratio of permeate to feed mass flow rate, as shown in eq.2. This value was used as a base for mass flow rate calculations while considering large-scale applications.

$$\mathrm{r_w} = \frac{\dot{\mathrm{m}}_\mathrm{p}}{\dot{\mathrm{m}}_\mathrm{f}} \tag{2}$$

Where $\dot{\mathrm{m}}_\mathrm{p}$ and $\dot{\mathrm{m}}_\mathrm{f}$ depict the mass flow rates of the permeate and feed, respectively.

During pilot-scale testing, a reconcentration study was also considered to study the MD system performance at different concentration levels and investigate the volume reduction factor of MD feed for the considered pilot-scale MD system. The volume reduction factor (VRF) of MD feed was assessed to determine the degree of feed concentration for the particular experimentation time using eq.3.

$$\mathrm{VRF} = \frac{\mathrm{V_p}}{\mathrm{V_f}} \tag{3}$$

where $\mathrm{V_p}$ and $\mathrm{V_f}$ show the permeate and initial MD feed volumes, respectively. The value of VRF can vary between 0-1

The volume reduction of MD feed leads to the concentration of contaminants. The concentration factor ($\mathrm{c'F_j}$) of the contaminants in MD feed can be described as a ratio of contaminant concentration in the retentate to contaminant concentration in the initial feed, as presented in eq.4.

$$c'F_j = \frac{c'_{j,r}}{c'_{j,f}} \tag{4}$$

where $c'_{j,r}$ shows the concentration of contaminant j in retentate and $c'_{j,f}$ depicts the concentration of component j in initial feed water (makeup water).

3.2.3 Energy analysis

Together with separation efficiency, thermal energy demand is another crucial aspect that is usually considered when determining the potential of large-scale MD systems for industrial applications. MD system involves latent heat transfer across the membrane that causes the change in enthalpy of the hot stream (feed) and cold stream (coolant). Enthalpy changes in the feed (Q_f) and coolant (Q_c) streams were calculated using eqs.5 and 6 to examine the thermal performance of the MD system.

$$Q_f = \dot{m}_f c_p (T_{f,i} - T_{f,o}) \tag{5}$$

$$Q_c = \dot{m}_c c_p (T_{c,o} - T_{c,i}) \tag{6}$$

where $\dot{m}_c$ is the mass flow rate of the coolant stream; $T_{f,i}$ and $T_{f,o}$ are inlet and outlet temperatures of the feed stream while coolant stream inlet and outlet temperatures are represented by $T_{c,i}$ and $T_{c,o}$. The heat capacity of water terms as c_p (4180 J/kgK). (For calculation purpose, it was supposed that the contribution of permeate stream is negligible, i.e. $\dot{m}_f \gg \dot{m}_p$ and $\dot{m}_c \gg \dot{m}_p$.)

The specific thermal energy demand ($\dot{Q}_f$) of the MD system was also estimated in terms of enthalpy change of hot feed per unit volume of permeate produced as a function of time. The specific thermal energy demand can be computed using eq.7.

$$\dot{Q}_f = \frac{\dot{m}_f c_p (T_{f,i} - T_{f,o})}{\dot{V}_p} \tag{7}$$

Moreover, the specific amount of heat transfer to the coolant stream ($\dot{Q}_c$) was also determined using eq.8.

$$\dot{Q}_c = \frac{\dot{m}_c c_p \left(T_{c,o} - T_{c,i}\right)}{\dot{V}_p} \tag{8}$$

It is instructive to define the net thermal energy demand for configurations where other processes can recover the dissipated heat. (For example, heat is supplied by the DH supply line with DH return line used as the heat sink). Eq.9 defines the net specific thermal energy demand ($\dot{Q}_n$) of the MD system as a function of the heat recovery factor.

$$\dot{Q}_n = \frac{\dot{m}_f c_p (T_{f,i} - T_{f,o}) - \varphi \dot{m}_c c_p \left(T_{c,o} - T_{c,i}\right)}{\dot{V}_p} \tag{9}$$

where φ describes the possibility of heat recovery by coolant, φ = 1 when heat can be recovered and φ = 0 for no heat recovery.

The specific amount of heat transfer to the permeate ($\dot{Q}_p$) was calculated with eq.10.

$$\dot{Q}_p = \frac{\dot{m}_p c_p (T_p - T_A)}{\dot{V}_p} \tag{10}$$

where T_p depicts as permeate temperature and T_A defines the atmospheric temperature at the infinity point when considering the module as the reference point.

Additionally, the specific amount of heat transfer from the module surface to the surrounding was evaluated in terms of free convective heat transfer ($\dot{Q}_{cv}$), as presented in eq.11.

$$\dot{Q}_{cv} = \frac{hA_s(T_s - T_A)}{\dot{V}_p} \tag{11}$$

where h is the heat transfer coefficient for free convection (approximately 10 W/m^2K for natural convective cooling by air) and A_s shows the module surface area. T_s denotes the module surface temperature.

Furthermore, specific electrical energy demand for operating feed recirculating pump was also calculated using eq.12 as a function of the flow rate of MD feed and pressure drop across the modules.

$$\dot{Q}_{el} = \frac{\dot{V}_f \Delta P}{\mu \dot{V}_p} \tag{12}$$

where $\dot{Q}_{el}$ presents specific electrical energy demand, ΔP is pressure drop across the modules, μ defines pump efficiency and $\dot{V}_f$ is the volumetric flow rate of the MD feed.

3.2.4 Exergy analysis

Applying only the first law of thermodynamics for evaluating energy utilization overlooks the quality of energy; instead, it only quantifies the energy amount. Therefore, it does not provide the qualitative assessment of heat losses and/or recovery and concentration changes in the AGMD system. However, exergy analysis considers both, first and second laws of thermodynamics for energy accounting and measures the extent of ideality and reversibility of the process. For MD separation systems, exergy is mainly associated with heat and material streams with different compositions and concentrations; therefore, the kinetic and potential exergies are not taken into account. Thus, the total exergy flow rate of an individual stream was calculated as the sum of the chemical and physical (thermal and mechanical) exergies associated with that particular stream, as shown in eqs.13-17.

$$Ex_{k,mech} = \dot{m}_k \frac{(P-P_R)}{\rho} \tag{13}$$

$$Ex_{k,th} = \dot{m}_k c_p \left[(T-T_R) - T_R \ln\frac{T}{T_R}\right] \tag{14}$$

$$Ex_{k,ch} = -\dot{m}_k c'_{solv} RT\ln\frac{c'_{solv}}{\left(c'_{solv} + \sum\frac{\beta_j c'_j}{\rho mw_j}\right)} \tag{15}$$

$$Ex_{k,T} = \dot{m}_k \left[\frac{P-P_R}{\rho} + c_p\,(T-T_R) - c_p T_R \ln\frac{T}{T_R} - c'_{solv} RT\ln\frac{c'_{solv}}{\left(c'_{solv} + \sum\frac{\beta_j c'_j}{\rho mw_j}\right)}\right] \tag{16}$$

$$c'_{solv} = \frac{\left[1000 - \sum\frac{c'_j}{\rho}\right]}{mw_{solv}} \tag{17}$$

$Ex_{k,mech}$, $Ex_{k,th}$ and $Ex_{k,ch}$ represent the mechanical, thermal and chemical exergies of the stream k, respectively. $Ex_{k,T}$ shows total exergy of stream k and $\dot{m}_k$ depicts the mass flow rate of the stream k. Reference temperature and pressure are nominated as T_R and P_R, respectively, P depicts total pressure, mw_j and mw_{solv} represent the molecular weight of contaminant j and solvent, respectively in the stream k, β denotes the number of dissociation species in contaminant j and c'_{solv} represents the solvent concentration in stream k.

Exergy can only be conserved for ideal and reversible processes and consumed or destroyed for real processes due to the definite and indefinite irreversibilities. In the MD system, the irreversibilities are linked with heat losses/recovery and composition/concentration changes. The irreversibility of any component ($Ex_{comp,ir}$) of the MD system can be calculated from the difference between exergy flow rates of inlet ($\sum Ex_{comp,i}$) and outlet ($\sum Ex_{comp,o}$) streams of that component and shown in eq.18.

$$Ex_{comp,ir} = \sum Ex_{comp,i} - \sum Ex_{comp,o} \tag{18}$$

The irreversible exergies associated with each component ($Ex_{comp,ir}$) and the entire process ($Ex_{sys,ir}$) were used to calculate the share of each component of the AGMD purification process towards the exergy destruction of the total system ($Ex_{comp,des}$), as expressed in eq.19.

$$\mathrm{Ex_{comp,des}} = \frac{\mathrm{Ex_{comp,ir}}}{\mathrm{Ex_{sys,ir}}} \times 100 \qquad (19)$$

Second-law efficiency or exergy efficiency determines the effectiveness of energy utilization in the process. The exergy efficiency (η) of the MD system can be described as the ratio of the minimum exergy required (minimum work of separation) to the total exergy input of the system, as shown in eq.20. The minimum exergy required for the MD process is the difference between exergy changes in feed streams and permeate stream exergy.

$$\eta = \frac{\mathrm{Ex_f} - \mathrm{Ex_r} - \mathrm{Ex_p}}{\mathrm{Ex_{sys,i}}} \times 100 \qquad (20)$$

where $\mathrm{Ex_f}$, $\mathrm{Ex_r}$, $\mathrm{Ex_p}$ are the exergy flow rates of feed, retentate and permeate, respectively. The exergy input of the system is denoted by $\mathrm{Ex_{sys,i}}$.

The electric power provided to the system for operating pumps, heater, and chiller was considered a pure exergy flow rate. Exergy analysis offers interesting understandings about the categories, localities, and reasons for losses and helps to achieve the optimum system design.

3.2.5 Performance of scaled-up system

For large-scale processes, the size of the MD system was needed to scale up based on the desired product yield. Here the pilot-scale Xzero MD system was considered as reference. Some assumptions were made including similar separation efficiencies, operating conditions (temperatures and flow rates), and specific performance parameters (transmembrane flux and specific heat demand) as in the base case, for specific applications. The following steps (1-8) show the opted procedure for scale-up.

1. Considering the desired product yield, the total required area of the membranes was estimated while using the reference membrane area and related permeate flow rate, as shown in eq.21.

$$\mathrm{A_{m,T}} = \dot{\mathrm{m}}_{\mathrm{p,T}} \frac{\mathrm{A_m}}{\dot{\mathrm{m}}_{\mathrm{p}}} \qquad (21)$$

where $\mathrm{A_{m,T}}$ and $\mathrm{A_m}$ depict total membrane area and reference membrane area, respectively while $\dot{\mathrm{m}}_{\mathrm{p,T}}$ and $\dot{\mathrm{m}}_{\mathrm{p}}$ are the desired product yield and reference MD permeate flow rate, respectively.

2. The number of required MD modules ($\mathrm{N_T}$) was calculated using a ratio of total to reference membrane areas, as presented in eq.22.

$$N_T = \frac{A_{m,T}}{A_m} \tag{22}$$

3. Further, based on the desired permeate flow rate and recovery ratio per cycle, the total MD feed flow rate ($\dot{m}_{f,T}$) was computed using eq.23.

$$\dot{m}_{f,T} = \frac{\dot{m}_{p,T}}{r_w} \tag{23}$$

4. The total thermal power demand ($Q_{f,T}$) was calculated as a function of the total desired permeate flow rate and specific heat demand, as expressed in eq.24.

$$Q_{f,T} = \dot{m}_{p,T}\dot{Q}_f \tag{24}$$

5. The rate of heat transfer to the coolant stream ($Q_{c,T}$), called as recovered thermal power was calculated in a similar manner using eq.25.

$$Q_{c,T} = \dot{m}_{p,T}\,\dot{Q}_c \tag{25}$$

6. Net thermal power demand was calculated as the difference between total and recovered thermal power, as shown in eq.26 (applicable when heat recovery is possible).

$$Q_{n,T} = Q_{f,T} - Q_{c,T} \tag{26}$$

7. Based on total and recovered thermal power, the required heat exchangers areas (A_{HX}) for large-scale systems were calculated using eq.27.

$$A_{HX} = \frac{Q_X}{U\Delta T} \tag{27}$$

where subscript X = f,T or c,T, U shows the overall heat transfer coefficient (for air: 10 W/m^2K and for water: 250 W/m^2K), and ΔT is the temperature difference between inlet and outlet streams.

8. Based on specific electrical energy consumption for operating feed recirculating pump, the total required electrical power (E_T) for the desired product yield was also calculated using eq.28.

$$E_T = \dot{m}_{p,T}\dot{Q}_{el} \tag{28}$$

Based on the flow rates of streams, commercial water tanks and pumps/compressors were considered to operate the industrial-scale MD system.

3.2.6 Economic analysis

Apart from technical evaluation in terms of system capacity and energy demands, the economic feasibility for large-scale MD plants was also determined. The economic model has been established using the performance of the Xzero semi-commercial AGMD system considering the waste heat/district heating integration along with required economic data from literature and manufacturers. Based on the level of water systems advancement, two scenarios have been considered for economic assessment: new wastewater facilities; and retrofitted facilities. In this work, plant capacity is referred as both, the desired product yield and the flow rate of makeup wastewater.

Capital investment

Total capital expenditure (CAPEX, $\mathrm{C_{TCI}}$) of the new facilities involves total depreciable capital ($\mathrm{C_{TDC}}$), total permanent capital ($\mathrm{C_{TPC}}$) and working capital ($\mathrm{C_{WC}}$), as presented in eq.29.

$$\mathrm{C_{TCI}} = \mathrm{C_{TDC}} + \mathrm{C_{TPC}} + \mathrm{C_{WC}} \tag{29}$$

Total depreciable capital is distributed among direct permanent capital ($\mathrm{C_{DPC}}$), contingencies fees ($\mathrm{C_{CF}}$), insurance ($\mathrm{C_{I}}$), and contractor fees ($\mathrm{C_{CO}}$). Eq. 30. shows that direct permanent capital ($\mathrm{C_{DPC}}$) is the sum of inside battery limits ($\mathrm{C_{ISBL}}$) and outside battery limits ($\mathrm{C_{OSBL}}$) where $\mathrm{C_{ISBL}}$ comprises the equipment cost and installation charges and $\mathrm{C_{OSBL}}$ includes the expenses of administration and storage facilities. $\mathrm{C_{OSBL}}$ is taken as 40% of the $\mathrm{C_{ISBL}}$.

$$\mathrm{C_{DPC}} = \mathrm{C_{ISBL}} + \mathrm{C_{OSBL}} \tag{30}$$

Based on the design stage, $\mathrm{C_{ISBL}}$ was calculated considering the Study (factored) Estimate Method [170]. In this approach, the purchased equipment cost ($\mathrm{C_{eq}}$) was estimated and factored up with the Lang Factor. (The Lang factor is described as a ratio of the installation expenses of a process to the equipment cost) The time effect was managed with the cost index, i.e., the Chemical Engineering Plant Cost Index ($\mathrm{i_{CEPCI}}$). For complementing economics of scale, the system size correction has also been considered, which is related to the overall plant capacity. Eq.31 expresses the chosen approach to estimate total equipment cost considering system size correction and time effect, whereas eq.32 determines $\mathrm{C_{ISBL}}$ considering Lang factor and location index.

$$\mathrm{C_{eq}} = \mathrm{i_{CEPCI}} \left[\sum \left(\frac{\mathrm{X_T}}{\mathrm{X_R}} \right)^{\mathrm{d}} \mathrm{C_{eq,R}} \right] \tag{31}$$

$$C_{ISBL} = C_{eq} L i_L \quad (32)$$

where $C_{eq,R}$ depicts the cost of reference equipment, X_R & X_T shows the reference and total capacity of the equipment, i_{CEPCI} is the value of CEPCI, L= 5.7 is the Lang factor for the fluid processing plant and i_L is the location index and taken as 1.20 for Europe. Moreover, d depicts the degression constant. For MD modules and heat exchangers, its value is 0.8, and for water tanks and pumps, it is equal to 0.667 [171].

Total depreciable capital (C_{TDC}) was calculated using eq.33.

$$C_{TDC} = C_{ISBL} + C_{OSBL} + C_{CO} + C_{CF} + C_I \quad (33)$$

The C_{WC} has been estimated as 8.33% of the C_{OSBL} while total permanent capital (C_{TPC}) includes land and site development costs (C_{LS}), and plant startup cost (C_{PS}). Total permanent capital (C_{TPC}) can be determined using eq.34.

$$C_{TPC} = C_{LS} + C_{PS} \quad (34)$$

Table 3.2 contains some constituents of capital costs that have been used for the economic model.

Table 3.2 Some constituents of total capital investment

Constituents	Cost [171]–[174]
Construction overhead (C_{CO})	15% of C_{eq} and labor cost
Contingency fee (C_{CF})	10% of C_{eq}
Insurance (C_I)	5 % of C_{eq}
Land cost and site development cost (C_{LS})	2 % of C_{TDC}
Plant startup (C_{PS})	10% of C_{TDC}

For retrofitted facilities, the total capital investment (C_{TCI}) only includes equipment, insurance, and retrofitting costs and can be calculated using eq.35.

$$C_{TCI} = C_{eq} + C_I + C_{rf} \quad (35)$$

where C_{rf} is the retrofitting cost, which is assumed as 4% of the total equipment cost.

Equipment cost

Purchased equipment cost includes the cost of MD modules, membranes, heat exchangers, pumps, sensors, security control systems and electrical subsystems. Table 3.3 summarizes the cost of reference equipment.

Table 3.3 Cost of reference equipment

Equipment	Cost
PTFE membrane	90 $/m^2 [172]
Module cost	6100 $/module [54], [175]
Plate and frame heat exchangers	325 $/m^2 [176]
Centrifugal pumps	5500 $/100 m^3/h [177]
Tanks	130 $/m^3/day [178]
Controls, sensors, and sub electrical systems	140 $/m^3/day [178]

The annual capital cost ($C_{a,cap}$) was calculated considering the net present value method where annual interest rate (z) of 5% [179] and plant lifetime (n) of 20 years were used, as shown in eq.36.

$$C_{a,cap} = \left(\frac{z(1+z)^n}{(1+z)^n - 1}\right) C_{TCI} \quad (36)$$

Operating and Maintenance Expenditure

Operating and maintenance expenditure (OPMEX) includes the cost of thermal energy, cooling water, electrical energy, sludge disposal, chemicals, equipment replacement, labor, operating supplies and services, and technical assistance. For calculating the annual operating and maintenance cost ($C_{a,om}$), the annual working period was assumed 8000 hours. The operational and maintenance costs are summarized in Table 3.4.

Table 3.4 Costs of different OPMEX components

OPMEX components	Costs
Thermal energy (DH retail price)	77 $/MWh [180]
Electrical energy	0.09 $/kWh [172], [181]
Service and maintenance	0.033 $/m^3 [172] [71]
Labor	0.03 $/m^3 [172], [178], [179]
Cleaning chemicals	0.0018 $/m^3 [172], [178]
Pretreatment chemical	0.02 $/m^3 [182]
Membrane replacement	15% of the total membrane cost [175]
Brine disposal	0.0015 $/m^3 [183]
Cooling water	0.02 $/m^3 of total cooling water [184]

Unit water treatment cost

Finally, unit water treatment cost (C_w) was estimated as a function of annual capital and operational expenses, and plant capacity, as shown in eq.37.

$$C_w = \frac{C_{a,cap} + C_{a,om}}{\dot{m}_{p,T}} \quad (37)$$

In this study, the permeate flow rate and makeup wastewater flow rate are taken similar; therefore, the same C_w can be associated with both. A sensitivity analysis was also performed to study the effect of various techno-economic factors on C_w. Figure 3.4 shows the total expenditure breakdown for new wastewater treatment facilities.

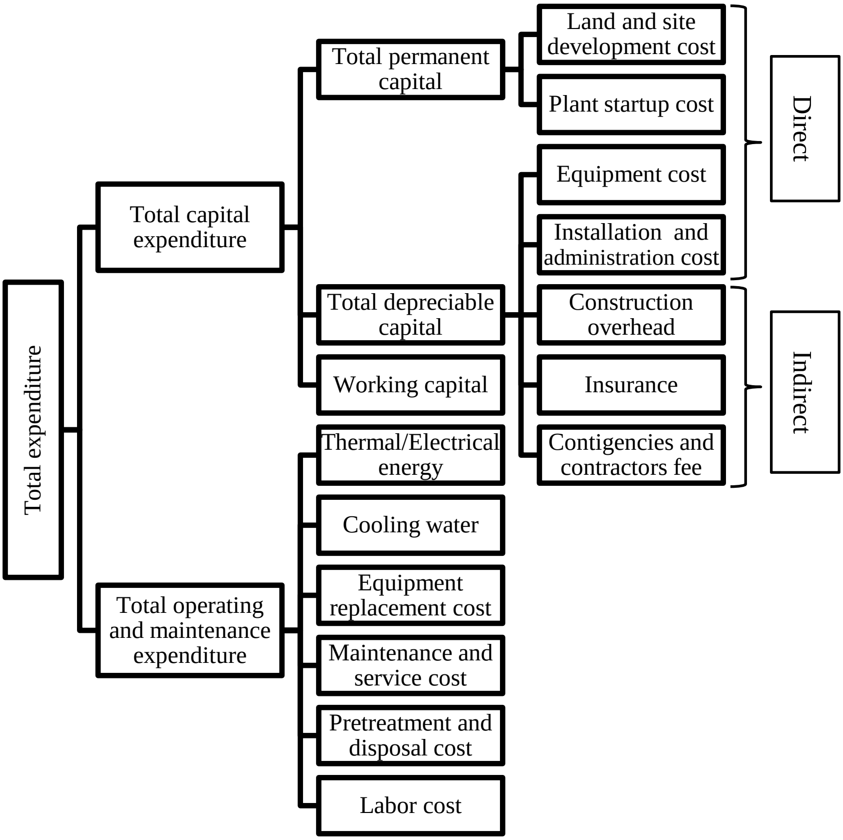

Figure 3.4 Breakdown of total expenditure for new wastewater treatment facilities

Chapter 4 Performance assessment of membrane distillation for wastewater treatment in nano-electronics facilities (Appended articles I, II and III)

In nano-electronics industries, photolithography and chemical mechanical planarization (CMP) are two of the key processes which release significant volumes of complex wastewaters [145], [150]. Based on the nature of the processes, the physicochemical properties of these wastewaters differ. For example, photolithographic wastewater mainly consists of tetramethylammonium hydroxide (TMAH) along with spent etching and stripping chemicals. TMAH, in its pure form, is a non-volatile, highly water-soluble strong alkali (pH ~12) with a thermal decomposition temperature of >65°C [185]. In contrast, the CMP wastewater generally involves nano-sized silica (SiO_2), alumina (Al_2O_3) and ceria (CeO_2) particles, and copper (Cu) with a combination of several chemical additives [151]. The CMP wastewater contains approximately 3-12 % solids by weight, and pH levels range from 6.8-10 [150], [186]–[188]. These wastewaters are highly alkaline and exhibit high corrosivity and acute toxicity. Moreover, they are considered as a source for eutrophication in recipient water bodies. Given this, the current challenge for the nano-electronics industries is to treat these wastewaters properly, according to the stringent environmental regulations. For this purpose, many technologies are explored.

For TMAH wastewater treatment, the list includes electrodialysis, catalytic oxidation, ion exchange, membrane bioreactor, reverse osmosis and biological treatment. Wang et al. [189] presented a combined process of electrodialysis, activated carbon and ceramic filtration for TMAH recovery. The outcomes show that TMAH can be concentrated up to 8%. Huang et al. [190] developed an oxidative degradation system while employing ultraviolet light-activated persulfate. The researchers were able to reduce the TMAH concentration up to 20 ppm. Citraningrum et al. [191] employed weak and strong acid cation resins for TMAH wastewater treatment and showed reasonable performance. Chen et al. [192] presented a combination of membrane bioreactor and reverse osmosis methods, and the outcomes showed that the high-quality water was recovered, with conductivity ~150 µS/cm and TOC ~2.5 ppm. You et al. [193] used membrane photoreactor, anoxic membrane bioreactor, and a combination of both for TMAH removal. The results show that the separation efficiency of TMAH was around 80%. Chen et al. [194] established autotrophic nitrogen removal over nitrite process in an anoxic up-flow bioreactor. The outcomes present that 90% of the total nitrogen was removed. Innocenzi et al. [145] reported the aerobic biodegradation process as a successful option for TMAH wastewater treatment in electronics industries. In this work, 99% of biodegradation was achieved. In a related study, Ferella et al. [195] presented the feasibility of aerobic biodegradation for TMAH wastewater treatment using microorganisms from the local wastewater treatment plant (WWTP).

Among these procedures, biodegradation and catalytic oxidation are the most relevant for today’s nano-electronics manufacturing. However, biodegradation needs comparatively bulky equipment and long residence times for TMAH degradation and leads to N_2O emissions. Moreover, the TMAH biodegradation process begins to inhibit above 150 ppm and may cease around 450 ppm [196]. In contrast, catalytic oxidation is cost-inefficient due to the expensive catalysts. Considering the mentioned issues, nano-electronics facilities usually collect the TMAH wastewater and send it for off-site thermal destruction. Thus, there is a clear need to find novel methods for the environmentally friendly and cost-efficient management of TMAH wastewater.

For handling CMP wastewater, several other treatment methods have been investigated by researchers, involving electrochemical separation, membrane separation, and other methods. Liu et al. [197] demonstrated electro-coagulation for treating CMP wastewater while using Fe electrodes. The results show that at a current density of 5.9 mA/cm^2, the particle separation efficiency was around 99%. Ohanessian et al. [8] tested and simulated dead-end and cross-flow UF and reported that the technique is suitable for CMP wastewater treatment when the silica nanoparticles concentration is less than 100 ppm. Juang et al. [9] used a combination of UF and RO for CMP wastewater treatment, which showed that high-quality permeate having conductivity ~6 µS/cm, turbidity ~0.01 NTU and TOC ~1.6 mg/L can be obtained. Hu et al. [198] reported the effective removal of surface-modified silica nanoparticles using micro-bubbles flotation (assisted with Dodecyl dimethyl betaine). Other methods for CMP wastewater treatment involve the magnetic seeds to improve aggregation and precipitation of silica nanoparticles. Kim et al. [199] examined the combined effect of chemical coagulation and magnetic separation on CMP wastewater treatment using 1.5 g/L magnetite and 0.2 g/L ferric chloride. The results showed that turbidity could be reduced up to 0.94 NTU. Ryu et al. [200] applied magnetite aggregation and sedimentation in the magnetic field to remove the silica nanoparticles. The researchers showed that 97% of silica could be separated using 16 ppm of magnetite.

The methods above have shown great potential in specific applications; however, fundamental challenges are preventing their widespread adaptation. Electro-coagulation has the issue of reduced treatment efficiency due to electrode blockage and also has high electrical energy demand. UF shows a severe problem of membrane blockage due to inorganic and organic fouling/scaling. RO membranes require high mechanical strength and are susceptible to biofouling (that demands to be handled using harsh chemicals). Moreover, the RO process demands relatively high electrical energy for operation. The magnetic seeding aggregation is cost-inefficient due to expensive magnetic seeds. Hence, these methods are unreliable, energy inefficient, and costly.

Considering these constraints, membrane processes are assessed as the most promising techniques assuming that the following aspects can be addressed adequately: reduced electrical energy demand, lower pretreatment requirements, minimum fouling propensity, and cost-efficiency. In this respect, MD is a promising technology that can treat the considered wastewaters in a more ecological and economical manner. To date, no study has investigated MD technology for TMAH and CMP wastewater treatment.

This chapter presents the potential applications of MD technology for wastewater treatment in nano-electronics industries where water recovery and reconcentration are achievable goals. The investigation includes experimental studies and energy and exergy analyses for complete technical evaluation. Moreover, the feasibility of the industrial waste heat driven large-scale MD systems was determined for wastewater treatment in nano-electronics facilities.

4.1 Technical performance of Xzero laboratory prototype

This section highlights the technical performance of the Xzero laboratory prototype when TMAH and CMP wastewaters are used as MD feedstocks. Some of the outcomes in terms of separation efficiencies, product yield, energy demand and exergy efficiencies are presented in sections 4.1.1. and 4.1.2. Detailed information can be found in [201], [202].

4.1.1 Separation efficiency

Wastewater from photolithography process

At the imec facilities, the photolithography process typically releases 200-300 L/h of TMAH wastewater, which is finally accumulated in the collection tank. The TMAH wastewater sample (550 L) was taken from the collection tank and later analyzed, which included mainly TMAH (646 ppm), ammonium hydroxide (1409 ppm), hydrogen fluoride (158 ppm) and hydrogen peroxide (3000 ppm). Since TMAH wastewater contains hydrogen peroxide (H_2O_2), so in the first pretreatment step, 175 g of 60µm mesh powdered manganese dioxide (MnO_2) was added in the sample for catalytic reduction of H_2O_2. The sample was continuously mixed, and the reduction rate was observed over time. (The concentration of H_2O_2 was measured with Quantofix peroxide test strips.) This step was completed in eight hours. After the first step, the pretreated sample (350 L) was filtered to separate the MnO_2 catalyst and then sent for the second pretreatment step, pH adjustment, to avoid ammonia slip. In this step, a total of 572 mL of 98% sulfuric acid (H_2SO_4) was added in steps for 110 minutes, and the pH reduction was determined. Finally, the acidified TMAH wastewater sample of 15 L was pumped in the MD feed tank of the Xzero laboratory MD system. The MD experiments were conducted for different MD feed inlet temperatures, i.e., 60˚C, 65˚C, and 70˚C. The feed, retentate and permeate samples of 0.5 L were collected and examined, and the concentrate volume was also assessed to estimate the volume reduction of TMAH wastewater.

Figure 4.1 shows the schematic diagram of the employed TMAH wastewater treatment system.

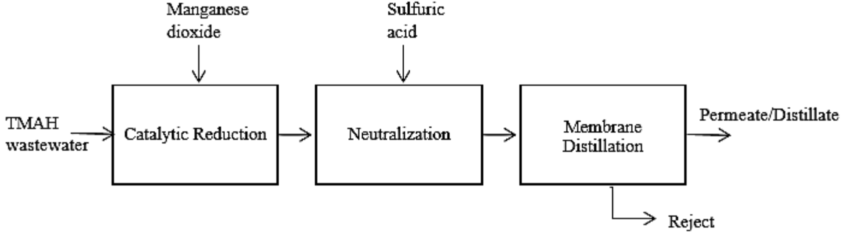

Figure 4.1 Schematic diagram of proposed TMAH wastewater treatment system

Figure 4.2 presents the effect of the addition of manganese dioxide on hydrogen peroxide reduction over time. It was found that more than 95% of H_2O_2 was catalytically reduced during the operation and converted into the H_2O and O_2 gas. (Foaming at the surface of TMAH wastewater and downward displacement of the wastewater was noticed). It was also seen that the trend exhibits an exponential decrease of H_2O_2 concentration level after each MnO_2 intake, which gradually stabilized over time. Eqs. 1 and 2 show the observed reduction reactions:

$$\mathrm{MnO_2 + 2H_2O_2 \rightarrow MnO_2 + O_2 + 2H_2O} \quad (1)$$

$$\mathrm{2H_2O_2 \rightarrow O_2 + 2H_2O} \quad (2)$$

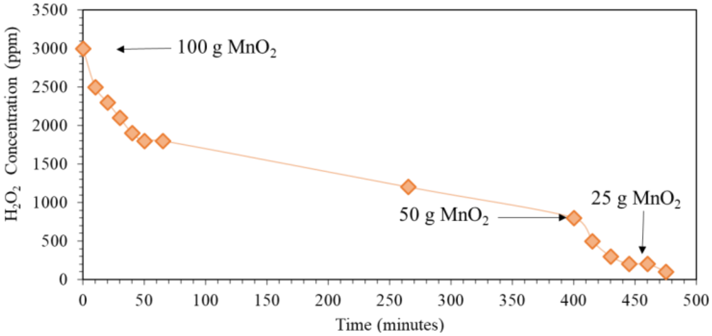

Figure 4.2 Effect of Catalytic reduction on hydrogen peroxide concentration as a function of time

The collected TMAH wastewater sample also includes NH_4OH and HF, whose equilibriums are considerably affected by changing pH and temperature levels. At higher pH levels, NH_4OH equilibrium is directed towards NH_3 gas, which is very likely to pass through the membrane at elevated feed temperatures. In order to avoid the NH_3 slip, acid neutralization is performed as pretreatment. Consequently, the pH value of the TMAH wastewater sample was reduced to 2.94 linked to the pKa value (3.18) of HF, while considering the Henderson-Hasselbach relation. With pH reduction, the desired NH_4OH equilibrium was achieved, where the NH_3 (volatile) was converted to NH_4^+ ions (nonvolatile). Eq. 3 shows the reversible equilibrium reaction of NH_4OH [203].

$$\mathrm{NH_3 + H_2O \rightleftarrows NH_4{}^{+} + OH^{-}} \qquad (3)$$

In parallel, the chemical equilibrium of HF (mentioned in eq. 4) has been directed from F^- ions (nonvolatile) to HF gas (volatile) that may release from the TMAH wastewater sample at elevated temperature.

$$\mathrm{H^{+} + F^{-} \rightleftarrows HF} \qquad (4)$$

Table 4.1 presents the results of physicochemical analyses of the TMAH wastewater sample, pretreated wastewater samples at room temperature and after heating at 60 °C, and permeate samples at different feed temperatures. It was noticed that after acid neutralization, the concentration of sulfate (SO_4^{-2}) ions was increased significantly in the pretreated TMAH wastewater due to the addition of H_2SO_4. Moreover, the nitrite (NO_2^-) ions were created and appeared in the wastewater owing to the oxidation of NH_4OH while the TMAH wastewater was stored in the collection tank. In contrast to the pretreated sample, the hot feed (preheated TMAH wastewater after pretreatment) sample showed a higher concentration of TMAH. The reason might be a higher water evaporation rate at elevated temperatures. However, at higher temperatures, the marginal degassing of HF gas was also observed.

Considering MD treated permeates, the concentration of NH_4OH and TMAH was reduced to an acceptable level. Moreover, the levels of analyzed metals, NO_2^- and Na^+ ions, and H_2O_2 were below the detection limits. However, the concentration of F^- ions in the permeate samples was considerably high, i.e., 125-147 ppm. The reason was the presence of highly volatile HF gas in hot MD feed, which was passed through the membrane to the permeate side. Other ions, including SO_4^{-2}, Cl^- and NO_3^- have quite low concentration. It is noteworthy that manganese (from catalyst MnO_2) did not appear in the permeate samples. While analyzing the MD performance at different feed temperatures, the results show that elevated temperatures lead to slightly enhanced separation efficiency due to improved driving force (vapor pressure difference) and, in some cases, owing to enhanced solubility. While analyzing the carbon content in permeate samples, no definite trend was noted with varying temperatures, which indicates that the thermal decomposition of TMAH was not observed. Nevertheless, it is known that TMAH thermal decomposition temperature is above 65°C; hence, for TMAH wastewater treatment, the recommended MD feed temperature is ≤ 65°C. The other water quality parameters were also studied and presented in [201].

During the reconcentration study, the achieved wastewater volume reduction factor was ~0.7 after eight hours of the MD separation process. The obtained permeate quality satisfies most local environmental standards for discharge to the recipient, except for F^- ions concentration. To handle F^- ions concentration, using strong base anion resin/activated alumina can be a favorable approach before disposal or reuse of the permeate as process water [204], [205].

Table 4.1 Concentration of contaminants in 1) real TMAH wastewater sample, 2) wastewater sample after catalytic reduction (CR) and acid neutralization (AN) and 3) pretreated wastewater sample after heating at 60°C and 4) permeate samples after the MD separation process while varying the wastewater temperature. ('<' indicates a value below the respective detection limit).

Contaminants	Units	TMAH wastewater	Pretreated wastewater	Pretreated wastewater after heating at 60°C	After CR + AN + MD		
					Trial 1	Trial 2	Trial 3
					Permeate, 60°C	Permeate, 65°C	Permeate, 70°C
H_2O_2	ppm	8000	<100	<50	<50	<50	<50
Al	ppm	0.1	0.1	0.3	<0.0004	<0.0004	<0.0004
Cr	ppm	<0.002	<0.002	<0.002	<0.002	<0.002	<0.002
Cu	ppm	0.3	0.1	0.1	<0.004	<0.004	<0.004
Zn	ppm	0.7	0.1	0.1	<0.002	<0.002	<0.002
F^-	ppm	158.1	162	150.5	124.2	133.5	147
Cl^-	ppm	12.3	10.4	11.6	0.1	0.1	0.1
NO_2^-	ppm	9.8	<0.05	<0.05	<0.05	<0.05	<0.05
NO_3^-	ppm	37.4	80.4	80.3	1.1	0.6	0.4
SO_4^{-2}	ppm	28.3	3529.7	3731.3	201.7	11.5	9
Na^+	ppm	1.2	0.6	0.7	<0.05	<0.05	<0.05
K^+	ppm	15.6	7	7.2	0.3	0.1	0.1
NH_4^+	ppm	1409.5	895	980.8	4.7	3.9	3.5
TMA^+	ppm	646.1	637.5	732.6	1.6	1.2	1
pH		10.55	2.94	2.89	2.81	2.81	2.80
TOC	ppm	8	9.2	9.4	1.2	0.8	1.4

Wastewater from chemical mechanical planarization

A total of 100 L of CMP wastewater was collected in five 20 L samples from imec, Belgium, during ten days (some variation in composition was inevitable owing to the changes in upstream trials). Samples 1, 2 and 3, were employed to examine the separation efficiency of the Xzero laboratory prototype for various conditions. Considering that concentration does not significantly affect the parametric study, the other two samples were used to study the permeate yield and energy requirement. The MD experiments (focused on determining the separation performance) were performed in two steps: i) no pretreatment using sample 1 (S1), and ii) with pretreatment while employing samples 2 and 3 (S2 and S3). In this case, acid neutralization was considered the only pretreatment where 0.5 mL of 40% H_2SO_4 was added per L of collected samples before their introduction into the MD modules. The proposed CMP wastewater treatment process is presented in Figure 4.3.

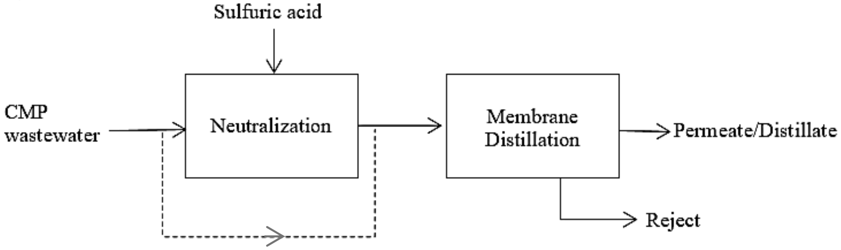

Figure 4.3 Schematic diagram of the proposed CMP wastewater treatment system

Samples S1, S2 and S3, were employed in Test 1, Test 2 and Test 3, respectively. These tests were performed at constant feed and coolant flow rates of 7.2 L/min and 8.3 L/min, respectively. The other operating conditions were as follows: the feed inlet temperature of 85°C for S1, 80°C for S2 and 75°C for S3; coolant inlet temperature of 35°C for S1, 30°C for S2 and S3; and elapsed time of 3h. Fluid flow conditions determine that average flow channel velocity was in a range of 0.025-0.055 m/s, assuming a U-type flow pattern from inlet to outlet. This condition corresponds to a Reynolds number range of 800-2500. The feed, retentate and permeate samples of 0.5 L were collected and examined, and the volume reduction was also determined.

Table 4.2 summarizes the physicochemical analysis of MD feed and the resulting permeate samples. In CMP wastewater samples, the primary metallic contaminants were silicon (Si), aluminum (Al), and copper (Cu), as anticipated. Along with these contaminants, phosphorus (P) was also in high concentration. It was also noticed that in all CMP wastewater samples, ionic concentration of NH_4^+, K^+, and PO_4^{-3} was high, while except S1, the other two samples (S2 and S3) also have a significantly high concentration of SO_4^{-2} ions owing to the neutralization step. The obtained permeate samples of S1, S2 and S3 were named D1, D2 and D3, respectively.

Table 4.2 The concentration of ionic and metallic contaminants in MD feed water samples and permeate samples (elapsed time of three hours) in three tests. (‘<’ indicates a value below the respective detection limit.)

Contaminants	Units	Test 1		Test 2		Test 3	
		S1	D1	S2	D2	S3	D3
Al	ppm	9.9	<0.0004	0.64	<0.0004	1.23	<0.0004
Ca	ppm	0.254	0.001	0.36	0.005	0.25	0.006
K	ppm	10.82	<0.01	10.69	<0.01	15.9	<0.01
Fe	ppm	0.025	<0.001	0.39	<0.001	0.02	<0.001
Ni	ppm	0.057	<0.005	0.034	<0.005	0.017	<0.005
Cu	ppm	3.5	<0.004	4.9	<0.004	3.05	<0.004
Zn	ppm	0.054	<0.002	0.048	<0.002	0.006	<0.002
P	ppm	3.9	<0.04	2.73	<0.04	9.04	<0.04
Ge	ppm	0.06	<0.01	0.014	<0.01	<0.01	<0.01
W	ppm	0.022	<0.01	<0.01	<0.01	<0.01	<0.01
Ti	ppm	<0.04	<0.04	<0.04	<0.04	<0.04	<0.04
Si	ppm	95.16	<0.1	6.4	<0.1	0.27	<0.1
Ta	ppm	0.271	<0.01	<0.01	<0.01	0.062	<0.01
NH_4^+	ppm	16.6	12.4	26.57	<0.05	30.2	<0.05
F^-	ppm	<0.05	<0.05	<0.05	<0.05	0.087	<0.05
Cl^-	ppm	1.3	<0.05	1.1	<0.05	5.9	<0.05
NO_3^-	ppm	0.84	<0.1	0.18	<0.1	0.5	<0.1
SO_4^{-2}	ppm	1.9	<0.1	115.3	<0.1	266.8	<0.1
PO_4^{-3}	ppm	12.26	0.037	9.7	<0.01	32.07	<0.01
Conductivity	mS/m	120	75.6	774	2.1	1580	18.5
pH		6.6	8	3	5.4	2.6	4.4
TOC	ppm	31.4	1.06	30.3	1.1	24.3	4.9
TDS	ppm	86.4	32.5	534.06	1.1	1036.4	7.2

Concerning MD permeate samples, the results show that the concentration of analyzed metals was below the detection limits except Ca, which was also considerably low. However, the separation efficiency of NH_4^+ ions was not substantial, i.e., ~25% owing to highly volatile NH_3 vapor in S1. With the pretreatment of other feed samples (S2 and S3), the formation of NH_4^+ ions (non-volatile) was favored in feed samples due to low pH. Consequently, the separation efficiency of NH_4^+ ions was improved by three-fold, following quite low concentrations of NH_4^+ ions (<0.05 ppm) in permeate samples. The other ions, including NO_3^-, Cl^-, SO_4^{-2} and F^-, remained undetectable in the permeate samples along with quite low levels of PO_4^{-3} (0.03 ppm in S1). The resulting quality allows the permeate to get released into the recipient water bodies or reuse it as process water. When comparing overall performance in terms of separation efficiency, MD displays promising results as opposed to other available methods, including electro micro-filtration [206], an integration of electro-dialysis and RO [207] and a combination of UF and RO [9].

Since the permeate was discharged from the MD system, the volume of the initial feed samples was reduced by the factor of ~0.3 in three hours, which led to a gradual increase in ionic and metallic concentration in the retentate samples. However, for metallic Ni and Cl^- ions, the initial feed has higher levels than the concentrated retentate. The reason might be that these contaminants were adsorbed on the membrane surface. Detailed results are included in [202].

4.1.2 Module performance

In addition to separation efficiency, permeate yield, energy analysis, and exergy efficiency of the Xzero laboratory prototype were also determined. As mentioned in the previous section, CMP wastewater samples were selected as MD feed, while assuming that composition and concentration change does not have any significant impact on the parametric study. During this study, ranges of feed inlet flow rates (3.5-7.2 L/min), coolant inlet flow rates (3.5-8.3 L/min), feed inlet temperatures (65-85°C), and coolant inlet temperatures (15-35°C) were considered.

Yield analysis

When performing yield analysis, the defining criterion for AGMD performance is transmembrane flux; therefore, it is critically investigated for the mentioned operating parameters. In the first set of experiments, the variation of transmembrane flux was linked to the feed and coolant inlet flow rates at constant feed temperature (80°C) and coolant temperature (25°C). The second set of tests considered the effect of feed and coolant temperatures on transmembrane flux with constant feed flow rate (7.2 L/min) and coolant flow rate (8.3 L/min). The outcomes from the first set of experiments demonstrate that the increase in feed and coolant flow rates at constant temperatures provide higher transmembrane flux, which adopts a positive linear trend, as presented in Figure 4.4. The reasons involve reduced boundary layer resistance, higher bulk temperature along the feed channel (at higher feed flow rates), and increased vapor condensation rate (at higher cold water flow rates). The transmembrane flux values vary from 9.7 to 11.7 L/m^{2}h, which are in line with the outcomes reported by Baaklini [208].

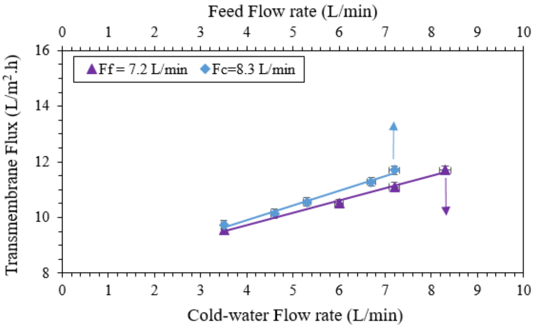

Figure 4.4 Variation of transmembrane flux as a function of MD feed and coolant flow rates while considering the other one constant. (Constant feed flow rate (F_f) was 7.2 L/min, and constant coolant (coolant) flow rate (F_c) was 8.3 L/min). MD feed temperature was 80°C, and the coolant temperature was 25°C.

Figure 4.5 points out the observed effect on transmembrane flux values for varying feed and coolant temperatures, at constant flow rates. The results obtained from the second set of experiments exhibit that with raising feed inlet temperatures, the transmembrane flux increases with linear to weakly exponential fashion. The observed trends might be associated with lower viscosity of water and changes in the vapor pressure of water at elevated feed temperatures, as shown by the Antoine relation using eq. 6.

$$\ln P_v = A + \frac{B}{C + T_f} \tag{6}$$

where A, B and C are the regression constants for the specific compounds, T_f and P_v represent MD feed temperature and vapor pressure. For water, A = 23.238; B = 3841; C = 45.

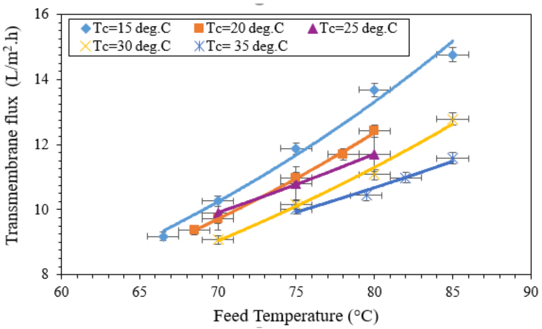

Figure 4.5 Effect of MD feed and coolant temperatures on transmembrane flux considering constant MD feed flow rate of 7.2 L/min and constant coolant flow rate of 8.3 L/min.

It was also found that lower coolant temperature provides higher transmembrane flux at constant feed temperature owing to the higher driving force. Nevertheless, at the same feed to coolant temperature difference (considering different feed and coolant temperatures), different transmembrane flux values were observed due to varying vapor pressure difference (driving force), conforming to the findings of Kujawa and Kujawski [209].

Energy analysis

While conducting energy analysis of the AGMD system, specific thermal energy demand was considered the critical parameter. Figure 4.6 displays the influence of feed and coolant inlet temperatures on specific thermal energy demand, at fixed feed and coolant flow rates (7.2 L/min and 8.3 L/min, respectively). Like transmembrane flux, specific thermal energy demand also adopts a positive linear trend with increasing feed temperature at constant coolant temperature. The reason behind this is the higher rate of heat transfer from MD feed to coolant, which leads to observe lower feed outlet temperature. Moreover, an increase in coolant temperature also results in higher specific thermal energy demand due to reduced transmembrane flux. Hence, specific heat demand significantly increases at elevated feed and coolant inlet temperatures, i.e., 1390–2170 kWh/m^3, in agreement with the values reported by Baaklini [208] and Woldemariam et al. [82].

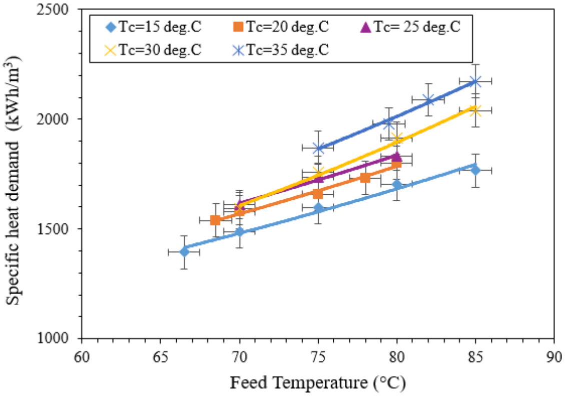

Figure 4.6 Effect of MD feed and coolant temperatures on specific heat demand considering the constant MD feed flow rate of 7.2 L/min and constant coolant flow rate of 8.3 L/min.

The amount of heat transferred to coolant, permeate, and surrounding was also calculated for a series of coolant temperatures (15-35°C), considering fixed feed inlet temperature (80°C), as displayed in Table 4.3. With an increase in coolant temperature, the amount of heat release through permeate increases due to higher permeate temperature, despite having lower transmembrane flux. A comparable trend was observed for convective heat transfer. The outcomes depict that most of the heat (~90%) was recovered by coolant, whereas the remaining was directed towards permeate and surrounding through module surfaces, pipes, and joints.

Table 4.3 Effect of coolant temperatures on specific heat transfer flow rates to coolant and via permeate and convection at a constant feed inlet temperature of 80°C.

Coolant temperature (°C)	$\dot{Q}_c$ (kWh/m^3)	$\dot{Q}_{cv}$ (kWh/m^3)	$\dot{Q}_d$ (kWh/m^3)
15	1574	38	19
20	1660	45	20
25	1683	52	22
30	1763	58	25
35	1813	66	27

Exergy analysis

Since MD is an energy-intensive separation process, therefore, it is essential to consider a realistic measure of energy evaluation for the system. For this reason, the exergy analysis of the Xzero AGMD laboratory unit is also performed. Figure 4.7 presents the process flow diagram of the Xzero AGMD laboratory prototype for exergy analysis.

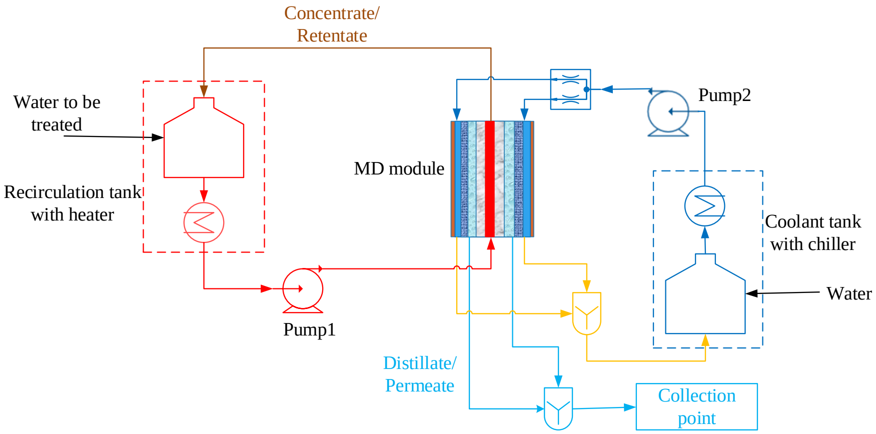

Figure 4.7 Flow diagram of Xzero laboratory unit

The considered conditions include the MD feed and coolant inlet flow rates of 7.2 L/min and 8.3 L/min, respectively; MD feed inlet temperature of 80°C and coolant inlet temperature of 30°C. For the purpose, the chemical composition and concentration of sample S2 (CMP wastewater) have been considered. The inlet and outlet exergies of principal components are shown in Table 4.4.

Table 4.4 Exergy flow rates of the main components of Xzero laboratory unit

Main Components	$Ex_{comp,\ in}$ (kW)	$Ex_{comp,\ out}$ (kW)
Recirculation tank (with heater)	3.68	2.44
MD feed pump (pump 1)	2.45	2.44
MD module	2.49	1.76
Coolant pump (pump 2)	0.047	0.046
Coolant tank (with chiller)	1.87	0.047

The total exergy gain by the AGMD system was determined using (1) initial water stream exergy at the restricted dead state, (2) heater and chiller exergies, and (3) pumps exergies. With considered operating conditions, the calculated exergy gain by the system was ~4 kW. In comparison, the exergy gain by the MD feed was only ~2 kW, including initial water stream exergy, heater exergy, and feed pump input exergy. Contrary to MD feed exergy gain, the required minimum work input for the treatment process was also calculated. The results determine that the minimum work input was ~0.75 kW, which indicates that the separation could be ideally performed using only ~0.75 kW instead of ~2 kW.

Moreover, it was determined that the exergy efficiency of the whole unit was 19%, in line with published results for other single-cassette MD systems [210]. In comparison, RO shows lower exergy efficiency due to higher pressure drop [211]. Second-law efficiency can further be increased while introducing the concept of internal heat recovery in MD systems [212]. Figure 4.8 displays the exergy destruction share of key components of the Xzero laboratory prototype. The outcomes show that the recirculation tank is accountable for ~32% exergy destruction. The reasons include evaporation through the tank covering and heat losses through the recirculation tank walls. The share of the coolant tank was ~47% in total exergy destruction, which was considerably higher since the coolant tank was entirely uncovered. MD module was responsible for ~20% exergy destruction owing to the heat transfer through convection and conduction, heat losses through condensation walls and permeate release. The exergy destruction in the pumps is below ~1%. The pumps are mainly responsible for overcoming the friction losses along the pipes. Therefore the exergy input (electrical) for the recirculation pumps might be destroyed across the pipes. These outcomes exhibit the need for an optimized MD unit in terms of its membrane material and condensation plates design. Moreover, the recirculation and coolant tanks' performance can be enhanced using proper insulation to minimize conductive and evaporative losses.

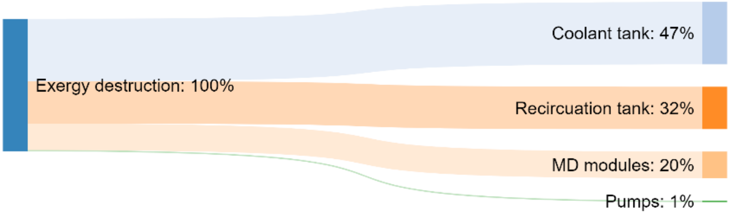

Figure 4.8 Exergy destruction share of the components in Xzero laboratory prototype

4.2 Integrated large-scale systems

A critical factor in the technology’s advancement links to handling the comparatively high thermal energy demand as opposed to other membrane processes [213], which is particularly significant at the industrial-scale. As mentioned in section 2.4, there are various waste heat sources available in typical fabs. Keeping in view of the characteristics of these heat sources, different industrial-scale semi-batch MD system configurations were designed and analyzed to treat selected wastewaters in a typical nano-electronics fab while considering the required pretreatment techniques (shown in Figure 4.9). Some assumptions were also taken into account for the analysis, i.e., (a) the system has steady-state flow; (b) the system allows purging of the concentrated stream to avoid caking and scaling on the membrane surface, and (c) MD feed and coolant have the similar flow rates. In the proposed design, the cascading of two MD modules was considered for enhanced energy efficiency through internal heat recovery. Moreover, the separation process was supposed to be multicycle to increase water recovery ratio; therefore, the retentate stream was recycled back several times through the MD system and combined with the makeup water in the feed tank. The count of the required MD modules and heat exchanger areas were estimated based upon the MD feed flow rate and specific heat demand to satisfy the requirement [54]. It was assumed that the specific heat demand is not sensitive to wastewater concentration when it is <10% (w/v %).

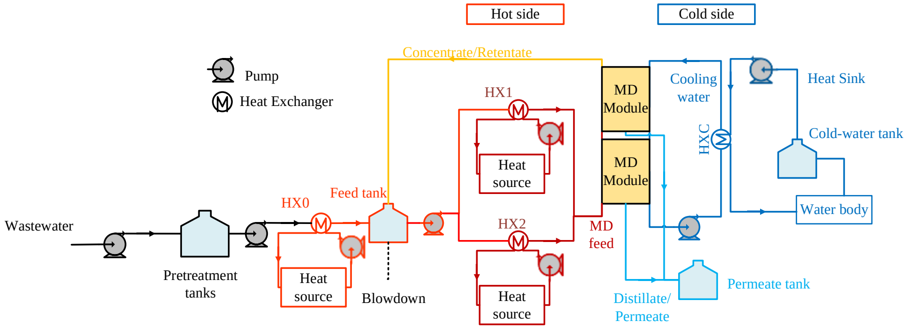

Figure 4.9 Flow diagram of proposed industrial-scale MD integrated system. In all cases, HX1 is considered as a primary heat recovery exchanger whereas; HX2 is for additional heating, and the HX0 is for preheating purposes. HXC presents the heat exchanger for the cold side.

4.2.1 TMAH wastewater treatment

Since the optimum temperature of MD feed for TMAH wastewater treatment is ≤65°C, this level is selected as the target temperature to be achieved. The chosen heat sources for the purpose are condenser outlet water of ~35°C from heat recovery chiller (for preheating), process cooling water released from manufacturing tools of ~85°C (for primary heating), and hot air of ~350°C from VOCs abatement systems (for additional heating).

According to the literature, the TMAH wastewater flow rate varies from under 0.2 m^3/h for small fabs up to 5m^3/h for large fabs [214], [215]. Based on the available information, industrial waste heat driven large-scale MD setup was investigated for the treatment of TMAH wastewater of flow rate 2.5 m^3/h (matching the amount releasing from a generic fab). The proposed industrial waste heat driven MD system (case 1) was further compared with DH driven MD system (case 2) for TMAH wastewater treatment. In case 2, the DH supply line of 85°C was selected as the primary heat source to satisfy the thermal power demand of the MD system. Despite the case, water from the external cooling source is taken as coolant. The estimations determine that for reaching the aimed temperature of 65°C from the initial temperature of 20°C, the total thermal power demand was approximately 1.8 MW. Considering the temperature levels and available thermal power of the selected heat sources, the outcomes show that the proposed configurations are able to meet the thermal power demand of the full-scale MD system; thus, both of the cases are technically feasible options for TMAH wastewater treatment. Additional results about the presented cases are included in [201].

Depending on the flow rates and thermal energy demands, the equipment was designed for both cases for the large-scale MD system. Considering 2.5 m^3/h of continuous TMAH wastewater flow rate, the estimated number of MD modules was 196. In case 1, three heat exchangers (HX0, HX1 and HX2) were connected to exploit the maximum potential of the available industrial waste heat, while in case 2, only one heat exchanger (HX1) was needed for DH integration. The specific electrical energy demand was around 0.5 kWh/m^3. Commercial water tanks and pumps were selected considering the flow rates and expected storage. Furthermore, the required cooling water and chemical amounts were also calculated. Table 4.5 summarizes the specifications of the main components and the necessary amount of raw materials.

Table 4.5 Design specification of industrial-scale MD integrated system.

Components		Specifications
MD modules		N = 196
Membranes		Area = 451 m^2
Hot side heat exchangers	Case 1	Total heat transfer area = 370 m^2
	Case 2	Total heat transfer area = 278 m^2
Cold side heat exchanger		Total heat transfer area = 278 m^2
Pumps	Case 1	Capacity 660 m^3/h, N = 8
	Case 2	Capacity 660 m^3/h, N = 6,
Water tanks		Capacity = 150 m^3/h, N = 6; Capacity = 5 m^3/h, N = 1
Pretreatment tanks		Capacity = 5 m^3/h, N = 2
Raw materials		Amount
Chemicals	Manganese dioxide	5 kg/year
	Sulfuric acid	23 m^3/year
Cooling Water		1.2 Mm^3/year

4.2.2 CMP wastewater treatment

There is no specific temperature restriction for CMP wastewater treatment using MD based process. Therefore, the selected target temperature is 80°C, and the chosen wastewater flow rate is 15 m^3/h (matching the amount of CMP wastewater releasing from typical fabs of 5000 m^2). In this case, condenser outlet water from chillers (for primary heating) and hot air from VOCs combustion abatement systems (for additional heating) were selected. (Contrary to the TMAH wastewater treatment case, this time upper-range of temperature (85-90°C) has been considered for condenser outlet water from chillers). Moreover, DH (supply line of 85°C and return line of 45°C) is taken into account as an external heat source in a case when industrial waste heat is not adequate to reach the target temperature of 80°C.

For this purpose, different configurations have been designed and examined for a continuous CMP wastewater flow rate of 15 m^3/h. These configurations were classified depending upon the origin of selected heat sources in each case, i.e., industrial waste heat integrated MD system (designated as case 1a), DH (supply line) integrated MD system (identified as case 1b), and industrial waste heat and DH integrated MD systems (referred as case 2a (preheating is done by DH return line) and case 2b (additional heating is provided by DH supply line)). More details about the integration cases are mentioned in [216]. The MD feed and coolant flow rates were regulated to keep the mass balance around the overall system. The total thermal power requirement of the MD system was 12.38 MW for reaching the aimed temperature of 80°C from the initial temperature of 20°C. The estimations show that 555 cascades arranged in parallel are required for a full-scale CMP wastewater treatment system. Table 4.6 shows the design specifications of the industrial-scale CMP wastewater treatment system.

Table 4.6 Design specification of industrial-scale MD integrated system.

Components		Specifications
MD modules		N = 1110
Membranes		Area = 2553 m^2
Hot-side heat exchangers	Case 1a	Total heat transfer area = 3140 m^2
	Case 1b	Total heat transfer area = 3093 m^2
	Case 2a	Total heat transfer area = 3199 m^2
	Case 2b	Heat transfer area = 3093 m^2
Cold-side heat exchanger		Heat transfer area = 3093 m^2
Pumps	Case 1a	Capacity = 670 m^3/h, N = 4; Capacity = 15 m^3/h, N = 2, one air compressor
	Case 1b	Capacity = 670 m^3/h, N = 4; Capacity = 15 m^3/h, N = 2
	Case 2a	Capacity = 670 m^3/h, N = 5; Capacity = 15 m^3/h, N = 2
	Case 2b	Capacity = 670 m^3/h, N = 4; Capacity = 15 m^3/h, N = 2
Water tanks		Capacity = 100 m^3/h, N = 14; Capacity = 15 m^3/h, N = 1
Pretreatment tank		Capacity = 15 m^3/h, N = 1
Raw materials		Amount
Sulfuric acid		60 m^3/year
Cooling Water		5.3 Mm^3/year

4.3 Economic assessment

In this section, thermally integrated large-scale MD systems for CMP wastewater treatment were chosen as a representation to investigate the economic feasibility. The economic model for the proposed systems was based on their equipment design and other operational requirements. Figure 4.10 summarizes total capital investment for four selected cases of thermal integrations for a full-scale wastewater treatment system of 15 m^3/h. The outcomes display that the MD modules are the main cost-capturing components and accountable for ~61–63% of overall equipment cost, and the heat exchanger takes second place with a share of ~21–23% of the total equipment cost. The heat exchanger cost contribution depends on the considered configuration and complexity of the process. Equipment specifications are quite comparable; therefore, the overall equipment cost and total depreciable capital are nearly indistinguishable in all integration cases. The total depreciable capital accounts for ~28 M$. , where the key cost-drivers are inside battery limits and outside battery limits. It is noteworthy that this work also regards land and site development cost and plant startup cost as a total permanent capital investment, contrary to most of the studies in the literature. The resulting total permanent capital investment was ~3.4 M$, and the overall working capital was 0.65 M$. The estimated annual CAPEX was ~2.5 M$/year for all the considered cases.

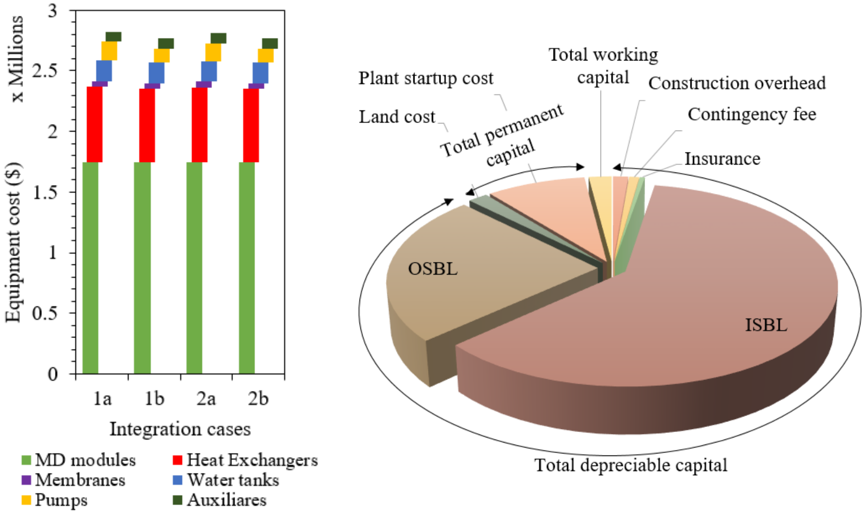

Figure 4.10 Distribution of total capital investment for all the integration cases.

Figure 4.11 displays the annual OPMEX breakdown for all integration cases. Usually, thermal energy cost is the most significant portion of the operating and maintenance cost ($C_{a,om}$), when the external heat sources are employed for satisfying the heat demand of the MD system. A related trend was noted for case 1b, where only DH cost accounts for 98% of $C_{a,om}$. In cases 2a & 2b, the share of thermal energy cost is 63% of $C_{a,om}$, whereas in case 1a, the heat cost is negligible since only industrial waste heat has been considered for the purpose. The cooling water contribution is also quite sensitive to the configurations and accounts for 2–83% of $C_{a,om}$. Service and labor cost was accountable for 0.1–6% of $C_{a,om}$. The OPMEX also covers membranes replacement cost (~0.1–6% of $C_{a,om}$), and chemicals and sludge disposal cost (0.04–2.2% of $C_{a,om}$). The electricity cost was ~0.05–3% of $C_{a,om}$. Among the mentioned cases, the case 1a is responsible for the lowest OPMEX, i.e., ~0.13 M$, whereas case 1b was subjected to the highest OPMEX, ~7.7 M$ owing to the highest thermal energy cost. The evaluation proves that Case 1a would be the preferred integration option when the operating cost is prioritized.

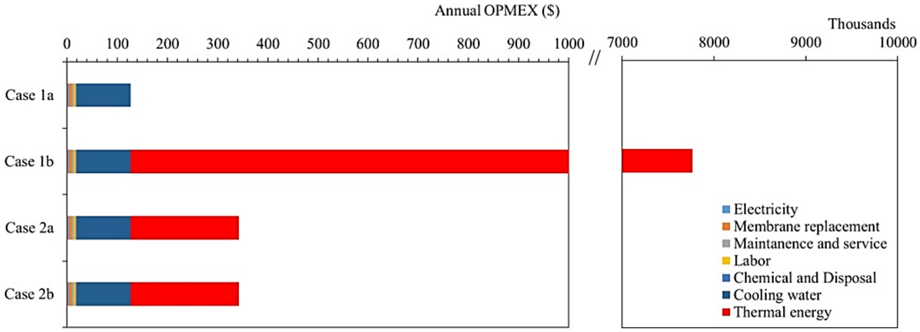

Figure 4.11 Annual OPMEX for all integration cases.

For determining the normalized CAPEX, two scenarios were selected: a new wastewater treatment plant (Scenario 1) and a retrofitted plant (Scenario 2). The outcomes show that the normalized CAPEX in scenario 1 (21 $\$/m^3$) is ten-fold higher than in scenario 2 due to the additional inevitable expenses. It was also found that the normalized OPMEX was widely fluctuated (1 to 65 $\$/m^3$) based on the type of thermal energy sources. The Case 1a exhibited the least wastewater treatment cost in both scenarios due to reasonable CAPEX and negligible thermal energy cost. The estimated unit water treatment cost is as low as 3.1 $\$/m^3$, ~95% less than the cost of CMP wastewater treatment while applying electrochemical systems (59 $\$/m^3$) [208]. (For TMAH wastewater, the expected unit water treatment cost using waste heat integrated MD system was ~16 $\$/m^3$ [201], which was approximately half of electrodialysis treatment cost: 36 $\$/m^3$ [189].) It was also revealed that the configuration of thermal energy sources has a negligible effect on the treatment cost; however, the chosen heat sources have a considerable impact on the economy.

As shown from the economic evaluation, MD modules and types of thermal energy sources are the two principal cost drivers. Therefore, the sensitivity analysis was conducted for these economic factors, as presented in Figure 4.12. The analysis has been performed for both scenarios (new and retrofitted wastewater treatment facilities) of Case 1a.

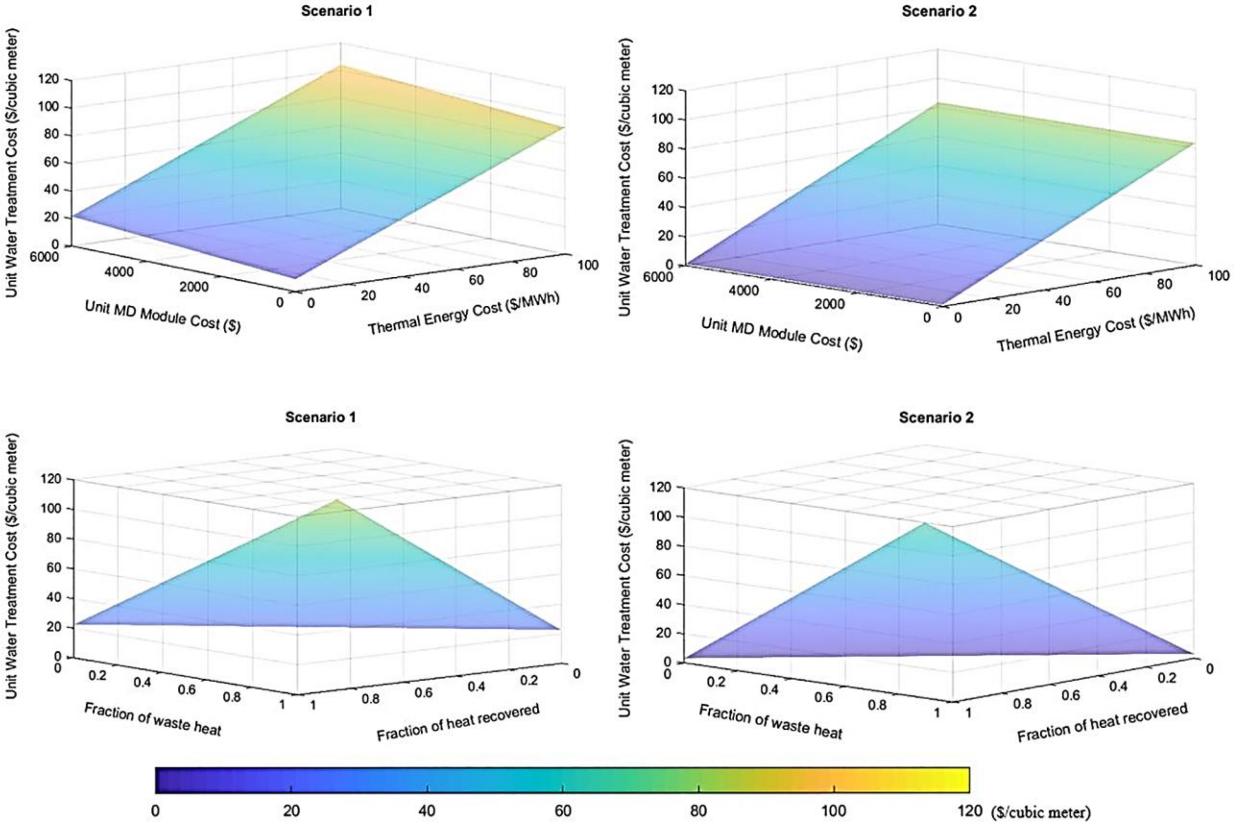

Figure 4.12 Sensitivity analysis of thermally integrated MD system.

While studying the effect of variation of the MD modules costs, it was found that treatment cost can be reduced up to 15.7 \$/m^3 in scenario 1 and up to 2.5 \$/m^3 in scenario 2, when module cost is decreased by 50%, and heat cost is supposed negligible. The cost per unit thermal energy varies depending on the heat sources, i.e., 0–100 \$/MWh in that case, unit water cost can also be altered between ~22-105 \$/m^3 in scenario 1, while it ranges from ~3-86 \$/m^3 in scenario 2, with reference MD module unit cost. Moreover, unit water treatment cost values were also estimated while varying the amount of waste heat used and total heat recovered. The outcomes show that when only external heat sources were considered without a heat recovery option, the water cost may increase to 86 \$/m^3 in scenario 1, with a heat cost of 77 \$/MWh. However, it can be reduced to 75% when only industrial waste heat sources were taken into account without heat recovery. Similar results can be obtained when the option of an external heat source with complete heat recovery was selected (quite impractical). In scenario 2, when industrial waste heat was considered, the unit water treatment cost can be as low as 3.12 \$/m^3.

4.4 Concluding remarks

This chapter presented the techno-economic performance of the membrane distillation (MD) process for the treatment of different wastewaters from nano-electronics industries. Case studies of imec, Belgium, have been chosen for the purpose, and the Xzero laboratory prototype was employed for experimental investigations. It was found that catalytic reduction and acid neutralization were the required pretreatment methods when wastewater from the photolithography process was considered. However, in the case of chemical mechanical planarization wastewater, only neutralization was needed before the MD separation step. Moreover, for the treatment of the photolithography process wastewater, the optimal MD feed temperature was 65°C since, above this temperature, the TMAH decomposition starts happening. The experimental results determine that high-quality permeate was recovered, having a reasonably low concentration of the major contaminants, in most cases, below detection limits. (The fluoride issue can be easily managed using an ion-exchanger, as an add-on step).

The parametric study of the Xzero laboratory prototype shows that the maximum transmembrane flux was 14.8 L/m^{2}h at the feed to the coolant temperature difference of 70°C. The specific thermal energy demand was ranged from 1390 to 2170 kWh/m^3 depending on the feed and coolant temperatures. In contrast, the achievable exergy efficiency was ~19%. The techno-economic system analysis of full-scale MD process shows that the estimated thermal energy demand can be readily managed using industrial waste heat sources of the nano-electronics facilities. Resultantly, the expected unit water treatment cost was around 3-16 \$/m^3, reasonably lower than the treatment cost associated with competitive methods. Sensitivity analysis confirms that thermal energy cost and the fraction of industrial waste heat utilization are the critical determinants, which can change the unit water treatment cost significantly.

Chapter 5 Water recovery from flue gas condensate in combined heat and power plants using membrane distillation (Appended articles IV and V)

In combined heat and power (CHP) plants, numerous wastewater treatment methods are considered for cleaning flue gas condensate in order to fulfill dual purposes: satisfying boiler feed water quality standards and meeting wastewater release limitations [217]. In this respect, filter bags, sand filters and lamella clarifiers are employed for removing the particulate and solids from the flue gas condensate. Separation of salts and heavy metals involves ion exchange [10]. These arrangements are found competent when the treated condensate is discharged to the recipient water body. However, in circumstances where the concentration of specific contaminants is quite high, or water recovery is obliged for producing boiler makeup water, membrane processes are favored due to their more reliable performance and reduced cost. Typically a sequence of process steps are considered [7], [218], e.g., microfiltration (MF) for separating colloids and large particles, ultrafiltration (UF) for removing remaining colloids and small particles, and reverse osmosis (RO) for separating water molecules from ions. Table 5.1 shows the existing flue gas condensate treatment methods in some major CHP facilities in Sweden, along with their fuel types.

Table 5.1 Flue gas condensate treatment methods in CHP plants in Sweden [219]–[221]

CHP Plants	Location	Fuel type	Purification methods
Värtaverket 8	Värtan	Forestry products	MF, UF and RO
Bristaverket	Brista	Wood residues and municipal solid waste	MF, UF, bag filter and RO
Högdalenverket	Högdalen	Municipal solid waste	MF, UF, bag filter and RO
E.ON (Åbyverket)	Örebro	Peat and wood chips	CO_2 degassing, MF, UF, RO, ion exchangers and ammonia removal
Söderenergi AB	Södertälje	Wood chips	MF, UF, RO, EDI and ammonia removal
Karlskoga Energi	Karlskoga	Animal waste, peat, recycled paper/plastic and wood chips	MF, UF, RO, EDI, ion exchanger, membrane degasser and mixed bed
Sävenäsverket	Gothenburg	Forestry products	MF, UF, water softeners, Bag filter and RO
Sevab Strängnäs Energi	Strängnäs	Municipal wastes and recycled wood	MF, UF, bag filter, RO, water softeners and EDI

These methods are highly recognized and generally useful, but there is still a need for a cost-efficient arrangement with increased water purity. Additionally, there are some technical issues, including bio-fouling, scaling, sludge disposal, and upper pressurization limits. The CHP plants have also reported poor separation efficiency of some contaminants in the RO based process. Hence, unique membrane separation techniques are of great concern, with benefits of the established processes. In this setting, MD is a potential membrane technology that has inherent advantages as compared to RO in that it can realize higher recovery ratios, has reduced fouling problems and requires less mechanical stress for the membranes due to low operating pressures [12]. These attributes warrant higher permeate yield, which in turn minimizes freshwater demand and lessened concentrate/sludge disposal requirements, following potentially lower capital and/or operating and maintenance expenditures. Moreover, heat sources and sinks required for the efficient operation of MD technology are well-suited for CHP integration.

A handful of studies have been performed to explore the potential of MD technology in the power industry. Ali et al. [124] demonstrated the performance of lab-scale DCMD while treating flue gas desulfurization wastewater. The researchers reported that all the non-volatiles were removed up to 99.5%. Conidi et al. [123] examined the lab-scale RO-DCMD integrated process to reduce salt-content from flue gas desulfurization wastewater and reclaim the purified water. In this study, RO-retentate was further concentrated using MD. The results showed that the non-volatiles were separated successfully, and up to 94% of the water was recovered. Yu et al. [125] assessed bench-scale DCMD to concentrate cooling tower blowdown. The researchers reported that 99.5% of salts were removed, and water recovery extent was increased from 68% to 87% with the use of antiscalant. Chuanfeg et al. [126] and Kullab et al. [127] conducted pre-studies on pilot-scale AGMD for flue gas condensate treatment. It was reported that heavy metals and particles from flue gas condensate could be separated successfully. However, ammonium could not be removed entirely. It is noteworthy that Kullab et al. [127] introduced the DH driven MD system in the study, but the strategy to address DH supply ━ MD heat demand balance and economic analyses of such integrations were not reported. Later, Fortkamp et al. [128] examined the flue gas condensate cleaning while applying the comparable AGMD system and determined that ammonium separation issues were still present.

Since the removal of ammonium ions from the flue gas condensate is essential before its release or reuse; therefore, it must be addressed along with the elimination of non-volatiles. Goldschmidt et al. [222] examined different commercially used alternatives for ammonium separation and suggested acid quenching as the best option due to its lower maintenance requirements. In 2014, Bristaverket (biofuel-fired) CHP facility employed an acid stream quench system that presented satisfactory outcomes. However, biofouling during the flue gas condensate treatment led to a shorter RO membrane lifetime [223].

The novel combination of MD separation with acid neutralization may exploit both methods' advantages for innovative flue gas condensate treatment. This chapter is focused on exploring this novel concept in detail. The investigations include experimental and techno-economic studies of MD based separation process for treating actual flue gas condensate feeds from municipal solid waste (MSW) and biofuel-fired CHP plants. Facilities operated by Stockholm Exergi AB were selected since they represent modern waste incineration and biofuel-fired CHP plants. The main emphasis of the experimental studies is the separation efficiency of major contaminants and water recovery. Moreover, the effect of parametric variation on the performance of the Xzero AGMD pilot plant was also studied. The work also involves the techno-economic analysis of large-scale systems for advanced flue gas condensate treatment in CHP plants.

5.1 Stockholm Exergi facilities

The Högdalenverket and Bristaverket, owned and operated by Stockholm Exergi AB, are the two considered CHP facilities. The Högdalenverket facility contains six boilers that consume up to 700,000 tonnes of waste per year and supply ~2200 GWh of heat annually. In contrast, the Bristaverket facility is comprised of an MSW CHP plant and a biofuel-CHP plant. The MSW CHP plant provides 500 GWh of heat annually by combusting 240,000 tons of MSW, whereas the biofuel-CHP facility supplies 760 GWh of heat per year while utilizing 350,000 tons of wood chips. Sections 5.1.1 and 5.1.2 include the description of the existing flue gas condensate treatment processes in the selected facilities. Moreover, proposed alternative MD based options are also introduced.

5.1.1 Högdalen CHP facilities

The flue gas condensate from Högdalen CHP facilities is usually heavily contaminated, which requires it to be treated before discharge to the recipient or return as the boiler feed water (for saving freshwater purchases). In this framework, the flue gas condensate from the condenser is first buffered and then filtered through vibrating screens to eliminate the suspended solids. After that, the flue gas condensate is directed to another buffer tank, and next, it passes through the UF modules to separate small particulates, resins and oils. This ultra-filtered flue gas condensate is then entered into the following buffer tank and is later sent to the bag filters for further cleaning. After this stage, RO modules are introduced for the advanced treatment of the flue gas condensate. Based on the seasonally dependent DH requirement, the flow rate of RO-treated flue gas condensate ranges from 10-100 m^3/h. The clean condensate is usually mixed with city water (when it is insufficient to meet the boiler water demand). The mixed water is further sent for additional treatment to satisfy boiler water quality standards. In the case when the clean condensate is in abundance, the excess amount is released to the recipient.

While the existing RO based system for flue gas condensate treatment has proven satisfactory, few operation and maintenance issues are worthy of note. For instance, UF modules encounter severe biofouling issues that have increased the maintenance frequency from two cleanings per year to one cleaning per week and have also reduced the yield by four-fold. The problem is resolved by sodium hypochlorite (NaOCl) dosing in the buffer tanks. Moreover, the membrane scaling in RO modules may cause serious concerns for the long-term operation of the modules. Furthermore, the RO removal efficiency of specific contaminants is no longer adequate due to tightened environmental controls. For example, this process faces the challenge of maintaining acceptable levels of ammonia (NH_3) and mercury (Hg), pointing to the need for additional investments in water treatment technology. The alternative arrangement involves off-loading the RO based system, downstream of the shaking screens with MD based system. Figure 5.1 shows the existing RO-based flue gas condensate treatment process in Stockholm Exergi (municipal solid waste (MSW) fired) Högdalen cogeneration facilities [223].

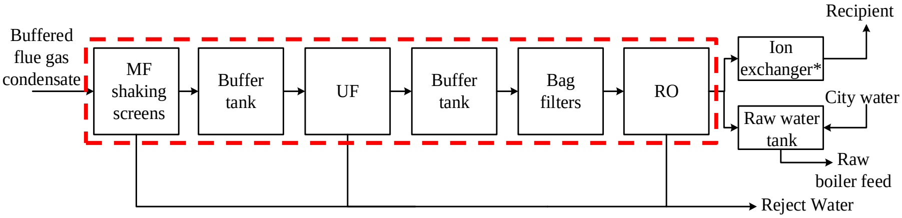

Figure 5.1 Process flow diagram of RO based flue gas condensate treatment in Stockholm Exergi Högdalen CHP facility. The Red dashed line shows an area of interest for introducing an MD based system. * indicates additional investment.

5.1.2 Bristaverket CHP facilities

The flue gas condensate treatment system of the Bristaverket CHP facilities is displayed in Figure 5.2. The flue gas condensate from the MSW incineration CHP plant is first passed through MF bag filters to remove the suspended solids. After that, it is sent to UF modules and subsequent set of bag filters to separate the residual solids and small particulates. For further cleaning, it then flows through RO filters. The RO treated flue gas condensate is next introduced to an ion exchanger before entering into a condensate collection tank. Ion exchangers are specifically used to remove the remaining metals, i.e., mercury (Hg). The typical volumetric flow rate of flue gas condensate from the MSW-CHP plant is around 20 m^3/h.

In the biofuel-fired CHP plant, the flue gas condensate is sent to MF shaking screens and is then exposed to ultraviolet (UV) light for microorganism control. Afterward, it follows an analogous route of flue gas condensate treatment for MSW incineration CHP plant (exception: ion exchangers are not considered in this case). From the biofuel-fired CHP plant, around 40 m^3/h of flue gas condensate is added into the collection tank.

Later, based on requirements, the clean condensate is sent to various destinations: 1) discharged to the recipient water bodies after pH adjustment; 2) sent for advanced treatment to produce boiler feed water; 3) directed to ash slag in the waste fired boiler.

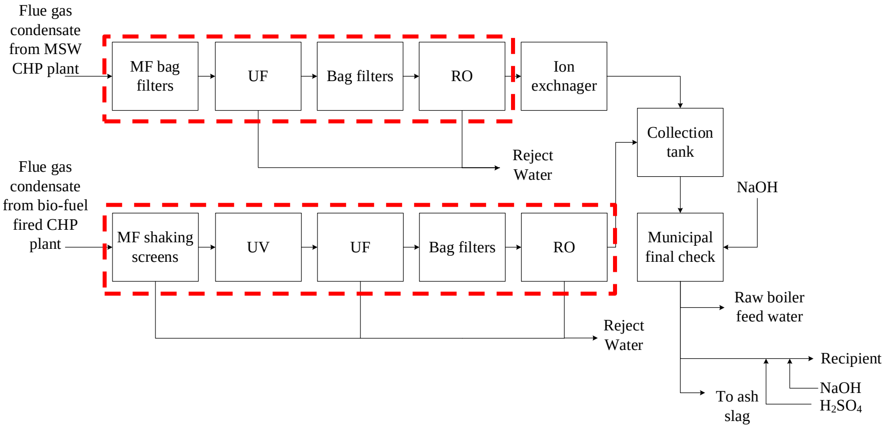

Figure 5.2 Process flow diagram of RO based flue gas condensate treatment in Stockholm Exergi Bristaverket CHP facility. The Red dashed lines show an area of interest for introducing an MD based system.

In the MSW incineration and biofuel-fired CHP plants, it is reported that the MF and UF modules are facing challenges concerning biofouling. These issues lead to the requirement for an advanced wastewater management system, which can potentially resolve the problem in an eco-friendly and economical manner.

5.2 Technical performance of Xzero laboratory prototype and pilot plant

This section includes experimental investigations for flue gas condensate treatment via the Xzero AGMD facilities, in which the primary focus is on the separation efficiency of the main contaminants and feed reconcentration (associated with volume reduction). Moreover, parametric studies are also presented to demonstrate the potential of the system.

5.2.1 Separation efficiency

The experimental study was conducted in two phases (A and B). In phase A, flue gas condensate samples from Högdalenverket were tested, while in phase B, flue gas condensate samples from Bristaverket were considered.

In phase A (linked to Högdalen CHP facilities), actual flue gas condensate samples were collected from MF shaking screens outlet and further referred as S1-A (while using Xzero laboratory unit) and S2-A (when Xzero pilot plant is employed). In addition, RO permeate was also collected from the RO outlet and considered as a reference sample (S3). Considering the limitation of MD for removal of volatile contaminants (ammonia), the need for acid neutralization was required to be investigated. Therefore, in lab-scale experiments, the MD tests were performed for two cases: no pretreatment and acid neutralization pretreatment, which was achieved by adding 0.9 mL of 40% concentrated sulfuric acid per L of collected samples to adjust the pH. After pretreatment, the sample S1-A was denoted as S1-A*. The 10 L flue gas condensate sample (S1-A/ S1-A*) was filled in the recirculation tank for each test. Each test ran for 3 hours. In pilot-scale trials, pretreatment was performed by neutralizing with 37% H_2SO_4 (1 mL/L); this feed was expressed as S2-A*. A total of 1 m^3 of the sample S2-A* was pumped through a 10-micron filter before filling the feed tank of the MD pilot facility. Owning to the limitation of available equipment, only module 5a of the Xzero pilot plant was used. The detailed experimental methods are explained in [224].

In phase B (at Bristaverket CHP facilities), the real raw flue gas condensate samples of a total of 40 L were collected from waste-fired and biofuel-fired CHP plants. The experiments were performed using the Xzero laboratory unit in two sections: section 1, when flue gas condensate from MSW CHP facility (S1-B) is considered, and section 2 when flue gas condensate from biofuel-fired CHP facility (S2-B) is tested. Similar to phase A, the MD experiments were performed in two steps for each section, (1) no-pretreatment and (2) with neutralization. In this phase, 0.5 mL of 40% H_2SO_4 has been added per L of flue gas condensate samples for neutralization, before their introduction to the MD system. After neutralization, the sample S1-B is referred to as S1-B*, and sample S2-B is named as S2-B*.

Feed, concentrate and permeate samples of 1 L were collected in glass bottles and sent to independent laboratories for physicochemical analysis (as mentioned in section 3.2.1). Figure 5.3 shows the considered scheme for flue gas condensate treatment, and Table 5.2 presents the operating parameters and conditions for experimental runs in phases A and B (for evaluating the separation efficiencies).

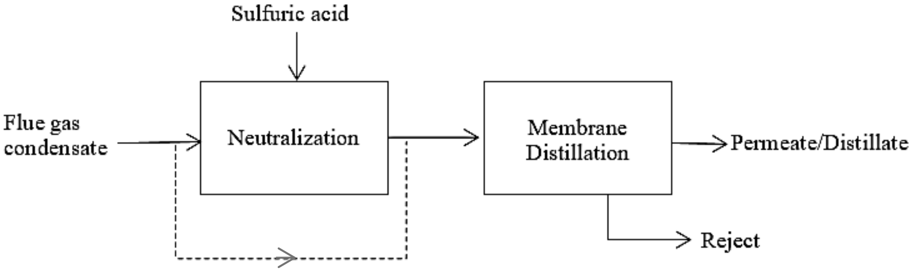

Figure 5.3 Schematic diagram of proposed flue gas condensate cleaning system

Table 5.2 Experimental conditions of phase A and B testing

	Phase A		Phase B
	Högdalen CHP facilities		Bristaverket CHP facilities
Parameters	Xzero laboratory prototype	Xzero pilot plant	Xzero laboratory prototype
Feed sample volume (L)	10	1000	10
Feed temperature (°C)	70	55, 70, 80	70
Coolant temperature (°C)	18	15	18
Feed flow rate (L/min)	4.9	10	4.9
Coolant flow rate (L/min)	6.8	10	6.8
Permeate sample Size (L)	1	1	1

Phase A (Hödgalen CHP facilities)

Table 5.3 summarizes the outcomes of physicochemical analysis of raw flue gas condensate samples (S1-A and S2-A), pretreated flue gas condensates (S1-A* and S2-A*) and their resulting permeate samples. The obtained permeate samples of S1-A and S2-A (no pretreatment) are named as D1-A and D2-A, whereas the permeates of S1-A* and S2-A* (with neutralization) are denoted as D1-A* and D2-A*, respectively.

Considering sample D1-A, most of the analyzed metals were under detection limits except Cd and Pb; however, their concentration was below the maximum acceptable levels. Moreover, the obtained concentrations of Na, Hg and Zn were lower in comparison to the related values of RO permeate (S3). In the case of ions, the separation efficiency of MD for Cl^- and SO_4^{-2} was >99%, whereas the concentration of ammonium ions was not substantially reduced, i.e., ~35% owing to the high volatility of ammonia. Resultantly, higher conductivity of sample D1-A was observed than that of the S3 sample. This finding points to the need for pretreatment via acid neutralization. It was found that after pH adjustment, ammonium concentration in D1-A* was <0.05 ppm, which was lower than the achievable value (3.32 ppm) for RO permeate (S3). When the quality of D1-A and D1-A* was compared, it was found that metallic concentrations were similar in MD permeate samples. The concentration levels of all analyzed metals in D1-A* were following regulated limits except Cd. Considering other water quality parameters, the values for D1-A* were found comparable to the respective values for the RO permeate sample (S3). Since acid neutralization was taken into account as a pretreatment step, the pH of samples D1-A* was comparatively low (~5). More results are discussed in [224].

Table 5.3 Performance of Xzero laboratory prototype and pilot plant for flue gas condensate treatment for Högdalen CHP facilities

Contaminants	Units	Xzero Laboratory Prototype				Xzero Pilot plant					RO permeate	Release limits
		S1-A	D1-A	S1-A*	D1-A*	S2-A	S2-A*	D2a-A*	D2b-A*	D2c-A*	S3	RL
K	ppm	0.61	<0.4	0.623	<0.4	0.74	0.98	<0.4	<0.4	<0.4	<0.4	-
Na	ppm	109	<0.5	112	<0.5	56	51	0.12	0.14	0.15	10.6	-
As	ppm	<0.0005	<0.0005	<0.0005	<0.0005	<0.0005	0.0012	<0.0005	<0.0005	<0.0005	<0.0005	0.005
Cd	ppm	0.0014	0.0002	0.0014	0.00064	0.0032	0.0025	0.0004	0.0003	0.0006	0.0001	0.0005
Co	ppm	<0.0002	<0.0002	<0.0002	<0.0002	<0.0002	0.0009	<0.0002	<0.0002	<0.0002	<0.0002	0.005
Cr	ppm	<0.0009	<0.0009	<0.0009	<0.0009	<0.0009	0.17	<0.0009	<0.0009	<0.0009	<0.0009	0.005
Cu	ppm	0.009	<0.001	0.01	<0.001	0.013	0.16	<0.001	<0.001	<0.001	<0.001	0.015
Hg	ppm	0.00027	<0.0001	0.0004	<0.0001	0.0003	0.0002	<0.0001	<0.0001	<0.0001	0.00017	0.00025
Ni	ppm	<0.0006	<0.0006	0.002	<0.0006	<0.0006	0.18	<0.0006	<0.0006	<0.0006	<0.0006	0.005
Pb	ppm	0.037	0.00084	0.037	0.004	0.032	0.055	0.002	0.0015	0.004	0.0016	0.005
Zn	ppm	0.229	<0.004	0.204	<0.004	0.29	1.7	0.0031	0.014	0.0098	0.0045	0.025
Tl	ppm	<0.0001	<0.0001	<0.0001	<0.0001	<0.0001	<0.0001	<0.0001	<0.0001	<0.0001	<0.0001	0.005
NH_4^+	ppm	35.8	23	35.3	<0.05	22	27	<0.05	<0.05	<0.05	3.32	7.5
Cl^-	ppm	26	<0.1	26	1.2	21	22	<0.1	<0.1	<0.1	1.2	-
SO_4^{-2}	ppm	91	0.39	390	3.4	23	450	<1	<1	<1	2.8	-
Total Hardness	°dH	<0.15	<0.15	<0.15	<0.15	<0.15	1.3	<0.15	<0.15	<0.15	<0.15	-
COD	ppm	<20	<20	7	<20	<20	<20	<20	<20	<20	<20	-
TDS	ppm	273	<20	544	<20	610	550	<20	<20	<20	37	-
TOC	ppm	0.21	0.29	0.93	<2	<2	<2	<2	<2	<2	<2	-
Conductivity	mS/m	66.1	12	187	0.6	38	250	<2	<2	<2	6.5	-
Turbidity	FNU	0.34	<0.2	<0.2	<0.2	0.39	<0.2	<0.2	<0.2	<0.2	<0.2	-
pH		8.3	8.6	2.58	4.88	7.5	2.4	4.6	5.4	5.2	7.6	-
Alkalinity	ppm HCO_3	220	72	<2.4	<2.4	150	<2.4	<2.4	<2.4	<2.4	32	-

Permeate sample at T_f = 55°C and T_c = 15°C: D2a-A*; Permeate sample at T_f = 70°C and Tc = 15°C: D2b-A*; Permeate sample at T_f = 80°C and Tc = 15°C: D2c-A*. '<' indicates a value below the detection limit. Note that samples of MD treated permeates and RO treated permeate were sent to two different external laboratories. Therefore, different detection limits were observed. However, in order to make the comparison easy, the higher value was chosen among both detection limits and expressed in this table. '-' shows that values are not available.

In phase A of testing, the Xzero pilot plant's performance was also evaluated for flue gas condensate treatment at different feed temperatures. Considering metallic concentration, it was observed that the quality of the permeate samples was not significantly affected by the feed and coolant temperature variation. Similar to lab-scale experiments, the concentrations of Hg and Na were seen lower compared to that of RO permeate (S3). Moreover, the removal efficiency of NH_4^+, Cl^- and SO_4^{-2} was more than 99.5%. It was also noticed that the concentration levels of the analyzed metals and ions in all MD permeate samples were ranged from under detection limits to below the permissible concentration levels. As a result of neutralization, the pH of the MD permeate samples was low, i.e., 4.6-5.4, which can be normalized to 7 when added with municipal water. Moreover, the values of other water quality parameters, including conductivity, TOC, TDS, COD, TOC, alkalinity and turbidity, were either equal to or lower than that of RO treated permeate (S3). The additional outcomes can be found in [224].

Moreover, the reconcentration study was performed using the Xzero pilot plant to examine the potential of achieving high recovery ratios for the available pilot-scale system. Here an initial volume of 2.5 m^3 was considered. The experiments were performed at constant feed and coolant temperatures of 50°C and 18°C, respectively; feed and coolant flow rates were 50 L/min, each. Moreover, the DH return line was selected as the thermal energy source, and the cold water was taken as a heat sink. The feed was reconcentrated for 105 hours, and the experiments were performed in five stages. The outcomes show that 92% of the water was recovered from the selected flue gas condensate sample while reducing the feed volume from 2500 L to 200 L. As a result, the concentration of the contaminants in the feed was increased, as anticipated, and the conductivity was also reached up to 1400 mS/m. In contrast, the concentration of analyzed contaminants in the permeate samples was found under acceptable values, except for Cd and Zn in some runs. The detailed results and discussion are presented in [224].

Phase B (Brista CHP facilities)

Table 5.4 presents the physicochemical analyses of the raw flue gas condensate samples from MSW and biofuel-fired CHP facilities (S1-B and S2-B, respectively), neutralized flue gas condensate samples (S1-B* and S2-B*) and related MD permeate samples. The resulting permeate samples of S1-B and S2-B (no pretreatment) are symbolized as D1-B and D2-B, whereas the permeate of S1-B* and S2-B* (with pretreatment) are shown as D1-B* and D2-B*, respectively. Moreover, the concentration of reference permeate samples from the particular CHP facilities are also mentioned and compared. (For MSW CHP facility, reference permeate is RO and ion exchange-treated condensate, whereas, for biofuel-fired CHP facility, it is RO permeate).

When considering the quality of samples S1-B and S2-B, it was observed that S1-B has a comparatively higher metallic and anionic concentration; however, S2-B has a significantly higher level of ammonium ions compared to S1-B. Nonetheless, the quality of S2-B seems relatively better than S1-B when the other water quality parameters are compared. However, when S1-A and S1-B were compared, the quality of S1-B was found better. The noted difference in samples' quality is certainly linked to different methods for flue gas cleaning and variable boiler feed.

The physicochemical analysis of D1-B reveals that the analyzed metals have concentration under detection limits, except for Cd and Pb, but their levels are quite low with a maximum of 0.8 ppb. The concentration level of NH_4^+ ions was also quite low (1.9 ppm), and the anions were not found in the D1-B sample. Compared to the related reference permeate, a higher concentration of Cd and Pb in D1-B was found. In contrast, reference permeate has a higher level of Na and As. The examination of D1-B* presented that NH_4^+ ions were not detectable in the permeate sample. The comparison of D1-B and D1-B* proves that D1-B has acceptable quality, and neutralization is not needed in this particular case, contrary to the results shown in the Högdalen case study (for D1-A). However, concerning the concentration levels of Cd and Pb in D1-A and D1-B samples, it was found that they were similar in both permeate samples. Though, the release limit for Cd in the Brista facilities is considerably tighter.

In terms of the metallic concentration of D2-B, it was determined that only Cd was detectable among all analyzed metals, though the level was adequately low. The anions concentration was under the detection limit; however, the NH_4^+ ions concentration was above the allowable limit, i.e., 12 ppm, with unsatisfactory removal efficiency. When compared with reference permeate, it was observed that Hg concentration in reference permeate was higher, whereas D2-B has a slightly higher concentration of Cd and NH_4^+ ions than reference permeate. A higher level of NH_4^+ ions in D2-B required acid neutralization, which eventually helped reduce NH_4^+ ions concentration up to 0.045 ppm, in D2-B*. However, it leads to other challenges such as the higher concentration of Pb, Cd and Hg, compared to D2-B and reference permeate.

Since the complete separation is not observed, the reasons may involve adsorption and permeation of particular contaminants (i.e., Hg, Cd and Pb, in their elemental and/or compound forms) through the membrane. In this respect, the two critical parameters are temperature and pH values, which affect the contaminants' concentration levels in feed, permeate, and retentate samples. (Diffusion of pollutants in a liquid phase has not been contemplated at this point.)

Table 5.4 Performance of Xzero laboratory prototype for flue gas condensate treatment in case of Bristaverket CHP facilities

Contaminants	Units	Waste to Energy CHP facility					Biofuel-fired CHP facility						
		S1-B	D1-B	S1-B*	D1-B*	Reference permeate	S2-B	D2-B	S2-B*	D2-B*	Reference permeate	HR	Release Limit
Na	ppm	27	<0.5	23	0.33	3.37	0.18	<0.5	1.2	0.22	<0.5	8.01	-
K	ppm	2.1	<0.4	2	<0.4	<0.4	0.15	<0.4	0.24	<0.4	<0.4	<0.4	-
As	ppm	<0.0005	<0.0005	0.00021	<0.0005	0.000507	<0.0005	<0.0005	<0.0005	<0.0005	<0.0005	<0.0005	0.001
Al	ppm	<0.01	<0.01	0.17	<0.01	<0.01	<0.01	<0.01	0.027	<0.01	<0.01	<0.01	-
Pb	ppm	0.0034	0.00082	0.0079	0.0017	<0.0005	0.001	<0.0005	0.0042	0.00095	<0.0005	<0.0005	0.0015
Cd	ppm	0.00054	0.00037	0.00061	0.00032	<0.00005	0.00039	0.00011	0.00053	0.00018	<0.00005	<0.00005	0.00008
Cu	ppm	0.0033	<0.001	0.14	0.0017	<0.001	<0.001	<0.001	0.011	<0.001	<0.001	<0.001	0.002
Hg	ppm	0.00059	<0.0001	0.00029	<0.0001	<0.0001	0.0016	<0.0001	0.0025	0.00099	0.00018	0.00021	0.0002
Mo	ppm	0.0006	<0.0005	0.00038	<0.0005	<0.0005	<0.0005	<0.0005	<0.0005	<0.0005	<0.0005	<0.0005	-
Ni	ppm	0.0012	<0.0006	0.058	<0.0006	<0.0006	<0.0006	<0.0006	0.015	<0.0006	<0.0006	<0.0006	0.001
Tl	ppm	<0.0001	<0.0001	<0.0001	<0.0001	<0.0001	<0.0001	<0.0001	<0.0001	<0.0001	<0.0001	<0.0001	0.0005
Zn	ppm	0.0089	<0.004	0.28	<0.004	<0.004	<0.004	<0.004	0.022	<0.004	<0.004	<0.004	0.01
Cl^-	ppm	14	<0.1	15	<0.1	-	7.5	<0.1	8.6	0.14	-	-	-
SO_4^{-2}	ppm	37	<1	360	<1	-	<1	<1	430	<1	-	<1	-
NH_4^+	ppm	1.1	1.9	0.46	<0.01	1.21	36	12	37	0.045	1.59	4.75	5
TOC	ppm	2.7	<2	4.5	<2	-	<2	<2	<2	<2	-	-	-
COD	ppm	<20	<20	< 20	<20	-	<20	<20	<20	<20	-	-	-
TDS	ppm	140	<20	450	<20	-	<20	<20	450	<20	-	-	-
Total Hardness	°dH	4.4	<0.15	4.2	<0.15	-	<0.15	<0.15	<0.15	<0.15	-	-	-
Turbidity	FNU	<0.1	0.13	1.2	<0.1	-	0.13	<0.1	0.71	<0.1	-	-	-
pH		7.9	7.2	2.4	4.8	5.5	7.6	8.8	2.3	3.7	5.2	-	-
Conductivity	mS/m	28	<2.0	210	<2.0	22	26	6.1	290	10	19	-	-
Alkalinity	ppm HCO_3	89	7.1	<2	<2	-	77	41	<2	<2	-	-	-

'<' indicates a value below the detection limit. Note that samples of MD treated permeate and RO treated permeates were sent to two different external laboratories. Therefore, different detection limits were observed. However, in order to make the comparison easy, the higher value was chosen among both detection limits and expressed in this table. '-' shows that values are not available.

The observed non-ideal separation of contaminants may attribute to the following potential mechanisms:

- Higher temperature levels increase the vapor pressure of some elements (or their compounds) as well as improve the solubility of various salts. For instance, elemental Hg shows high vapor pressure (volatility) at elevated temperatures; on the other hand, the increase in solubility of $HgCl_2$ (rich in flue gas condensate) can be observed at the higher temperature, that may lead to the presence of Hg both in permeate and concentrate [225]. The elemental Cd is also quite volatile and insoluble; however, $CdCl_2$ (abundant in flue gas condensate) is very soluble in water, and its solubility improves with an increase in temperature [226]. The other contaminants, for example, $PbCl_2$ is sparingly soluble but highly volatile; however, at elevated temperatures, it also shows higher solubility.
- The variation in the pH level may alter the speciation of elements in the solution as well as change the surface charge of the polymeric (PTFE) membrane.
    - Depending upon the chemical and thermodynamic stability of the elements and their compounds in the solution, their speciation at a certain pH level can be defined by the Pourbaix diagram [227]. For instance, oxides of Hg, Pb and Cd may not be observed when the pH of the solution is <4 [227]–[229]. Therefore, the acidic flue gas condensate might not contain these oxides. Moreover, at lower pH levels, the NH_3 concentration is negligible since the equilibrium favors the formation of NH_4^+ in aqueous solution [230].
    - The change in pH level alters the electrostatic interactions among the membrane surface and charged solutes, which determine the permeation or retention of the contaminants; counter-ions attract towards the membrane surface; however, co-ions show the opposite behavior [231]–[233]. This might be another explanation of the presence of Hg, Cd and Pb in the permeate samples.
    - Additionally, the solubility of some salts is also affected by their associated anions and pH levels, which can be described by Le Chatelier's principle [234]. In the acidic flue gas condensate samples, the solubility of almost all sparingly soluble salts (whose anion is the conjugate base of a weak acid) is enhanced dramatically. However, with pH change, no to little effect can be recorded on the solubility of the salt whose anion is the conjugate base of a strong acid or stronger weak acid, respectively (for instance, sulfates and chlorides).

Thus the performance of the MD systems may considerably be influenced by higher temperatures and lower pH values due to the change in properties of the MD membrane and contaminants.

Combined Scenario

At the Bristaverket facilities, clean condensates from both plants are typically mixed and referred as HR. The comparison of D1-B and D2-B* with HR indicates that MD permeate samples have a relatively higher concentration level of Pb, Cd and Hg (only in case of D2-B*); however, HR shows comparatively higher amounts of Hg (in case of D1-B), Na, and NH_4^+ ions. The final comparison of the values of MD permeates with release limits (RL) reports that D1-B and D2-B* have partially fulfilled the RL requirement. For improving the performance of the MD system, the mixing of permeates is considered as one of the options. The results tell that when D2-B and D2-B* are mixed in the ratio of 4 to 1, the quality of the mixed permeate (M1) was much closer to the desired outcome. Moreover, when M1 is added in the equal amount of D1-B, the mixed permeate (M12) fulfills the regulatory requirements, except for Cd. The detailed outcomes are presented in [235]. To manage the concentration of Cd, existing ion exchangers with cation resins can be employed as an add-on before releasing the clean condensate to water bodies or reuse as boiler/process feed water. [236].

5.2.2 Module performance

Apart from determining the removal efficiencies of MD systems, a parametric study was conducted for analyzing the system performance at different operating flow rates and temperatures. For understanding the impact of these parameters on the performance of MD pilot plant, ranges of feed and coolant flow rates (10-25 L/min, in increments of 5 L/min), feed inlet temperatures (50-90°C, in increments of 5°C), and coolant inlet temperatures (15-55°C, in increments of 5°C) were employed. For this study, neutralized flue gas condensate sample, S2-A* (from Högdalen CHP facilities) was taken as MD feed, considering that composition and concentration change does not significantly affect the parametric study.

Yield analysis

Figure 5.4 and Figure 5.5 present the effect of MD feed and coolant temperatures and flow rates on transmembrane flux. The outcomes show that lower coolant temperatures and higher feed temperatures were linked to comparatively higher transmembrane flux due to improved driving force. Moreover, the higher feed to coolant temperature difference resulted in greater flux. It is noteworthy that, for the same temperature difference between feed and coolant streams, slightly higher transmembrane flux was obtained at higher feed temperatures. The maximum achievable flux was 7.2 L/m^2h, at the feed temperature of 80°C and coolant temperatures of 15°C. Concerning the effect of flow rates at constant temperatures, it was found that an increase in MD feed and coolant flow rates improved the transmembrane flux and exhibited a positive linear trend. These outcomes are in line with the results shown in section 4.1.2

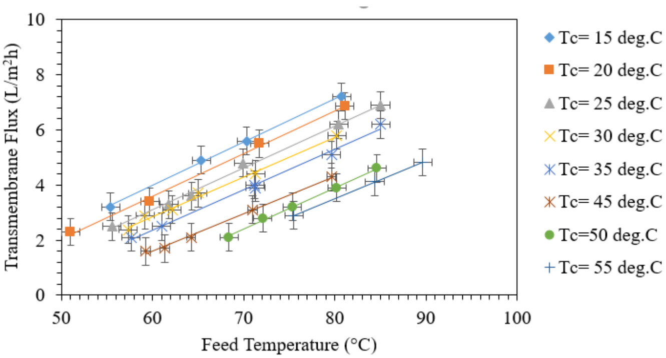

Figure 5.4 Effect of MD feed and coolant temperatures (T_f and T_c) on transmembrane flux considering constant MD feed and coolant flow rate of 20 L/min.

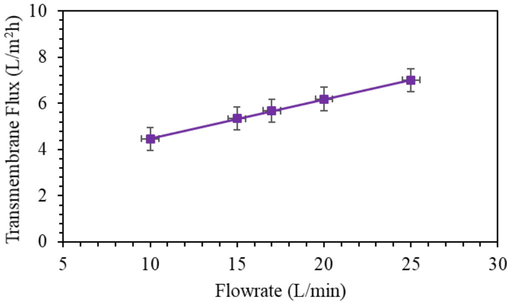

Figure 5.5 Effect of MD feed and coolant flow rates on transmembrane flux considering constant MD feed temperature of 80°C and coolant flow rate of 25°C.

<u>Energy analysis</u>

Figure 5.6 shows the effect of various feed and coolant temperatures at specific thermal energy demand of a single module of the Xzero pilot-plant. The results show that the specific thermal energy demand varied between 450-1000 kWh/m^3 when the feed temperatures were increased from 50°C to 90°C, and coolant temperatures ranged between 15°C to 55°C (at constant feed and coolant flow rates of 20 L/min, each). The higher specific thermal energy demand was primarily subjected to the higher temperature drop of the feed stream across the MD module (at elevated feed temperature) and the lower amount of permeate produced (at higher coolant temperature). Figure 5.7 reveals that the net thermal energy demand showed a similar trend at elevated coolant temperature with constant feed temperature, owing to lower product yield. However, it conferred the opposite direction for higher feed temperatures at fixed coolant temperatures due to the increased heat transfer rate to the coolant. The minimum net thermal energy demand was about 17 kWh/m^3, considering feed to coolant temperature difference of 65°C, and MD feed and coolant flow rates of 20 L/min each. Moreover, it was

found that the specific electrical energy demand varies from 0.05 kWh/m^3 to 0.22 kWh/m^3, depending upon the MD feed flow rates.

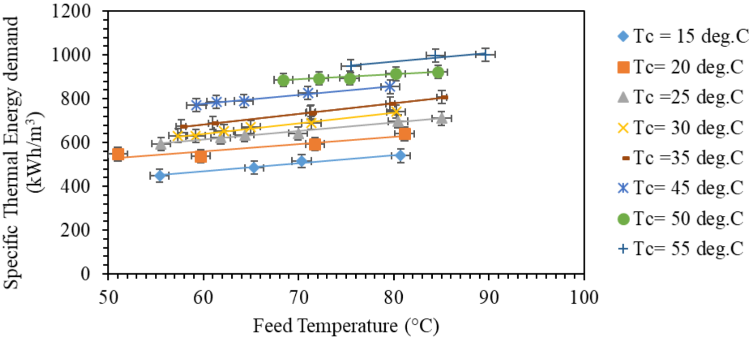

Figure 5.6 Effect of MD feed and coolant temperatures (T_f and T_c) on specific thermal energy demand considering constant MD feed and coolant flow rates of 20 L/min.

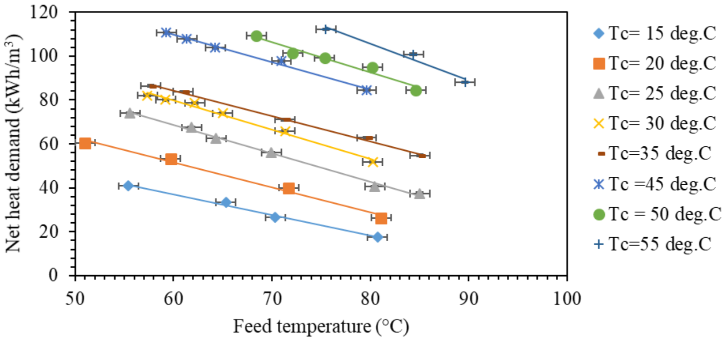

Figure 5.7 Effect of MD feed and coolant temperatures (T_f and T_c) on net heat demand considering constant MD feed and coolant flow rates of 20 L/min.

5.3 Integrated large-scale systems

The principal challenge in managing an industrial-scale MD system is addressing its relatively high thermal energy demand. In CHP facilities, one possibility is to employ DH network lines to operate the large-scale MD system for advanced flue gas condensate treatment. In this study, simulations have been performed for the MD plant capacity of 100 m^3/h (matching the flue gas condensate amount released from Högdalen CHP facility) while analyzing two different thermal integrations. In case 1, the DH supply line of temperature 95°C is adopted as a heat source, while the DH return line of 40°C is taken as a heat sink for the MD system. In case 2, the DH return line of 60°C is employed for heating the MD feed whereas, an external cooling source of 10°C, i.e., municipal water or water from the cooling tower, is selected as a heat sink. Figure 5.8 a and b present the proposed semi-batch process configurations of the DH-MD systems for cleaning flue gas condensate in CHP facilities while considering acid neutralization as the only considered pretreatment method. The assumptions for designing the process are the same, as mentioned in section 4.2. For improved energy efficiency, cascading of every two MD modules was assumed. The design supported the concentrate to recycle back to the system to enhance the extent of water recovery. When the concentration limit was achieved, it was supposed that the concentrate was purged from the system to satisfy the safety controls.

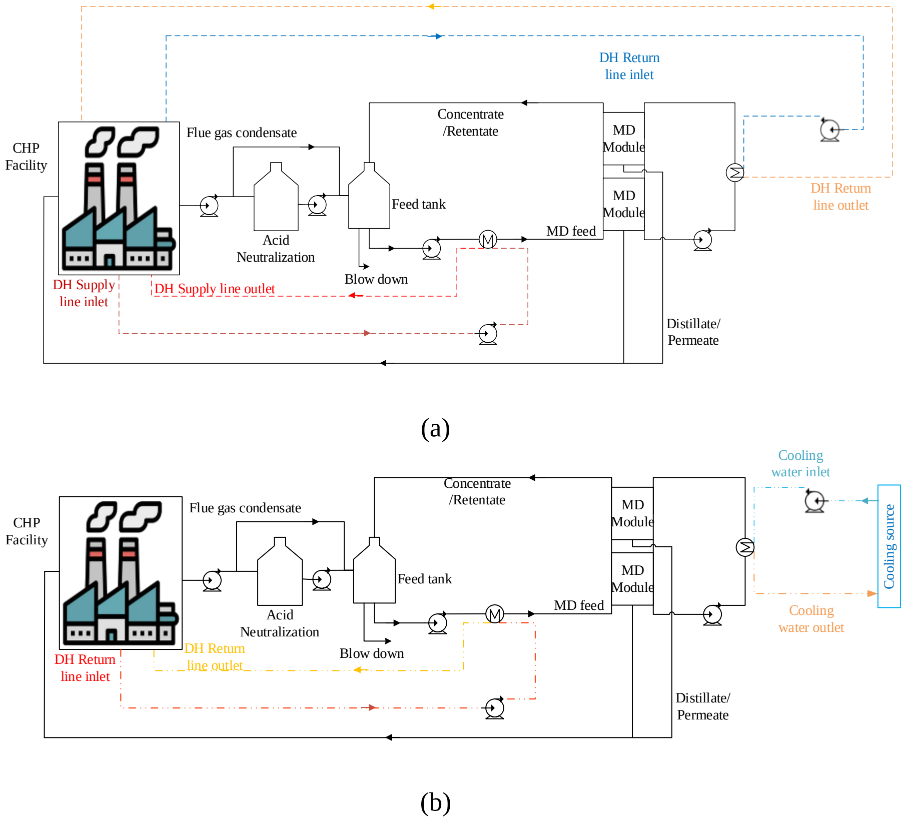

Figure 5.8 Flow diagrams of the proposed industrial-scale DH-MD integrated systems; (a) scheme for case 1 (DH supply line as a heat source and DH return line as a heat sink), (b) scheme for case 2 (DH return line as a heat source and other cooling sources as a heat sink).

Table 5.5 compiles the outcomes of the studied configurations of the DH-MD system for flue gas condensate treatment. The estimates show that for case 1, the transmembrane flux was relatively higher due to elevated feed temperatures and the higher temperature difference between feed and coolant. Moreover, in case 1, the total thermal power demand was nearly 102 MW, where 83% of the total was transferred to the DH return line; consequently, the net thermal power consumption was only 18 MW. In comparison, the transmembrane flux was reduced up to 1.6 times in case 2, and there was no option available for heat recovery. As a result, the net thermal power consumption in case 2 was relatively higher, i.e., 46.5 MW.

Table 5.5 Estimated parameters for considered cases of integrated MD system.

Parameters	Case1		Case 2	
	MD1	MD2	MD1	MD2
MD feed inlet temperature (°C)	90	80.9	55	52.7
Feed outlet/concentrate temperature (°C)	80.9	74.8	52.7	50.8
Coolant inlet temperature (°C)	45	52.8	15	17.9
Coolant outlet temperature (°C)	52.8	58.3	17.3	19.1
Average transmembrane flux (L/m^2h)	4.78		2.91	
Total specific heat demand (kWh/m^3)*	1020		464	
Total thermal power demand (MW)*ʃ	102		46.5	
Net thermal power consumption (MW)*ʃ	17.7		46.5	

*Initial flue gas condensate temperature of 25 °C and cascading of two MD modules were considered.
ʃMD system of capacity 100 m^3/h was selected.

Depending upon the results mentioned above, the required membrane area and the total count of MD modules were estimated for each case. In case 1, owing to relatively higher transmembrane flux, the number of necessary MD modules was lesser compared to case 2. Similarly, the required heat exchanger area was 1.6 times higher in case 2, linked to the higher MD feed flow rate to realize the target capacity of the system. The number of pumps and the amount of cooling water was also estimated by matching the flow rates for both configurations of the system. It is assumed that all the raw flue gas condensate needs to be treated before its introduction to the MD system. The outcomes of the equipment design are presented in Table 5.6.

Table 5.6 Design specification of industrial-scale integrated MD system for both cases

Components	Specifications	
	Case 1	Case 2
MD modules	N=9084	N=14921
Membranes	Area = 20894 m^2	Area = 34319 m^2
Heat exchangers	N= 2, Heat transfer area = 25315 m^2	N= 2, Heat transfer area = 41580 m^2
Pumps	Capacity 5500 m^3/h, N=4 Capacity 100 m^3/h, N=2	Capacity 9000 m^3/h, N=4 Capacity 100 m^3/h, N=2
Raw material	Amount	
40% concentrated sulfuric acid	800 m^3/year	800 m^3/year
Cooling water	-	72 Mm^3/year

5.4 Economic assessment

Based on the technical requirements, the process economy of the proposed large-scale DH-MD systems was determined, where the ultimate measure is unit clean condensate cost. The outcomes show that MD modules and heat exchangers are the two principal components of the capital investment, which were responsible for 87 % of the total equipment cost. On the other hand, utilities (thermal energy and cooling water) are the leading players in annual operating and maintenance costs and have 98% shares in both cases. The comparison of annual capital investment shows that choosing the configuration of case 1 over case 2 can result in a yearly potential cost reduction of approximately 0.5 M$. Moreover, when normalized thermal energy cost is considered, it is found that case 1 is accountable for 13.6 $/m^3, whereas case 2 is responsible for 35.8 $/m^3. These values represent the importance of choosing different heat source and sink options. Thus, case 1 is a preferable configuration while considering the unit water treatment cost. Table 5.7 summarizes annual expenditures and unit clean condensate cost while considering the DH-MD system of capacity 100 m^3/h.

Table 5.7 Process economy of industrial-scale MD system for water recovery from flue gas condensate in cogeneration plants of capacity 100 m^3/h.

Economic Parameters	Case 1	Case 2
CAPEX, M$	13.8	20.4
Annual CAPEX, M$	1.1	1.6
Annual heat cost, M$	10.9	28.6
Annual OPMEX, M$	11.1	30.3
Normalized CAPEX, $/m^3	1.4	2.05
Normalized OPMEX, $/m^3	13.8	37.8
Clean condensate cost, $/m^3	15.2	39.8

Moreover, the effect of various techno-economic parameters on unit clean condensate cost was also determined. Figure 5.9 exhibits the sensitivity of unit clean condensate cost while changing different techno-economic parameters. Among all the examined technical factors, it was found that plant life and plant capacity were two parameters that have affected the clean condensate cost. For decreasing the plant life by half (10 years), the estimated clean condensate cost was increased by 6% for case 1 and 3.5% for case 2. In contrast, an increase in plant capacity up to 50% reduces the clean condensate cost only by 1 % for case 1 and 4% for case 2. It is noteworthy that the clean condensate cost is very susceptible to thermal energy costs; therefore, when the thermal energy cost decreases by half, the clean condensate cost is reduced by almost 45% for both configurations. However, when the MD module' cost is reduced by half (3000 $/unit), the clean condensate cost can only be varied by a maximum of 3-4%. Considering the interest rate, when it becomes double, the clean condensate cost increases up to 2.5% for case 1 and 1.1% for case 2. Furthermore, the clean condensate cost was merely affected by variations of heat exchanger prices, membrane replacement frequency, membrane price and pretreatment extent.

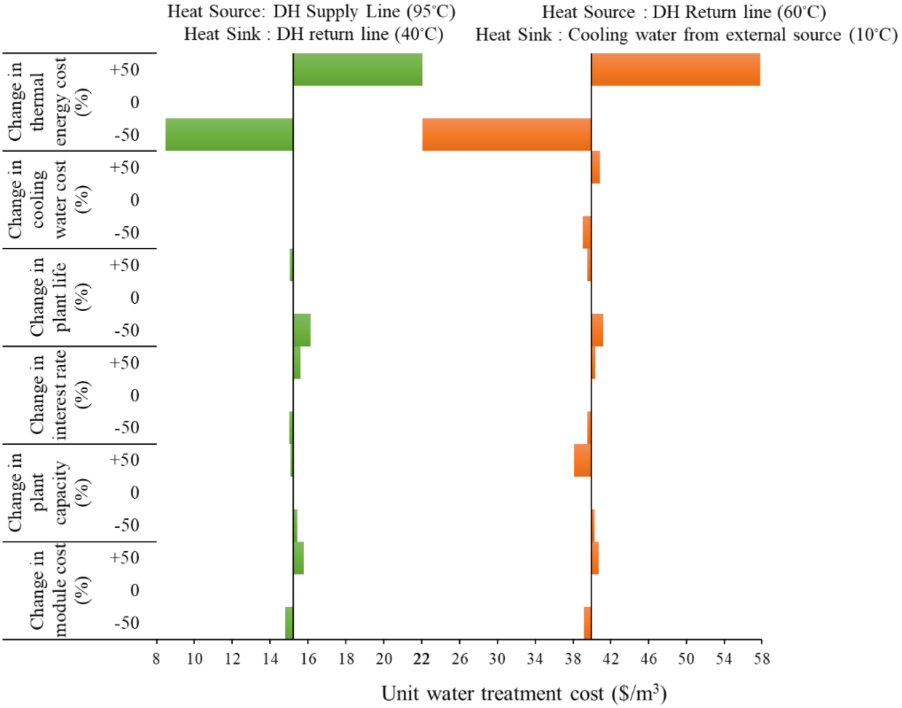

Figure 5.9 Sensitivity analysis of clean condensate cost for different techno-economic parameters

As mentioned above, plant capacity hardly changes the unit clean condensate cost. However, it can significantly affect the operation of the MD system in terms of its thermal power demand, as shown in Figure 5.10. Due to the practical limitation of the use of locally produced district heating, a boundary line is needed to define, i.e., only 10% of total locally produced district heating can be employed for operating the MD system for flue gas condensate treatment in CHP plants. This limit can determine the feasible plant capacity to reach the thermal power balance (linked to DH supply-MD demand) for both thermal integration options. For example, Hödgalen produces 2174 GWh of heat yearly; based on its 10%, the limit for MD plant capacity can be up to 150 m^3/h while considering the configuration of case 1. In contrast, this value is reduced to almost 2.5 times when case 2 is considered. For Bristaverket, where total heat generation is 1253 GWh, case 1 seems practical for up to 80 m^3/h; however, for case 2, the maximum MD capacity can only be around 35 m^3/h.

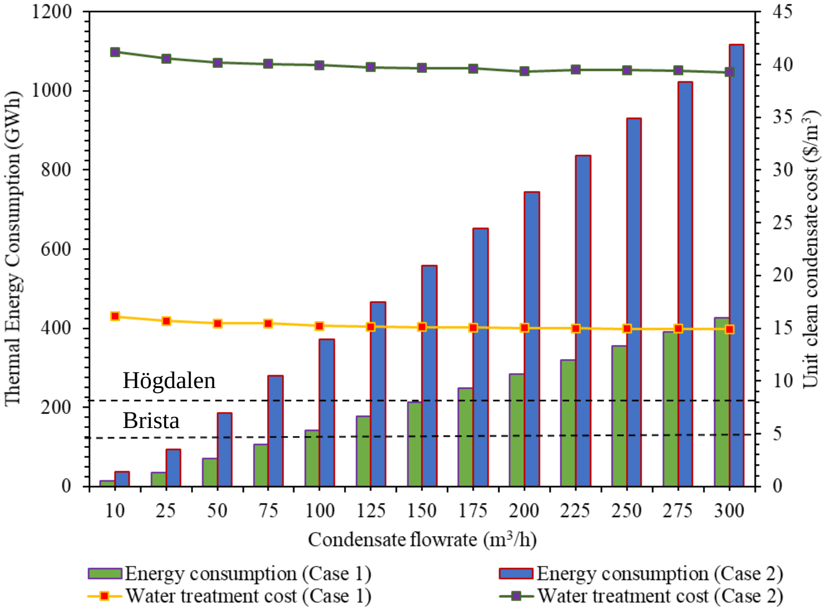

Figure 5.10 Annual district heating energy consumption for flue gas condensate cleaning using the MD system

It is noteworthy to mention that this study has considered a conservative approach when taking the district heating price (77 \$/MWh, retail price); however, the actual DH production cost may vary from 5-15 \$/MWh. In the latter condition, the flue gas condensate treatment cost in case 1 can be reduced up to 2.43 $\$/m^3$, with the normalized operational cost of ~0.8 $\$/m^3$ comparable to the cost for RO based treatment [223]. Furthermore, in waste-fired CHP plants, case 1 configuration would incur an added fuel (MSW) volume, which in turn leads to the economic benefit of MSW power plant and, at a larger scale, to environmental benefit. However, handling Cd accounts for an additional 0.5 $\$/m^3$ to 4 $\$/m^3$ for adsorption. This cost includes adsorbent, sludge treatment, and electricity costs [237].

5.5 Concluding remarks

This chapter presented the performance of membrane distillation (MD) technology for advanced flue gas condensate treatment in combined heat and power plants, with the Högdalenverket and Bristaverket facilities selected for experimental campaigns at the laboratory and pilot-scale. Considering the separation efficiencies and quality of permeate, the findings reveal that the MD based system is well suited for the waste-fired CHP facilities. The need for pretreatment (acid-neutralization) mainly depends on the ammonia content in MD feed. Compared to the performance of the existing RO based treatment system, the MD treated permeate quality was improved, i.e., a higher number of elements showed concentrations under detection limits; lower heavy metals concentrations were observed; lower levels of ammonium were obtained; and lower values of conductivity, alkalinity and TDS were maintained. During the reconcentration study, more than 92% of the water was recovered, and removal efficiency remained high, except for cadmium and zinc in some tests. For the biofuel-fired CHP facility, the high-quality permeate can be achieved according to strict environmental regulations with the mixing of the permeates of raw and neutralized flue gas condensates. The issue of cadmium can be resolved using existing ion exchangers. The parametric study shows that the thermal specific heat demand of a single module of the Xzero pilot plant varies between 400-1000 kWh/m^3, depending on MD feed and coolant temperatures. The technical analysis of the industrial-scale MD system of capacity 100 m^3/h tells that the annual thermal energy consumption can be approximately 140 GWh, when district heating supply and return lines are used to operate the MD system as the heat source and sink, respectively. Process economy evaluation determines that the expected unit clean condensate cost can be as low as 2.5 \$/m^3 for the system, as mentioned above.

Chapter 6 Conclusion and future work

In this thesis, the potential of waste heat driven membrane distillation systems has been explored in terms of their techno-economic feasibility, covering applications in two major water-intensive industries, nano-electronics facilities and cogeneration plants. The techno-economic evaluation of these systems embodied the principal research objective.

In nano-electronics facilities, the main purpose was to remove pollutants from the effluent streams of photolithography and chemical mechanical planarization processes. The analysis of the photolithography wastewater has determined the presence of four key contaminants: tetramethylammonium hydroxide (TMAH), hydrogen peroxide, ammonium hydroxide and hydrogen fluoride. A sequence of catalytic reduction (to decompose hydrogen peroxide), acid neutralization (to avoid ammonia slip) and membrane distillation process (to separate non-volatiles) was used to remove the mentioned substances to acceptable limits except for fluoride, which can be efficiently handled using strong alkali resins. Since TMAH has a thermal degradation temperature above 65°C, the MD feed temperature should be prudently chosen. For the chemical mechanical planarization wastewater, the primary contaminants were nano-sized silica and alumina particles, and copper; however, the analysis determined that along with key pollutants, ammonium hydroxide was also present. The combination of acid neutralization and membrane distillation provided complete removal of all analyzed contaminants. Thus, disposing of the MD treated wastewater into recipient water bodies is acceptable under EU Directive 91/271/EEC concerning urban wastewater treatment and can also be reused further in cooling towers, wet scrubbers and other facilities.

In cogeneration plants, advanced cleaning of flue gas condensate for water recovery was investigated considering municipal solid waste and biofuel-fired boilers. The raw flue gas condensate was mainly an aqueous mixture of heavy metals, salts, acids and particulate solids. The investigation of the integrated acid neutralization-membrane distillation process exhibited encouraging results in terms of the complete removal of the analyzed contaminants, except for cadmium in a few runs. The reconcentration study determined that the volume of tested flue gas condensate was reduced by 12.5 times, and more than 90% of clean water could be recovered for further reuse as boiler feed water. The proposed approach pointed out that it is technically expedient to partially offload the RO based cleaning processes with membrane distillation based processes.

The parametric study presented that product yield and specific thermal energy demand fluctuated with varying feed and coolant temperatures and flow rates. Product yield could be enhanced by increasing the driving forces, primarily feed temperature and feed to coolant temperature difference. In contrast, at elevated feed and coolant temperatures, a less energy-efficient process is observed. Compared with pilot plant trials, the laboratory prototype showed comparatively higher specific thermal energy demand due to the absence of an internal heat recovery system. The specific electrical energy demand was directly proportional to the flow rates and pressure drop across the MD modules. Moreover, the exergy analysis determined that more customized membrane materials, proper insulation and improved condensation plates design can optimize the performance of MD systems.

For large-scale systems, the critical test is to satisfy the high thermal energy demand of the MD systems. The waste heat released from the nano-electronics industries and district heating generated by the CHP plants were found adequate to perform the necessary operation for treating local effluent streams, i.e., wastewaters or flue gas condensate. Different thermal integrations schemes for MD systems were compared and categorized based on their technical feasibility and origin of considered heat sources/sinks. These schemes could also improve sustainability and help reduce carbon dioxide emissions. Therefore, they may recognize twofold benefit systems in environmental perspectives.

Finally, the detailed economic model was developed for new and retrofitted industrial-scale MD facilities. For capital investment, MD modules were shown as key contributors, whereas, in the operating expenses, the thermal energy cost took the lead when no free heat is available. This indicates that any advancement in system design that focuses on improving the MD modules’ performance while minimizing the thermal energy demand will eventually magnify the economic superiority of such applications. In supplement to financial gains, a zero liquid discharge scenario could also be realized with the MD technology. The final check was the unit water treatment cost. The estimate of unit water treatment cost showed that the proposed processes for specific applications are economically viable compared to current practices when the thermal energy cost is negligible.

In summation, membrane distillation presents technical, environmental and economic advantages for the examined applications. These findings add to a growing body of literature on membrane distillation industrial applications. Moreover, this study provides a paradigm for related applications of membrane distillation in the future. Furthermore, installing such MD systems in the respective industries would lead to lower freshwater use while reducing wastewater pollution and reusing the recovered water.

6.1 Future work

Though the studied methods proved promising, there may still be limitations on the resource side, i.e., availability of local waste heat sources (associated with managing heat recovery for handling the locally generated effluent). Therefore, for practical implementations of the proposed systems, the analysis should be extended to incorporate operational factors of the particular industry and their corresponding influence on available thermal energy and wastewater treatment. Proper business models for these projects have not been presented in this work but would support further analysis. Investigation of dynamic aspects of proposed thermal integrations would be a reasonable extension of this study, which may provide a better understanding of system performance and how the proposed approaches can be optimized in techno-economic terms. Moreover, other thermal integration options should be studied, such as steam extraction from turbines to operate the MD system in CHP plants. In nano-electronics industries, an integrated approach to treat combined (all in one) wastewater streams, while using the available waste-heat sources, needs to be further studied. More investigations would be required to examine the performance of a large-scale MD system installed in-field (for managing continuous input of wastewater). Additionally, the improvement in existing MD units (including module structure, membrane material and condensation plate material) is required for operating the industrial-scale MD system more efficiently. Furthermore, the suggested post-treatments would need to be appropriately investigated in combination with analyzed methods. The repercussions of the fouling and concentrate disposal can be other concerning issues. Beyond this, a detailed life cycle assessment of the proposed systems should be performed.

References

[1] "Aquastat Main Database," *Food and Agriculture Organization of the United Nations (FAO)*, 2016. [Online]. Available: http://www.fao.org/nr/water/aquastat/data/query/index.html. [Accessed: 04-Sep-2020].

[2] M. Palaniappan *et al.*, "Clearing the waters: a focus on water quality solutions," United Nations Environment Programme, Nairobi, ISBN: 978-92-807-3074-6, 2010.

[3] T. Luo, R. Young, and P. Reig, "Ranking the World's Most Water-Stressed Countries in 2040," *World Resources Institute*, 2015. [Online]. Available: https://www.wri.org/blog/2015/08/ranking-world-s-most-water-stressed-countries-2040.

[4] United States Environmental Protection Agency, "Water Use and Water Waste at Industrial Facilities." [Online]. Available: https://www.epa.gov/sustainability/lean-water-toolkit-chapter-2. [Accessed: 05-Jul-2020].

[5] M. S. Branham, "Semiconductors and Sustainability : Energy and Materials Use in Integrated Circuit Manufacturing," Masters Thesis Report, Massachusetts Institute of Technology, 2008.

[6] T. J. Feeley *et al.*, "Water: A critical resource in the thermoelectric power industry," *Energy*, vol. 33, no. 1, pp. 1–11, Jan. 2008.

[7] K. Kylhammar, "Comparative Evaluation of Membrane Based Condensate Treatment Systems for Biomass-fired CHP Plants," Masters Thesis Report, Lund University, 2018.

[8] K. Ohanessian *et al.*, "Dead-end and crossflow ultrafiltration process modelling: Application on chemical mechanical polishing wastewaters," *Chem. Eng. Res. Des.*, vol. 158, pp. 164–176, Jun. 2020.

[9] L.-C. Juang, D.-H. Tseng, H.-Y. Lin, C.-K. Lee, and T.-M. Liang, "Treatment of Chemical Mechanical Polishing Wastewater for Water Reuse by Ultrafiltration and Reverse Osmosis Separation," *Environ. Eng. Sci.*, vol. 25, no. 7, pp. 1091–1098, Aug. 2008.

[10] N. P. Cheremisinoff, "Membrane Separation Technologies," in *Handbook of Water and Wastewater Treatment Technologies*, Elsevier, 2002, pp. 335–

371.

[11] M. Khayet and T. Matsuura, *Membrane Distillation: Principles and Applications*. Elsevier, 2011.

[12] A. Deshmukh *et al.*, “Membrane distillation at the water-energy nexus: limits, opportunities, and challenges,” *Energy Environ. Sci.*, vol. 11, no. 5, pp. 1177–1196, Mar. 2018.

[13] B. R. Bodell, “Distillation of saline water using silicone rubber membrane,” US3361645A, 1963.

[14] P. K. Weyl, “Recovery of demineralized water from saline waters,” US3340186A, 1967.

[15] M. E. Findley, “Vaporization through Porous Membranes,” *Ind. Eng. Chem. Process Des. Dev.*, vol. 6, no. 2, pp. 226–230, Apr. 1967.

[16] M. Gryta, M. Tomaszewska, and K. Karakulski, “Wastewater treatment by membrane distillation,” *Desalination*, vol. 198, no. 1–3, pp. 67–73, Oct. 2006.

[17] K. W. Lawson and D. R. Lloyd, “Membrane distillation,” *J. Memb. Sci.*, vol. 124, no. 1, pp. 1–25, Feb. 1997.

[18] A. M. Alklaibi and N. Lior, “Membrane-distillation desalination: Status and potential,” *Desalination*, vol. 171, no. 2, pp. 111–131, Jan. 2005.

[19] A. Ali, R. A. Tufa, F. Macedonio, E. Curcio, and E. Drioli, “Membrane technology in renewable-energy-driven desalination,” *Renew. Sustain. Energy Rev.*, vol. 81, pp. 1–21, Jan. 2018.

[20] E. Curcio and E. Drioli, “Membrane Distillation and Related Operations—A Review,” *Sep. Purif. Rev.*, vol. 34, no. 1, pp. 35–86, Jan. 2005.

[21] E. Drioli, A. Ali, and F. Macedonio, “Membrane distillation: Recent developments and perspectives,” *Desalination*, vol. 356, pp. 56–84, Jan. 2015.

[22] M. S. El-Bourawi, Z. Ding, R. Ma, and M. Khayet, “A framework for better understanding membrane distillation separation process,” *J. Memb. Sci.*, vol. 285, no. 1–2, pp. 4–29, Nov. 2006.

[23] A. Alkhudhiri, N. Darwish, and N. Hilal, “Membrane distillation: A comprehensive review,” *Desalination*, vol. 287, pp. 2–18, Feb. 2012.

[24] M. Khayet, “Solar desalination by membrane distillation: Dispersion in energy consumption analysis and water production costs (a review),” *Desalination*, vol. 308, pp. 89–101, Jan. 2013.

[25] M. Khayet, “Membranes and theoretical modeling of membrane distillation: A review,” *Adv. Colloid Interface Sci.*, vol. 164, no. 1–2, pp. 56–88, May 2011.

[26] P. Wang and T.-S. Chung, “Recent advances in membrane distillation processes: Membrane development, configuration design and application exploring,” *J. Memb. Sci.*, vol. 474, pp. 39–56, Jan. 2015.

[27] N. Thomas, M. O. Mavukkandy, S. Loutatidou, and H. A. Arafat, “Membrane distillation research & implementation: Lessons from the past five decades,” *Sep. Purif. Technol.*, vol. 189, pp. 108–127, Dec. 2017.

[28] F. Tibi, A. Charfi, J. Cho, and J. Kim, “Fabrication of polymeric membranes for membrane distillation process and application for wastewater treatment: Critical review,” *Process Saf. Environ. Prot.*, vol. 141, pp. 190–201, Sep. 2020.

[29] B. Jiao, A. Cassano, and E. Drioli, “Recent advances on membrane processes for the concentration of fruit juices: a review,” *J. Food Eng.*, vol. 63, no. 3, pp. 303–324, Aug. 2004.

[30] V. Belessiotis, S. Kalogirou, and E. Delyannis, “Membrane Distillation,” in *Thermal Solar Desalination*, Elsevier, 2016, pp. 191–251.

[31] R. S and Z. H, “Modelisation of Membrane Distillation: Mass and Heat Transfer in Air Gap Membrane Distillation,” *J. Membr. Sci. Technol.*, vol. 6, no. 2, pp. 1–9, Jun. 2016.

[32] C. Cabassud and D. Wirth, “Membrane distillation for water desalination: How to chose an appropriate membrane?,” *Desalination*, vol. 157, no. 1–3, pp. 307–314, Aug. 2003.

[33] L. Eykens, K. De Sitter, C. Dotremont, L. Pinoy, and B. Van der Bruggen, “How To Optimize the Membrane Properties for Membrane Distillation: A Review,” *Ind. Eng. Chem. Res.*, vol. 55, no. 35, pp. 9333–9343, Sep. 2016.

[34] M. Mahdi, A. Shirazi, and A. Kargari, “A Review on Applications of Membrane Distillation (MD) Process for Wastewater Treatment,” *J. Membr. Sci. Res.*, vol. 1, no. 3, pp. 101–112, Oct. 2015.

[35] S. Roy, M. Bhadra, and S. Mitra, “Enhanced desalination via functionalized carbon nanotube immobilized membrane in direct contact membrane distillation,” *Sep. Purif. Technol.*, vol. 136, pp. 58–65, Nov. 2014.

[36] L. D. Tijing *et al.*, “Superhydrophobic nanofiber membrane containing carbon nanotubes for high-performance direct contact membrane distillation,” *J. Memb. Sci.*, vol. 502, pp. 158–170, Mar. 2016.

[37] J.-G. Lee *et al.*, “Theoretical modeling and experimental validation of transport and separation properties of carbon nanotube electrospun membrane distillation,” *J. Memb. Sci.*, vol. 526, pp. 395–408, Mar. 2017.

[38] H. Ramlow, R. K. M. Ferreira, C. Marangoni, and R. A. F. Machado, “Ceramic membranes applied to membrane distillation: A comprehensive review,” *Int. J. Appl. Ceram. Technol.*, vol. 16, no. 6, pp. 2161–2172, Nov. 2019.

[39] F. Liu, N. A. Hashim, Y. Liu, M. R. M. Abed, and K. Li, “Progress in the production and modification of PVDF membranes,” *J. Memb. Sci.*, vol. 375, no. 1–2, pp. 1–27, Jun. 2011.

[40] J. Zhang, J.-D. Li, and S. Gray, “Effect of applied pressure on performance of PTFE membrane in DCMD,” *J. Memb. Sci.*, vol. 369, no. 1–2, pp. 514–525, Mar. 2011.

[41] H. J. Hwang, K. He, S. Gray, J. Zhang, and I. S. Moon, “Direct contact membrane distillation (DCMD): Experimental study on the commercial PTFE membrane and modeling,” *J. Memb. Sci.*, vol. 371, no. 1–2, pp. 90–98, Apr. 2011.

[42] L. Camacho *et al.*, “Advances in Membrane Distillation for Water Desalination and Purification Applications,” *Water*, vol. 5, no. 1, pp. 94–196, Jan. 2013.

[43] D. Hou, H. Fan, Q. Jiang, J. Wang, and X. Zhang, “Preparation and characterization of PVDF flat-sheet membranes for direct contact membrane distillation,” *Sep. Purif. Technol.*, vol. 135, pp. 211–222, Oct. 2014.

[44] S. Munirasu, F. Banat, A. A. Durrani, and M. A. Haija, “Intrinsically superhydrophobic PVDF membrane by phase inversion for membrane distillation,” *Desalination*, vol. 417, pp. 77–86, Sep. 2017.

[45] N. Peng *et al.*, “Evolution of polymeric hollow fibers as sustainable technologies: Past, present, and future,” *Prog. Polym. Sci.*, vol. 37, no. 10, pp. 1401–1424, Oct. 2012.

[46] S. Zare and A. Kargari, “Membrane properties in membrane distillation,” in *Emerging Technologies for Sustainable Desalination Handbook*, Elsevier, 2018, pp. 107–156.

[47] Y. M. Manawi, M. Khraisheh, A. K. Fard, F. Benyahia, and S. Adham, “Effect of operational parameters on distillate flux in direct contact membrane distillation (DCMD): Comparison between experimental and model predicted performance,” *Desalination*, vol. 336, no. 1, pp. 110–120, Mar. 2014.

[48] S. Cerneaux, I. Strużyńska, W. M. Kujawski, M. Persin, and A. Larbot, “Comparison of various membrane distillation methods for desalination using hydrophobic ceramic membranes,” *J. Memb. Sci.*, vol. 337, no. 1–2, pp. 55–60, Jul. 2009.

[49] Z. Xie, T. Duong, M. Hoang, C. Nguyen, and B. Bolto, “Ammonia removal by sweep gas membrane distillation,” *Water Res.*, vol. 43, no. 6, pp. 1693–1699, Apr. 2009.

[50] M. . García-Payo, C. . Rivier, I. . Marison, and U. von Stockar, “Separation of binary mixtures by thermostatic sweeping gas membrane distillation,” *J. Memb. Sci.*, vol. 198, no. 2, pp. 197–210, Apr. 2002.

[51] L. Francis, N. Ghaffour, A. A. Alsaadi, and G. L. Amy, “Material gap membrane distillation: A new design for water vapor flux enhancement,” *J. Memb. Sci.*, vol. 448, pp. 240–247, Dec. 2013.

[52] F. He, J. Gilron, and K. K. Sirkar, “High water recovery in direct contact membrane distillation using a series of cascades,” *Desalination*, vol. 323, pp. 48–54, Aug. 2013.

[53] J. H. Hanemaaijer, “Memstill® — low cost membrane distillation technology for seawater desalination,” *Desalination*, vol. 168, p. 355, Aug. 2004.

[54] D. Woldemariam, A. Kullab, U. Fortkamp, J. Magner, H. Royen, and A. Martin, “Membrane distillation pilot plant trials with pharmaceutical residues and energy demand analysis,” *Chem. Eng. J.*, vol. 306, pp. 471–483, Dec. 2016.

[55] W. Heinzl, S. Büttner, and G. Lange, “Industrialized modules for MED Desalination with polymer surfaces,” *Desalin. Water Treat.*, vol. 42, no. 1–3, pp. 177–180, Apr. 2012.

[56] M. Burhan, M. W. Shahzad, D. Ybyraiymkul, S. J. Oh, N. Ghaffour, and K. C. Ng, “Performance investigation of MEMSYS vacuum membrane distillation system in single effect and multi-effect mode,” *Sustain. Energy Technol. Assessments*, vol. 34, pp. 9–15, Aug. 2019.

[57] O. R. Lokare, S. Tavakkoli, V. Khanna, and R. D. Vidic, “Importance of feed recirculation for the overall energy consumption in membrane distillation systems,” *Desalination*, vol. 428, pp. 250–254, Feb. 2018.

[58] D. González, J. Amigo, and F. Suárez, “Membrane distillation: Perspectives for sustainable and improved desalination,” *Renew. Sustain. Energy Rev.*, vol. 80, pp. 238–259, Dec. 2017.

[59] J.-G. Lee, W.-S. Kim, J.-S. Choi, N. Ghaffour, and Y.-D. Kim, “Dynamic solar-powered multi-stage direct contact membrane distillation system: Concept design, modeling and simulation,” *Desalination*, vol. 435, pp. 278–292, Jun. 2018.

[60] G. Zaragoza, A. Ruiz-Aguirre, and E. Guillén-Burrieza, “Efficiency in the use of solar thermal energy of small membrane desalination systems for decentralized water production,” *Appl. Energy*, vol. 130, pp. 491–499, Oct. 2014.

[61] A. Chafidz, E. D. Kerme, I. Wazeer, Y. Khalid, A. Ajbar, and S. M. Al-Zahrani, “Design and fabrication of a portable and hybrid solar-powered membrane distillation system,” *J. Clean. Prod.*, vol. 133, pp. 631–647, Oct. 2016.

[62] R. G. Raluy, R. Schwantes, V. J. Subiela, B. Peñate, G. Melián, and J. R. Betancort, “Operational experience of a solar membrane distillation demonstration plant in Pozo Izquierdo-Gran Canaria Island (Spain),” *Desalination*, vol. 290, pp. 1–13, Mar. 2012.

[63] M. Asim, M. Imran, M. K. H. Leung, N. T. Uday Kumar, A. R. Martin, and

F. Kashif, “Experimental analysis of solar thermal integrated MD system for cogeneration of drinking water and hot water for single family villa in Dubai using flat plate and evacuated tube solar collectors,” *Desalin. WATER Treat.*, vol. 92, pp. 46–59, Oct. 2017.

[64] Y. Wang, Z. Xu, N. Lior, and H. Zeng, “An experimental study of solar thermal vacuum membrane distillation desalination,” *Desalin. Water Treat.*, pp. 1–11, Jun. 2014.

[65] G. Mohan, U. Kumar, M. K. Pokhrel, and A. Martin, “A novel solar thermal polygeneration system for sustainable production of cooling, clean water and domestic hot water in United Arab Emirates: Dynamic simulation and economic evaluation,” *Appl. Energy*, vol. 167, pp. 173–188, Apr. 2016.

[66] K. Nakoa, K. Rahaoui, A. Date, and A. Akbarzadeh, “An experimental review on coupling of solar pond with membrane distillation,” *Sol. Energy*, vol. 119, pp. 319–331, Sep. 2015.

[67] F. Suárez and R. Urtubia, “Tackling the water-energy nexus: an assessment of membrane distillation driven by salt-gradient solar ponds,” *Clean Technol. Environ. Policy*, vol. 18, no. 6, pp. 1697–1712, Aug. 2016.

[68] K. Rahaoui *et al.*, “Sustainable Membrane Distillation Coupled with Solar Pond,” *Energy Procedia*, vol. 110, pp. 414–419, Mar. 2017.

[69] M. R. Qtaishat and F. Banat, “Desalination by solar powered membrane distillation systems,” *Desalination*, vol. 308, pp. 186–197, Jan. 2013.

[70] A. Chafidz, S. Al-Zahrani, M. N. Al-Otaibi, C. F. Hoong, T. F. Lai, and M. Prabu, “Portable and integrated solar-driven desalination system using membrane distillation for arid remote areas in Saudi Arabia,” *Desalination*, vol. 345, pp. 36–49, Jul. 2014.

[71] F. E. Ahmed, R. Hashaikeh, and N. Hilal, “Solar powered desalination – Technology, energy and future outlook,” *Desalination*, vol. 453, pp. 54–76, Mar. 2019.

[72] B. Tomaszewska *et al.*, “Use of low-enthalpy and waste geothermal energy sources to solve arsenic problems in freshwater production in selected regions of Latin America using a process membrane distillation – Research into model solutions,” *Sci. Total Environ.*, vol. 714, p. 136853, Apr. 2020.

[73] R. Sarbatly and C.-K. Chiam, “Evaluation of geothermal energy in

desalination by vacuum membrane distillation," *Appl. Energy*, vol. 112, pp. 737–746, Dec. 2013.

[74] F. Y. C. Huang, L. Laumbach, R. Reprogle, and C. Medin, "Geothermal Membrane Distillation in Industrial Greenhouse Applications: Membrane Fabrication and Characterization," *Environ. Eng. Sci.*, vol. 35, no. 8, pp. 815–828, Aug. 2018.

[75] S. Bouguecha and M. Dhahbi, "Fluidised bed crystalliser and air gap membrane distillation as a solution to geothermal water desalination," *Desalination*, vol. 152, no. 1–3, pp. 237–244, Feb. 2003.

[76] S. Bouguecha, B. Hamrouni, and M. Dhahbi, "Small scale desalination pilots powered by renewable energy sources: case studies," *Desalination*, vol. 183, no. 1–3, pp. 151–165, Nov. 2005.

[77] A. Mahmoudi, M. Fazli, and M. R. Morad, "A recent review of waste heat recovery by Organic Rankine Cycle," *Appl. Therm. Eng.*, vol. 143, pp. 660–675, Oct. 2018.

[78] C. Liu and A. Martin, "Applying membrane distillation in high purity water production for semiconductor industry," *Ultrapure Water*, vol. 23, no. 3, pp. 32–38, Apr. 2006.

[79] C. W. Morrow, B. P. Dwyer, S. W. Webb, and S. J. Altman, "Water Recovery Using Waste Heat from Coal Fired Power Plants," Sandia National Laboratories, California, Report No. SAND2011-0258, 2011.

[80] R. Schwantes *et al.*, "Membrane distillation: Solar and waste heat driven demonstration plants for desalination," *Desalination*, vol. 323, pp. 93–106, Aug. 2013.

[81] N. E. Koeman-Stein, R. J. M. Creusen, M. Zijlstra, C. K. Groot, and W. B. P. van den Broek, "Membrane distillation of industrial cooling tower blowdown water," *Water Resour. Ind.*, vol. 14, pp. 11–17, Jun. 2016.

[82] D. Woldemariam, A. Kullab, E. U. Khan, and A. Martin, "Recovery of ethanol from scrubber-water by district heat-driven membrane distillation: Industrial-scale technoeconomic study," *Renew. Energy*, vol. 128, pp. 484–494, Dec. 2018.

[83] E. U. Khan, B. Mainali, A. Martin, and S. Silveira, "Techno-economic analysis of small scale biogas based polygeneration systems: Bangladesh

case study," *Sustain. Energy Technol. Assessments*, vol. 7, pp. 68–78, Sep. 2014.

[84] X. Song *et al.*, "An anaerobic membrane bioreactor – membrane distillation hybrid system for energy recovery and water reuse: Removal performance of organic carbon, nutrients, and trace organic contaminants," *Sci. Total Environ.*, vol. 628–629, pp. 358–365, Jul. 2018.

[85] E. U. Khan and Å. Nordberg, "Thermal integration of membrane distillation in an anaerobic digestion biogas plant – A techno-economic assessment," *Appl. Energy*, vol. 239, pp. 1163–1174, Apr. 2019.

[86] F. Yilmaz, M. Ozturk, and R. Selbas, "Design and thermodynamic assessment of a biomass gasification plant integrated with Brayton cycle and solid oxide steam electrolyzer for compressed hydrogen production," *Int. J. Hydrogen Energy*, Mar. 2020.

[87] L. Huang *et al.*, "Solar-driven co-generation of electricity and water by evaporation cooling," *Desalination*, vol. 488, p. 114533, Aug. 2020.

[88] J. A. Andrés-Mañas, L. Roca, A. Ruiz-Aguirre, F. G. Acién, J. D. Gil, and G. Zaragoza, "Application of solar energy to seawater desalination in a pilot system based on vacuum multi-effect membrane distillation," *Appl. Energy*, vol. 258, p. 114068, Jan. 2020.

[89] W. Peng and I. C. Escobar, "Rejection Efficiency of Water Quality Parameters by Reverse Osmosis and Nanofiltration Membranes," *Environ. Sci. Technol.*, vol. 37, no. 19, pp. 4435–4441, Oct. 2003.

[90] B. Ozbey-Unal, D. Y. Imer, B. Keskinler, and I. Koyuncu, "Boron removal from geothermal water by air gap membrane distillation," *Desalination*, vol. 433, pp. 141–150, May 2018.

[91] H. C. Duong *et al.*, "A novel application of membrane distillation to facilitate nickel recovery from electroplating wastewater," *Environ. Sci. Pollut. Res.*, vol. 26, no. 23, pp. 23407–23415, Aug. 2019.

[92] S. K. Hubadillah *et al.*, "Removal of As(iii) and As(v) from water using green, silica-based ceramic hollow fibre membranes *via* direct contact membrane distillation," *RSC Adv.*, vol. 9, no. 6, pp. 3367–3376, Jan. 2019.

[93] X.-Y. Lou, Z. Xu, A.-P. Bai, M. Resina-Gallego, and Z.-G. Ji, "Separation and Recycling of Concentrated Heavy Metal Wastewater by Tube

Membrane Distillation Integrated with Crystallization," *Membranes (Basel).*, vol. 10, no. 1, p. 19, Jan. 2020.

[94] B. G. Reis, A. L. B. Araújo, M. C. S. Amaral, and H. C. Ferraz, "Comparison of Nanofiltration and Direct Contact Membrane Distillation as an alternative for gold mining effluent reclamation," *Chem. Eng. Process. - Process Intensif.*, vol. 133, pp. 24–33, Nov. 2018.

[95] H. Liu and J. Wang, "Treatment of radioactive wastewater using direct contact membrane distillation," *J. Hazard. Mater.*, vol. 261, pp. 307–315, Oct. 2013.

[96] I. V. Korolkov *et al.*, "Modification of PET ion track membranes for membrane distillation of low-level liquid radioactive wastes and salt solutions," *Sep. Purif. Technol.*, vol. 227, p. 115694, Nov. 2019.

[97] F. Ricceri *et al.*, "Desalination of Produced Water by Membrane Distillation: Effect of the Feed Components and of a Pre-treatment by Fenton Oxidation," *Sci. Rep.*, vol. 9, no. 1, p. 14964, Dec. 2019.

[98] S. Tavakkoli, O. Lokare, R. Vidic, and V. Khanna, "Shale gas produced water management using membrane distillation: An optimization-based approach," *Resour. Conserv. Recycl.*, vol. 158, p. 104803, Jul. 2020.

[99] I. A. Said, T. R. Chomiak, Z. He, and Q. Li, "Low-cost high-efficiency solar membrane distillation for treatment of oil produced waters," *Sep. Purif. Technol.*, vol. 250, p. 117170, Nov. 2020.

[100] M. Shi, Q. He, L. Feng, L. Wu, and S. Yan, "Techno-economic evaluation of ammonia recovery from biogas slurry by vacuum membrane distillation without pH adjustment," *J. Clean. Prod.*, vol. 265, p. 121806, Aug. 2020.

[101] A. Zoungrana, İ. H. Zengin, O. K. Türk, and M. Çakmakcı, "Ammoniacal nitrogen reclamation by membrane distillation from high ammonia polluted solutions," *Chem. Pap.*, vol. 74, no. 6, pp. 1903–1915, Jun. 2020.

[102] N. Khumalo *et al.*, "Water recovery from hydrolysed human urine samples via direct contact membrane distillation using PVDF/PTFE membrane," *Sep. Purif. Technol.*, vol. 211, pp. 610–617, Mar. 2019.

[103] X. Li, J. Li, and L. Wu, "Vacuum membrane distillation to remove ethyl acetate from aqueous solutions," *Desalin. Water Treat.*, vol. 52, no. 25–27, pp. 5158–5164, Jul. 2014.

[104] S. Pedram, H. R. Mortaheb, and F. Arefi-Khonsari, “Plasma treatment of polyethersulfone membrane for benzene removal from water by air gap membrane distillation,” *Environ. Technol.*, vol. 39, no. 2, pp. 157–171, Jan. 2018.

[105] J. Zhang, N. Li, D. Ng, I. A. Ike, Z. Xie, and S. Gray, “Depletion of VOC in wastewater by vacuum membrane distillation using a dual-layer membrane: mechanism of mass transfer and selectivity,” *Environ. Sci. Water Res. Technol.*, vol. 5, no. 1, pp. 119–130, 2019.

[106] S. Kalla, S. Upadhyaya, K. Singh, and R. Baghel, “Development of heat and mass transfer correlations and recovery calculation for HCl–water azeotropic separation using air gap membrane distillation,” *Chem. Pap.*, vol. 73, no. 10, pp. 2449–2460, Oct. 2019.

[107] M. Madhumala, D. Madhavi, T. Sankarshana, and S. Sridhar, “Recovery of hydrochloric acid and glycerol from aqueous solutions in chloralkali and chemical process industries by membrane distillation technique,” *J. Taiwan Inst. Chem. Eng.*, vol. 45, no. 4, pp. 1249–1259, Jul. 2014.

[108] Z. Si, D. Han, Y. Liu, Y. Li, and K. Chen, “Performance analysis of treating sulfuric acid solution by the combined system of vacuum membrane distillation and mechanical vapor recompression,” *Chem. Eng. Process. - Process Intensif.*, vol. 150, p. 107890, Apr. 2020.

[109] Z. Si *et al.*, “Study on vacuum membrane distillation coupled with mechanical vapor recompression system for the concentration of sulfuric acid solution,” *J. Brazilian Soc. Mech. Sci. Eng.*, vol. 41, no. 11, p. 473, Nov. 2019.

[110] H. Julian, F. Yaohanny, A. Devina, R. Purwadi, and I. G. Wenten, “Apple juice concentration using submerged direct contact membrane distillation (SDCMD),” *J. Food Eng.*, vol. 272, p. 109807, May 2020.

[111] C. A. Quist-Jensen *et al.*, “Direct contact membrane distillation for the concentration of clarified orange juice,” *J. Food Eng.*, vol. 187, pp. 37–43, Oct. 2016.

[112] S. Ahmad *et al.*, “Mass transfer modelling of hollow fiber membrane contactor for apple juice concentration using osmotic membrane distillation,” *Sep. Purif. Technol.*, vol. 250, p. 117209, Nov. 2020.

[113] M. M. A. Shirazi, A. Kargari, D. Bastani, M. Soleimani, and L. Fatehi,

"Study on commercial membranes and sweeping gas membrane distillation for concentrating of glucose syrup," *J. Membr. Sci. Res.*, vol. 6, no. 1, pp. 47–57, 2020.

[114] R. Kumar, A. K. Ghosh, and P. Pal, "Fermentative ethanol production from Madhuca indica flowers using immobilized yeast cells coupled with solar driven direct contact membrane distillation with commercial hydrophobic membranes," *Energy Convers. Manag.*, vol. 181, pp. 593–607, Feb. 2019.

[115] O. Gupta, S. Roy, and S. Mitra, "Microwave Induced Membrane Distillation for Enhanced Ethanol–Water Separation on a Carbon Nanotube Immobilized Membrane," *Ind. Eng. Chem. Res.*, vol. 58, no. 39, pp. 18313–18319, Oct. 2019.

[116] O. Gupta, S. Roy, and S. Mitra, "Low temperature recovery of acetone–butanol–ethanol (ABE) fermentation products via microwave induced membrane distillation on carbon nanotube immobilized membranes," *Sustain. Energy Fuels*, vol. 4, no. 7, pp. 3487–3499, May. 2020.

[117] C. A. Nayak and N. K. Rastogi, "Comparison of osmotic membrane distillation and forward osmosis membrane processes for concentration of anthocyanin," *Desalin. Water Treat.*, vol. 16, no. 1–3, pp. 134–145, Apr. 2010.

[118] S. Varavuth, R. Jiraratananon, and S. Atchariyawut, "Experimental study on dealcoholization of wine by osmotic distillation process," *Sep. Purif. Technol.*, vol. 66, no. 2, pp. 313–321, Apr. 2009.

[119] A. Hausmann, P. Sanciolo, T. Vasiljevic, U. Kulozik, and M. Duke, "Performance assessment of membrane distillation for skim milk and whey processing," *J. Dairy Sci.*, vol. 97, no. 1, pp. 56–71, Jan. 2014.

[120] K. Gethard, O. Sae-Khow, and S. Mitra, "Carbon nanotube enhanced membrane distillation for simultaneous generation of pure water and concentrating pharmaceutical waste," *Sep. Purif. Technol.*, vol. 90, pp. 239–245, Apr. 2012.

[121] S. Leaper, A. Abdel-Karim, T. A. Gad-Allah, and P. Gorgojo, "Air-gap membrane distillation as a one-step process for textile wastewater treatment," *Chem. Eng. J.*, vol. 360, pp. 1330–1340, Mar. 2019.

[122] N. M. Mokhtar, W. J. Lau, A. F. Ismail, S. Kartohardjono, S. O. Lai, and H. C. Teoh, "The potential of direct contact membrane distillation for

industrial textile wastewater treatment using PVDF-Cloisite 15A nanocomposite membrane," *Chem. Eng. Res. Des.*, vol. 111, pp. 284–293, Jul. 2016.

[123] C. Conidi *et al.*, "Treatment of Flue Gas Desulfurization Wastewater by an Integrated Membrane-Based Process for Approaching Zero Liquid Discharge," *Membranes (Basel).*, vol. 8, no. 4, p. 117, Nov. 2018.

[124] A. Ali, A. Criscuoli, F. Macedonio, P. Argurio, A. Figoli, and E. Drioli, "Direct contact membrane distillation for the treatment of wastewater for a cooling tower in the power industry," *H2Open J.*, vol. 1, no. 1, pp. 57–68, Jul. 2018.

[125] X. Yu, H. Yang, H. Lei, and A. Shapiro, "Experimental evaluation on concentrating cooling tower blowdown water by direct contact membrane distillation," *Desalination*, vol. 323, pp. 134–141, Aug. 2013.

[126] L. Chuanfeng and A. Martin, "Membrane Distillation and Applications for Water Purification in Thermal Cogeneration : A Pre-study," Värmeforsk NV - 909, 2005.

[127] A. Kullab and A. Martin, "Membrane distillation and applications for water purification in thermal cogeneration plants," *Sep. Purif. Technol.*, vol. 76, no. 3, pp. 231–237, Jan. 2011.

[128] U. Fortkamp, H. Royen, M. Klingspor, Ö. Ekengren, A. Martin, and D. M. Woldemariam, "Membrane Distillation pilot tests for different wastewaters," IVL Swedish Environmental Research Institute Ltd., Stockholm, Report No. B 2236, 2015.

[129] J. S. Kilby, "Miniaturized electronic circuits," US3138743 A, 1964.

[130] P. Van Zant, *Microchip Fabrication, Sixth Edition: A Practical Guide to Semiconductor Processing*. McGraw-Hill Education, 2013.

[131] S. Boyd and D. Dornfeld, "Semiconductor Manufacturing," in *Green Manufacturing*, Springer, Boston, MA, 2013, pp. 153–178.

[132] P. van Gerven, "ASML for beginners," 2017. [Online]. Available: https://bits-chips.nl/artikel/asml-for-beginners/. [Accessed: 06-Jun-2020].

[133] C. L. Lai and S. H. Lin, "Treatment of chemical mechanical polishing wastewater by electrocoagulation: system performances and sludge settling

characteristics," *Chemosphere*, vol. 54, no. 3, pp. 235–242, Jan. 2004.

[134] G. Corlett, "Targeting water use for chemical mechanical polishing," *Solid State Technol.*, vol. 43, no. 6, pp. 201–202, Jun. 2000.

[135] G. E. McGuire, *Semiconductor Materials and Process Technology Handbook: For Very Large Scale Integration (VLSI) and Ultra Large Scale Integration (ULSI)*. Noyes Publications, 1988.

[136] K. Reinhardt and W. Kern, *Handbook of Silicon Wafer Cleaning Technology, 2nd Edition*. Elsevier Science, 2008.

[137] D. G. Gilles and R. C. Loehr, "Waste Generation and Minimization in Semiconductor Industry," *J. Environ. Eng.*, vol. 120, no. 1, pp. 72–86, Jan. 1994.

[138] C. Shen, P. Tran, and P. Minh Ly, "Chemical Waste Management in the U.S. Semiconductor Industry," *Sustainability*, vol. 10, no. 5, p. 1545, May 2018.

[139] C. N. Haas and V. Tare, "Application of ion exchangers to recovery of metals from semiconductor wastes," *React. Polym. Ion Exch. Sorbents*, vol. 2, no. 1–2, pp. 61–70, Jan. 1984.

[140] C. R. Simpson, *Environmental Issues in the Electronics/semiconductor Industries and: Electrochemical/photochemical Methods for Pollution Abatement*. Electrochemical Society, 1998.

[141] Y. C. Wong, V. Moganaragi, and N. A. Atiqah, "Physico-chemical Investigation of Semiconductor Industrial Wastewater," in *Ecological Technologies for Industrial Wastewater Management: Petrochemicals, Metals, Semi-Conductors, and Paper Industries*, Apple Academic Press, 2015, pp. 153–165.

[142] T. Ouslimane, S. Aoudj, M. Amara, and N. Drouiche, "Removal of Copper and Fluoride from Mixed Cu-CMP and Fluoride-Bearing Wastewaters by Electrocoagulation," *Int. J. Environ. Res.*, vol. 11, no. 5–6, pp. 677–684, Dec. 2017.

[143] K. Mitsumori and N. Inoue, "Silicon etching," in *Scientific Wet Process Technology for Innovative LSI/FPD Manufacturing*, 2016.

[144] H. Sugawara and T. Imaoka, "Chemical waste reclamation technology," in

Scientific Wet Process Technology for Innovative LSI/FPD Manufacturing, 2016.

[145] V. Innocenzi *et al.*, “Treatment of TMAH solutions from the microelectronics industry: A combined process scheme,” *J. Water Process Eng.*, vol. 31, p. 100780, Oct. 2019.

[146] S. Ojima and T. Ohmi, “Wet vapor resist stripping technology,” in *Scientific Wet Process Technology for Innovative LSI/FPD Manufacturing*, 2016.

[147] C.-F. Chen and J.-J. Liang, “Using a source–receptor approach to characterize the volatile organic compounds from control device exhaust in a science park,” *Environ. Sci. Pollut. Res.*, vol. 20, no. 3, pp. 1526–1536, Mar. 2013.

[148] Y. D. Chaniago, J.-K. Kim, M.-J. Park, K.-K. Koo, and M. Lee, “Design and modeling of optimal distillation sequence for recovery of valuable components from a waste photoresist stripper,” *J. Mater. Cycles Waste Manag.*, vol. 18, no. 2, pp. 366–376, Apr. 2016.

[149] H.-H. Cheng, T.-T. Pien, Y.-C. Lee, I.-C. Lu, and L.-M. Whang, “Effects of copper on biological treatment of NMF- and MDG-containing wastewater from TFT-LCD industry,” *Chemosphere*, vol. 258, p. 127125, Nov. 2020.

[150] S. Babu, *Advances in Chemical Mechanical Planarization (CMP)*. Elsevier Science, 2016.

[151] D. E. Speed, “Environmental aspects of planarization processes,” in *Advances in Chemical Mechanical Planarization (CMP)*, S. Babu, Ed. Elsevier, 2016, pp. 229–269.

[152] M. Krishnan, J. W. Nalaskowski, and L. M. Cook, “Chemical Mechanical Planarization: Slurry Chemistry, Materials, and Mechanisms,” *Chem. Rev.*, vol. 110, no. 1, pp. 178–204, Jan. 2010.

[153] G. B. Basim, “Effect of slurry aging on stability and performance of chemical mechanical planarization process,” *Adv. Powder Technol.*, vol. 22, no. 2, pp. 257–265, Mar. 2011.

[154] TRANE-A business of American Standard Companies, “Water-side heat recovery,” *TRANE*, 2007. [Online]. Available: https://www.trane.com/content/dam/Trane/Commercial/global/products-

systems/education-training/engineers-newsletters/waterside-design/admapn023en_0207.pdf. [Accessed: 28-Dec-2017].

[155] R. P. Kathey Ferland, "Industrial Waste heat Recovery [Roundtable Meeting]," *Texas Industries of the Furure*, 2007. [Online]. Available: https://texasiof.ceer.utexas.edu/PDF/Documents_Presentations/Roundtables/RoundTable_0807.pdf. [Accessed: 28-Dec-2017].

[156] O. Suenaga, T. Ohmi, and S. Kobayashi, "Semiconductor manufacturing facility," US6370897B1, 2002.

[157] I. Dubov, "Heat recovery, energy savings for semiconductor plant," *ASHRAE J.*, vol. 46, no. 12, pp. 56-58+60, Dec. 2005.

[158] Y.-C. Chang, "A novel energy conservation method—optimal chiller loading," *Electr. Power Syst. Res.*, vol. 69, no. 2–3, pp. 221–226, May 2004.

[159] B. Bängtsson, *Bäcken Industrifysik*. Personal Communication, 2019.

[160] A. Neuber, *Applied Materials*. Personal Communication, 2019.

[161] General Electric, "The Distributed Energy Transformation," 2018.

[162] E. Thorin, J. Sandberg, and J. Yan, "Combined Heat and Power," in *Handbook of Clean Energy Systems*, Chichester, UK: John Wiley & Sons, Ltd, 2015, pp. 1–11.

[163] "KMW Energi, Sweden." [Online]. Available: https://kmwenergy.com/.

[164] S. Zhao *et al.*, "Simultaneous heat and water recovery from flue gas by membrane condensation: Experimental investigation," *Appl. Therm. Eng.*, vol. 113, pp. 843–850, Feb. 2017.

[165] National Research Council (US) Committee on Health Effects of Waste Incineration. Waste Incineration & Public Health. 3, "Incineration Processes and Environmental Releases." Washington (DC): National Academies Press (US); 2000. [Online]. Available: https://www.ncbi.nlm.nih.gov/books/NBK233627/

[166] H. Gadd and S. Werner, "Achieving low return temperatures from district heating substations," *Appl. Energy*, vol. 136, pp. 59–67, Dec. 2014.

[167] S. Werner, “District heating and cooling in Sweden,” *Energy*, vol. 126, pp. 419–429, May 2017.

[168] D. Lundqvist, “District Energy in Sweden,” *Euroheat & Power*, 2019. [Online]. Available: https://www.euroheat.org/knowledge-hub/district-energy-sweden/. [Accessed: 07-Aug-2020].

[169] K.-M. Steen, U. Sagebrand, and H. Walletun, “Att använda fjärrvärme i industriprocesser,” Energiforsk, Stockholm, ISBN 978-91-7673-155-0, Report No. 2015:155, 2015.

[170] D. W. Green and R. H. Perry, *Perry’s Chemical Engineers’ Handbook, Eighth Edition*. McGraw-Hill Education, 2007.

[171] D. Winter, “Membrane Distillation – A Thermodynamic, Technological and Economic Analysis,” Doctoral Thesis Report, University of Kaiserslautern, 2014.

[172] E. Drioli, E. Curcio, G. Di Profio, F. Macedonio, and A. Criscuoli, “Integrating Membrane Contactors Technology and Pressure-Driven Membrane Operations for Seawater Desalination: Energy, Exergy and Costs Analysis,” *Chem. Eng. Res. Des.*, vol. 84, no. 3, pp. 209–220, Mar. 2006.

[173] M. S. Peters and K. D. Timmerhaus, *Plant design and economics for chemical engineers*. McGraw-Hill, 1991.

[174] W. D. Seider, J. D. Seader, D. R. Lewin, and S. Widagdo, “Cost Accounting and Capital Cost Estimation,” in *Product and Process Design Principles: Synthesis, Analysis and Design*, Third., J. Welter, Ed. Donald Fowley, 2004, p. 768.

[175] Medesol Report, “Performance and cost estimations of final industrial-size of MEDESOL-2 technology,” University of La Laguna, Spain, 2010.

[176] G. F. Hewitt and S. J. Pugh, “Approximate Design and Costing Methods for Heat Exchangers,” *Heat Transf. Eng.*, vol. 28, no. 2, pp. 76–86, Feb. 2007.

[177] H. P. Loh, J. Lyons, and C. W. White, “Process Equipment Cost Estimation, Final Report,” National Energy Technology Laboratory, Pittsburgh, PA, and Morgantown, WV (United States), Report No. DOE/NETL-2002/1169, Jan. 2002.

[178] K. K. Sirkar, *Pilot-scale Studies for Direct Contact Membrane Distillation-based Desalination Process*. US Department of the Interior, Bureau of Reclamation, 2009.

[179] U. K. Kesieme, N. Milne, H. Aral, C. Y. Cheng, and M. Duke, “Economic analysis of desalination technologies in the context of carbon pricing, and opportunities for membrane distillation,” *Desalination*, vol. 323, pp. 66–74, Aug. 2013.

[180] S. Werner, “European district heating price series,” Energiforsk, Stockholm, ISBN 978-91-7673-316-5, Report No. 2016:316, 2016.

[181] Eurostat, “Electricity price statistics,” 2019. [Online]. Available: https://ec.europa.eu/eurostat/statistics-explained/index.php/Electricity_price_statistics#Electricity_prices_for_non-household_consumers. [Accessed: 29-Nov-2019].

[182] ICIS, “Indicative chemical prices,” *Chemical Industry News, Chemical Prices & Chemical Suppliers from ICIS.*, 2019. [Online]. Available: https://www.icis.com/explore/commodities/chemicals/channel-info-chemicals-a-z/. [Accessed: 27-Sep-2019].

[183] R. Schwantes, K. Chavan, D. Winter, C. Felsmann, and J. Pfafferott, “Techno-economic comparison of membrane distillation and MVC in a zero liquid discharge application,” *Desalination*, vol. 428, pp. 50–68, Feb. 2018.

[184] R. Turton, R. C. Bailie, W. B. Whiting, and J. A. Shaeiwitz, *Analysis, Synthesis, and Design of Chemical Processes*. Prentice Hall, 2009.

[185] Y. Nishi and R. Doering, *Handbook of Semiconductor Manufacturing Technology*. Taylor & Francis, 2000.

[186] J.-C. Tsai, M. Kumar, S.-Y. Chen, and J.-G. Lin, “Nano-bubble flotation technology with coagulation process for the cost-effective treatment of chemical mechanical polishing wastewater,” *Sep. Purif. Technol.*, vol. 58, no. 1, pp. 61–67, Dec. 2007.

[187] W. Den and C. Huang, “Electrocoagulation for removal of silica nano-particles from chemical–mechanical-planarization wastewater,” *Colloids Surfaces A Physicochem. Eng. Asp.*, vol. 254, no. 1–3, pp. 81–89, Mar. 2005.

[188] R. Lo and S.-L. Lo, “A pilot plant study using ceramic membrane microfiltration, carbon adsorption and reverse osmosis to treat CMP (chemical mechanical polishing) wastewater,” *Water Supply*, vol. 4, no. 1, pp. 111–118, Feb. 2004.

[189] Y. Wang, Z. Zhang, C. Jiang, and T. Xu, “Electrodialysis Process for the Recycling and Concentrating of Tetramethylammonium Hydroxide (TMAH) from Photoresist Developer Wastewater,” *Ind. Eng. Chem. Res.*, vol. 52, no. 51, pp. 18356–18361, Dec. 2013.

[190] J. Huang, K.-S. Wang, and C. Liang, “Oxidative degradation of tetramethylammonium hydroxide (TMAH) by UV/persulfate and associated acute toxicity assessment,” *J. Environ. Sci. Heal. Part A*, vol. 52, no. 9, pp. 930–937, Jul. 2017.

[191] H. M. Citraningrum, J. C. Liu, and J. M. Chern, “Removal of Tetramethylammonium Hydroxide From Solution Using Ion Exchange,” *IEEE Trans. Semicond. Manuf.*, vol. 26, no. 2, pp. 214–220, May 2013.

[192] T. K Chen and N. J. Chen, “Combined membrane bioreactor (MBR) and reverse osmosis (RO) system for thin-film transistor - Liquid crystal display TFT-LCD, industrial wastewater recycling,” *Water Sci. Technol.*, vol. 50, pp. 99–106, Feb. 2004.

[193] S.-J. You, G. U. Semblante, Y.-P. Chen, and T.-C. Chang, “Combined photocatalysis and membrane bioreactor for the treatment of feedwater containing thin film transistor-liquid crystal display discharge,” *Environ. Technol.*, vol. 36, no. 21, pp. 2681–2690, Nov. 2015.

[194] S.-Y. Chen, L.-A. Lu, and J.-G. Lin, “Biodegradation of tetramethylammonium hydroxide (TMAH) in completely autotrophic nitrogen removal over nitrite (CANON) process,” *Bioresour. Technol.*, vol. 210, pp. 88–93, Jun. 2016.

[195] F. Ferella *et al.*, “Aerobic Treatment of Waste Process Solutions from the Semiconductor Industry: From Lab to Pilot Scale,” *Sustainability*, vol. 11, no. 14, p. 3923, Jul. 2019.

[196] T.-H. Hu *et al.*, “Biological treatment of TMAH (tetra-methyl ammonium hydroxide) in a full-scale TFT-LCD wastewater treatment plant,” *Bioresour. Technol.*, vol. 113, pp. 303–310, Jun. 2012.

[197] Y.-H. Liu, C.-Y. Lin, J.-H. Huang, and S.-C. Yen, “Particle removal

performance and its kinetic behavior during oxide-CMP wastewater treatment by electrocoagulation,” *J. Taiwan Inst. Chem. Eng.*, vol. 60, pp. 520–524, Mar. 2016.

[198] N. Hu *et al.*, “BS12-assisted flotation for the intensification of SNPs separation from CMP wastewater using a novel flotation column,” *J. Hazard. Mater.*, vol. 344, pp. 788–796, Feb. 2018.

[199] Y.-G. Kim, J.-B. Song, D. Yang, W. J. Kim, S.-H. Kim, and H. Lee, “Purification of Chemical Mechanical Polishing Wastewater via Superconducting High Gradient Magnetic Separation System with Optimal Coagulation Process,” *IEEE Trans. Appl. Supercond.*, vol. 25, no. 3, pp. 1–5, Jun. 2015.

[200] H.-D. Ryu, H.-S. Kang, and S.-I. Lee, “Enhancing the separation of silica nanoparticles from backside grinding (BG) wastewater with synthesized magnetite,” *Sep. Purif. Technol.*, vol. 165, pp. 130–136, Jun. 2016.

[201] I.- Noor, J. Coenen, A. Martin, O. Dahl, and M. Åslin, “Experimental investigation and techno-economic analysis of tetramethylammonium hydroxide removal from wastewater in nano-electronics manufacturing via membrane distillation,” *J. Memb. Sci.*, vol. 579, pp. 283–293, Jun. 2019.

[202] I.- Noor, J. Coenen, A. Martin, and O. Dahl, “Performance assessment of chemical mechanical planarization wastewater treatment in nano-electronics industries using membrane distillation,” *Sep. Purif. Technol.*, p. 116201, Oct. 2019.

[203] S. Körner, S. K. Das, S. Veenstra, and J. E. Vermaat, “The effect of pH variation at the ammonium/ammonia equilibrium in wastewater and its toxicity to Lemna gibba,” *Aquat. Bot.*, vol. 71, no. 1, pp. 71–78, Sep. 2001.

[204] M. T. Samadi, M. Zarrabi, M. N. Sepehr, S. M. Ramhormozi, S. Azizian, and A. Amrane, “Removal of fluoride ions by ion exchange resin: kinetic and equilibrium studies,” *Environ. Eng. Manag. J.*, vol. 13, no. 1, pp. 205–214, Jan. 2014.

[205] J. Singh, P. Singh, and A. Singh, “Fluoride ions vs removal technologies: A study,” *Arab. J. Chem.*, vol. 9, no. 6, pp. 815–824, Nov. 2016.

[206] G. C. . Yang, T.-Y. Yang, and S.-H. Tsai, “Crossflow electro-microfiltration of oxide-CMP wastewater,” *Water Res.*, vol. 37, no. 4, pp. 785–792, Feb. 2003.

[207] G. C. . Yang and T.-Y. Yang, “Reclamation of high quality water from treating CMP wastewater by a novel crossflow electrofiltration/electrodialysis process,” *J. Memb. Sci.*, vol. 233, no. 1–2, pp. 151–159, Apr. 2004.

[208] D. Baaklini, “Performance analysis of Air Gap Membrane Distillation: Comparison of PTFE membranes,” Master Thesis Report, KTH Royal Institute of Technology, 2011.

[209] J. Kujawa and W. Kujawski, “Driving force and activation energy in air-gap membrane distillation process,” *Chem. Pap.*, vol. 69, no. 11, pp. 1438–1444, Jan. 2015.

[210] D. Woldemariam, A. Martin, and M. Santarelli, “Exergy Analysis of Air-Gap Membrane Distillation Systems for Water Purification Applications,” *Appl. Sci.*, vol. 7, no. 3, p. 301, Mar. 2017.

[211] Y. Cerci, “Exergy analysis of a reverse osmosis desalination plant in California,” *Desalination*, vol. 142, no. 3, pp. 257–266, Mar. 2002.

[212] S. Al-Obaidani, E. Curcio, F. Macedonio, G. Di Profio, H. Al-Hinai, and E. Drioli, “Potential of membrane distillation in seawater desalination: Thermal efficiency, sensitivity study and cost estimation,” *J. Memb. Sci.*, vol. 323, no. 1, pp. 85–98, Oct. 2008.

[213] H. Susanto, “Towards practical implementations of membrane distillation,” *Chem. Eng. Process. Process Intensif.*, vol. 50, no. 2, pp. 139–150, Feb. 2011.

[214] A. Chuang, “The Opportunities and Challenges of Waste-Recycling for Semiconductor Plants,” *Semicon Taiwan*. [Online]. Available: http://www.semicontaiwan.org/en/sites/semicontaiwan.org/files/data16/docs/K1-TSMC_Arthur Chuang-presentation slide.pdf. [Accessed: 19-Jul-2018].

[215] K. Hirano, J. Okamura, T. Taira, K. Sano, A. Toyoda, and M. Ikeda, “An efficient treatment technique for TMAH wastewater by catalytic oxidation,” *IEEE Trans. Semicond. Manuf.*, vol. 14, no. 3, pp. 202–206, Aug. 2001.

[216] I.- Noor, A. Martin, and O. Dahl, “Techno-economic system analysis of membrane distillation process for treatment of chemical mechanical planarization wastewater in nano-electronics industries,” *Sep. Purif. Technol.*, p. 117013, May 2020.

[217] M. Hellman, “Handbook-Water treatment for energy producing plants,” Energiforsk, Stockholm, ISBN 978-91-7673-113-0, Report No. 2015:113, 2015.

[218] J. Uotila, “Heat Recovery and Environmental Impacts of Flue Gas Condensing,” Masters Thesis Report, Aalto University, 2015.

[219] L. Wiig, K. Lundkvist, B. Goldschmidt, and H. Östfeldt, “Mikrobiell tillväxt i rökgaskondensatreningar,” Energiforsk, Stockholm, ISBN 978-91-7673-489-6, Report No. 2018:489, 2018.

[220] “Radscan Intervex Projects.” [Online]. Available: www.radscan.se. [Accessed: 12-Dec-2019].

[221] M. Teppler, J. Wood, and P. Buzzell, “Flue Gas Condensate and Energy Recovery,” The Mcilvaine Company, Karlskoga, Report No. IWC-08-17, 2017.

[222] B. Goldschmidt, L. Wiig, and M. Lord, “Minskning av ammoniumhalt i rökgaskondensat,” Energiforsk, Stockholm, ISBN 978-91-7673-194-9, Report No. 2015:194, 2015.

[223] J. Lundgren, *Stockholm Exergi*. Personal Communication, 2018.

[224] I.- Noor, A. Martin, and O. Dahl, “Water recovery from flue gas condensate in municipal solid waste fired cogeneration plants using membrane distillation,” *Chem. Eng. J.*, vol. 399, p. 125707, Nov. 2020.

[225] J. Gaffney and N. Marley, “In-depth review of atmospheric mercury: sources, transformations, and potential sinks,” *Energy Emiss. Control Technol.*, p. 1, Aug. 2014.

[226] B. J. Lerner, “Removal of mercury and cadmium and their compounds from incinerator flue gases,” US5569436A, 29-Oct-1996.

[227] M. Pourbaix, *Atlas of electrochemical equilibria in aqueous solutions*, 2nd ed. National Association of Corrosion Engineers, 1974.

[228] A. Spyropoulou, Y. G. Lazarou, and C. Laspidou, “Mercury Speciation in the Water Distribution System of Skiathos Island, Greece,” *Proceedings*, vol. 2, no. 11, p. 668, Aug. 2018.

[229] S. B. Lyon, “Corrosion of Lead and its Alloys,” in *Shreir’s Corrosion*,

Elsevier, 2010, pp. 2053–2067.

[230] K. Emerson, R. C. Russo, R. E. Lund, and R. V Thurston, “Aqueous Ammonia Equilibrium Calculations: Effect of pH and Temperature,” *J. Fish. Res. Board Canada*, vol. 32, no. 12, pp. 2379–2383, Dec. 1975.

[231] J. López-García, F. Cupessala, P. Humpolíček, and M. Lehocký, “Physical and Morphological Changes of Poly(tetrafluoroethylene) after Using Non-Thermal Plasma-Treatments,” *Materials (Basel).*, vol. 11, no. 10, p. 2013, Oct. 2018.

[232] J. Kheriji, D. Tabassi, and B. Hamrouni, “Removal of Cd(II) ions from aqueous solution and industrial effluent using reverse osmosis and nanofiltration membranes,” *Water Sci. Technol.*, vol. 72, no. 7, p. 1206, Sep. 2015.

[233] A. K. An, J. Guo, S. Jeong, E.-J. Lee, S. A. A. Tabatabai, and T. Leiknes, “High flux and antifouling properties of negatively charged membrane for dyeing wastewater treatment by membrane distillation,” *Water Res.*, vol. 103, pp. 362–371, Oct. 2016.

[234] H. L. Le Chatelier, “A general statement of the laws of chemical equilibrium,” *Comptes rendus*, vol. 99, pp. 786–789, Jan. 1884.

[235] I.- Noor, A. Martin, and O. Dahl, “District heating driven membrane distillation for advanced flue gas condensate treatment in combined heat and power plants,” *J. Clean. Prod.*, In press, p. 125979, Jan. 2021.

[236] K. Pyrzynska, “Removal of cadmium from wastewaters with low-cost adsorbents,” *J. Environ. Chem. Eng.*, vol. 7, no. 1, p. 102795, Feb. 2019.

[237] G. Kyzas and M. Kostoglou, “Green Adsorbents for Wastewaters: A Critical Review,” *Materials (Basel).*, vol. 7, no. 1, pp. 333–364, Jan. 2014.

Appendix

Table A1 Uncertainty levels associated with different analysis

Analysis	Uncertainty	Reference
Turbidity	30%	SS-EN ISO 7027-1:2016
pH	0.2	SS-EN ISO 10523:2012
Alkalinity	10%	SS-EN ISO 9963-2:1996
Conductivity	10%	SS-EN 27888:1994
Cl^-	10%	SS-EN ISO 10304-1:2009
SO_4^{-2}	15%	StMeth 4500-SO_4, E 1998 mod
F^-	25%	St Meth 4500-F, E 1998 mod
TOC	20%	SS EN 1484:1997
COD	20%	ISO 15705:2002(E)
NH_3	15%	SS-EN 11732:2005
NH_4-N	15%	SS-EN 11732:2005
NO_3-N	20%	SS 028133:1991 mod
Na	15%	SS-EN ISO 17294-2, edition 1
K	15%	SS-EN ISO 17294-2, edition 1
Ca	15%	SS-EN ISO 17294-2, edition 1
Fe	25%	EN ISO 17294-2:2016 / EN ISO 15587-2:2002
Mg	15%	SS-EN ISO 17294-2, edition 1
Mn	20%	EN ISO 17294-2:2016 / EN ISO 15587-2:2002
Al	25%	EN ISO 17294-2:2016 / EN ISO 15587-2:2002
As	30%	EN ISO 17294-2:2016 / EN ISO 15587-2:2002
Ba	25%	EN ISO 17294-2:2016 / EN ISO 15587-2:2002
Pb	20%	EN ISO 17294-2:2016 / EN ISO 15587-2:2002
Cd	25%	EN ISO 17294-2:2016 / EN ISO 15587-2:2002
Co	20%	EN ISO 17294-2:2016 / EN ISO 15587-2:2002
Cu	20%	EN ISO 17294-2:2016 / EN ISO 15587-2:2002
Cr	20%	EN ISO 17294-2:2016 / EN ISO 15587-2:2002
Hg	20%	SS-EN ISO 17852:2008
Mo	20%	EN ISO 17294-2:2016 / EN ISO 15587-2:2002
Ni	25%	EN ISO 17294-2:2016 / EN ISO 15587-2:2002
Tl	20%	EN ISO 17294-2:2016 / EN ISO 15587-2:2002
Ti	20%	SS-EN ISO 15587-2, edition 1/ SS-EN ISO 11885:2009
V	20%	EN ISO 17294-2:2016 / EN ISO 15587-2:2002
Zn	20%	EN ISO 17294-2:2016 / EN ISO 15587-2:2002
TDS	unspecified	EN 15216:2007
Total hardness	-	Calculation (Ca + Mg)